

**Meereswissenschaftliche Berichte**  
**MARINE SCIENCE REPORTS**

No. 47

Data report of R/V "Meteor" cruise 48/3  
ANBEN'2000

by

H. U. Lass, V. Mohrholz, G. Nausch, C. Pohl, L. Postel, D. Rüß  
M. Schmidt, A. da Silva and N. Wasmund

**Institut für Ostseeforschung**  
**Warnemünde**  
**2001**

The cruise M48/3 of R/V "Meteor" was the third one in a framework of cruises, which were focussed on the dynamics of the Southeast Atlantic ecosystem. The field work started in 1997 with the R/V "Kottsov" expedition at the Angola-Benguela Frontal Zone and was continued with the R/V "Poseidon" cruise in March/April 1999, which provided a large scale view from the equator to the northern Benguela. The cruise M48/3 was granted by the Deutsche Forschungsgemeinschaft (DFG) Grant no. Ba 725/4-1 and LA 1137/3-1.

# Contents

	page
<b>Zusammenfassung</b>	<b>3</b>
<b>Summary</b>	<b>4</b>
<b>1 Background</b>	<b>6</b>
<b>2 Cruise Information</b>	<b>10</b>
2.1 Scientific programme	10
2.2 Strategy of measurements	11
2.3 List of cruise participants	12
2.4 The extent of measurements	13
2.5 Survey Chronology	18
2.6 List of principle Investigators	19
<b>3 Measurements and methods</b>	<b>20</b>
3.1 Underway measurements	20
3.1.1 Navigation	20
3.1.2 Meteorology	22
3.1.3 Thermosalinograph Measurements	23
3.1.4 Continuous determination of phosphate in the surface water	24
3.2 Vessel mounted Acoustic Doppler Current Profiler	25
3.3 CTD measurements	26
3.4 Salinometer	32
3.5 Reversing Thermometers	32
3.6 Lowered Acoustic Doppler Current Profiler (LADCP)	33
3.7 ARGOS Drifter	34
3.8 Hydrographic measurements	36
3.8.1 Sample salinity measurements	36
3.8.2 Sample oxygen measurements	37
3.8.3 Nutrient measurements	38
3.8.4 Trace Metals	39
3.8.5 Sample phytoplankton measurements	40
3.9 Net sampling	42
3.9.1 Phytoplankton net	42
3.9.2 Zooplankton sampling	42
3.10 Light measurements	44
<b>4 Data postprocessing</b>	<b>45</b>
4.1 Underway measurements	45

4.1.1	Navigation	45
4.1.2	Meteorology	45
4.1.3	Thermosalinograph	45
4.1.4	Surface phosphate measurements	47
4.1.5	Output file format	47
4.2	Vessel mounted ADCP	47
4.3	CTD data validation	49
4.4	LADCP	49
4.5	Phytoplankton	50
4.6	Primary production	51
4.7	Zooplankton	51
4.8	Data storage and distribution	52
<b>5</b>	<b>Preliminary Results</b>	<b>54</b>
5.1	Meteorological conditions	54
5.2	Hydrographical measurements	54
5.2.1	Surface water masses	54
5.2.2	The South Atlantic Central Water	59
5.2.3	The Anrarctic Intermediate Water	60
5.2.4	The North Atlantic Deep Water	61
5.2.5	Currents	82
5.3	Chemical measurements	89
5.3.1	Nutrients	89
5.3.2	Trace metals	99
5.4	Biological measurements	102
5.4.1	Chlorophyll-a and primary production	102
5.4.2	Zooplankton biomass	103
	<b>Acknowledgement</b>	<b>107</b>
	<b>Bibliography</b>	<b>108</b>
	<b>Appendix</b>	
<b>A</b>	<b>Station lists</b>	<b>115</b>

## Zusammenfassung

Die Meteor Expedition M48/3, an der deutsche, namibische und angolansische Wissenschaftler teilnahmen, diente der großräumigen Untersuchung des Ökosystems im östlichen Südatlantik. Die Messungen umfassten das Gebiet des Angoladoms und der Angola-Benguela Frontal Zone (ABFZ). Auf einem Netz hydrographischer Stationen wurden CTD-Profile, Strömungsmessungen und Nährstoffanalysen sowie Phyto- und Zooplanktonuntersuchungen durchgeführt. Diese Daten wurden mit kontinuierlichen Messungen eines Thermosalinographen, eines Phosphat-Autoanalysers und der Schiffswetterstation ergänzt.

Die hydrographischen Bedingungen im Untersuchungsgebiet entsprachen den klimatologischen Daten. Das Windfeld teilte sich in ein Gebiet mit schwachen südlichen Winden im Norden und in einen starken Südost-Passat Bereich im Süden, die durch eine Windfront bei 16°S getrennt sind.

Entsprechend seines jahreszeitlichen Zyklus konnte der Angoladom nicht nachgewiesen werden. Die Angola-Benguela Front Zone lag bei 16°S. Die meridionalen Gradienten in der ABFZ waren generell schwach. Nördlich der ABFZ wurde die Deckschicht von tropischen Oberflächenwasser dominiert. Lokale Auftriebszellen wurden an der angolansischen Küste nachgewiesen. Südlich der Front generierten die südöstlichen Winde moderaten Auftrieb an der namibischen Küste.

An der Windfront, die mit der ABFZ zusammenfiel, verursachte der negative Wind Stress Curl ein schwaches Auftriebssignal. Der Angolastrom (AC) wurde an der angolansischen Küste bis in 120 m Tiefe gefunden. Eine Fortsetzung des AC durch die ABFZ nach Süden konnte mit den direkten Strömungsmessungen nicht gezeigt werden. Ein im AC ausgesetzter Oberflächendrifter konnte die Front jedoch durchqueren und driftete erst weit südlich der Front nach Westen. Das deutet auf eine zumindest zeitweise Fortsetzung des AC durch die ABFZ nach Süden. Die Verteilung der Wassermassen unterstützt die Annahme eines mittleren polwärtigen Transportes unterhalb der Thermokline.

Die Verteilung von Sauerstoff und Nährstoffen ist eng verknüpft mit der Produktion und dem Abbau organischen Materials und den physikalischen Transportprozessen. Im Auftriebsgebiet südlich der ABFZ wurden im Oberflächenwasser hohe Konzentrationen von Phosphat und Nitrat gefunden, die nach Westen abnehmen. Die Silikatkonzentrationen waren ungewöhnlich niedrig. Die Nährstoffkonzentrationen im Oberflächenwasser sind nördlich von 16°S generell niedrig, mit Ausnahme der lokalen Auftriebsgebiete an der angolansischen Küste. Unterhalb der euphoten Schicht wurden hohe Nährstoffkonzentrationen nachgewiesen. Die Produktion in den küstenfernen Gebieten war meist Nitrat-limitiert. Im gesamten Untersuchungsgebiet trat bei etwa 300 m Tiefe ein Sauerstoffminimum auf. Das sauerstoffarme Wasser erstreckte sich von der Thermokline bis in 400 m Tiefe und setzte sich südwärts durch die ABFZ fort. Die seewärtige Ausdehnung dieser Wassermasse reicht nördlich von 19°S bis zur westlichen Grenze des Untersuchungsgebietes bei 8°E. Südlich von 19°S verengt sie sich auf einen etwa 200 km breiten Streifen an der Küste. Anoxische Verhältnisse in der Wassersäule wurden während der Expedition nicht gefunden.

Die Untersuchungen zu den Cadmium(Cd)-Konzentrationen in Angola-Benguela Front System zeigen, dass die erhöhten Cd-Konzentrationen an der Küste zwei Quellen haben. Nördlich der ABFZ werden die hohen Cd-Konzentrationen durch das im AC südwärts transportierte Kongo-Flusswasser verursacht. Südlich der ABFZ können die erhöhten Cd-Konzentrationen mit dem Auftrieb an der Küste erklärt werden.

Die Phytoplanktonverteilung korreliert mit der Nährstoffverteilung an der Oberfläche. Geringe Konzentrationen wurden nördlich der ABFZ gefunden. Südlich der Front steigen die Phytoplanktonkonzentrationen stark an und weisen eine hohe räumliche Varianz auf. Die Verteilung des Zooplanktons wurde in fünf Größenklassen an ausgewählten Stationen bestimmt. Zur Einschätzung der Biodiversität in Abhängigkeit von der Wassermassenverteilung wurden taxonomische Untersuchungen der Arten durchgeführt. Die aschefreie Trockenmasse wurde bestimmt und mit der Echointensität eines akustischen Stömungsmessers verglichen. Zoogeographisch teilt sich das Untersuchungsgebiet in drei Bereiche. Der nördlichste Teil, der vom Kongo-Flusswasser beeinflusst wird, zeigt die höchsten Zooplanktonkonzentrationen. Südlich davon erstreckt sich bis zur ABFZ ein zooplanktonarmes Gebiet. Südlich der ABFZ steigen die Zooplanktonkonzentrationen, bedingt durch den Auftrieb nährstoffreichen Wassers, wieder an.

## Summary

The Meteor cruise 48/3 was focussed on a large scale view of the Southeast Atlantic ecosystem. The cruise was a joint survey of scientists from Germany, Namibia and Angola. The measurements covered the Angola Dome area and the Angola-Benguela Front. On a grid of hydrographic stations CTD measurements have been carried out combined with direct current measurements and chemical, phytoplankton and zooplankton investigations. These data are supplemented by underway measurements with Thermosalinograph, Automatic Phosphate Analyser, vessel mounted ADCP and ship's weather station.

The hydrographic conditions in the investigation area coincides with the climatology. The wind field was characterised by weak southerly winds in the north and well developed south-easterly trade in the south. Both were separated by a pronounced front near 16°S.

In accordance with the known seasonal cycle the Angola Dome was not observed. The Angola-Benguela Frontal Zone (ABFZ) was met at 16°S. The meridional gradients in the ABFZ were generally weak. North of the ABFZ the upper layer was covered with tropical surface water. At the Angolan coast some local upwelling cells were detected. South of the front the south-easterly winds drive a moderate upwelling at the Namibian coast.

The negative wind stress curl caused an weak upwelling signal at this wind front, whose position coincides with the ABFZ. The Angola Current (AC) was detected at the Angolan coast down to 120 m. A poleward continuation of the AC through the ABFZ was not found in the direct current measurements. However, the surface drifter released in the AC crossed the ABFZ and turned westward well south of the front. This points to an intermit-

ting continuation of the AC into the northern Benguela. The distribution of watermasses supports the suggestion of a southward net transport below the thermocline.

The general distribution of oxygen and nutrients is closely related to the production and degradation of organic material and the transport processes. The upwelling area south of the ABFZ was characterized by high phosphate and nitrate concentrations in the surface layer, which are decreasing westwards. The silicate concentrations were unusually low. North of 16°S the surface nutrient concentrations are generally low, except in the local upwelling patches at the Angolan coast. Below the euphotic zone high nutrient concentrations were detected. The production in the open sea areas was limited most probably by nitrate. In the whole investigation area a minimum of oxygen content was found at about 300 m depth. The oxygen depleted water mass reaches from the thermocline down to 400 m depth and continues southward through the ABF. The off shore extension of this water mass is beyond 8°W north of 19°S and becomes a 200 km wide stripe along the coast south of 19°S. However, no anoxic conditions have been met in the water column during the cruise.

Investigations in the surface Cd-concentrations in the Angola-Benguela frontal system showed, that elevated Cd-levels in the coastal region may have two sources. North of the frontal system higher Cd-concentrations are attributed to the southward transport of Kongo riverwater by the AC. South of the frontal system increasing Cd-concentrations can be explained by coastal upwelling of the Benguela Current.

The phytoplankton distribution coincides with the surface nutrient distribution. Low concentrations were found north of the ABFZ. South of 16°S the phytoplankton concentrations increase rapidly but with a high patchiness. The distribution of zooplankton in five size categories was estimated at selected stations. Taxonomic analysis was carried out to investigate biodiversity patterns in relation to the water masses. The ash free dry mass was estimated and compared with the echo intensity of the acoustic current meter. The results show three sub-regions in the area of investigation. The northern most is influenced by the Congo river plume and has the highest zooplankton concentrations. It is followed by a region poor in zooplankton which extends southward to the ABFZ. South of the ABFZ the zooplankton concentrations increase due to the upwelling of nutrient rich water.

## 1 Background

The main aim of the investigations performed during the cruise M48/3 is to study the integration of both the Angola and Benguela current into the surface circulation of the South East Atlantic. This circulation is for the most parts determined by the spatial variations and the temporal fluctuations of the surface winds in both the Equatorial Atlantic and the South East Atlantic.

The prevailing winds off the Southwest African coast are determined by the South Atlantic anticyclone centred approximately at  $28^{\circ}$  S and  $7^{\circ}$  E, the equatorial zone of low pressure and the pressure field over the adjacent subcontinent. The resulting wind field of the tropical Atlantic is described by HELLERMANN (1980). The south east tradewinds prevail over the central and western parts of the tropical South Atlantic. Along the African coast and the Gulf of Guinea, the winds are predominantly meridional. Stronger winds in the south are separated there by a front from weaker winds in the north. This front is located at about  $15^{\circ}$  S at the African coast and stretches from there towards the equator at about  $15^{\circ}$  W. The wind pattern determines the distribution of the curl of the wind stress vector which is characterised by positive values in the south western part and by negative values in the north eastern part of the tropical South Atlantic ocean. In the area of the negative wind stress curl the minimum of the curl is aligned along the front between the areas of strong and weak tradewind.

The dynamic topography indicates a cyclonic gyre in the Angola Basin centered at about  $13^{\circ}$  S and  $4^{\circ}$  E, MOROSHKIN et al. (1970), GORDON and BOSLEY (1991). The gyre has a closed clockwise circulation covering the area between the Angolan coast and  $5^{\circ}$  W, and  $5^{\circ}$  S and  $15^{\circ}$  S, respectively. On the northern side the gyre is closed by the eastward flowing South Equatorial Undercurrent (SEUC), REID (1964), MOLINARI et al. (1981), MOLINARI (1982) and the South Equatorial Counter Current (SECC). According to WACOGNE and PITON (1992) both currents are driven by different dynamics. The SEUC appears to be tied to the equatorial thermostat, whereas the SECC is determined by the Sverdrup balance with local minimum of negative wind stress curl. At the coast the Angola Current (AC) forms the eastern part of the gyre. The AC consists of a pole-ward directed surface current with a vertical extent of about 50 m and a pole-ward undercurrent. The Angola Current is considered to be the continuation of the SECC which bends southward at the Angolan coast. Another source is the Gaboon-Congo Undercurrent, a pole-ward undercurrent at the shelf break at  $1^{\circ}$  S to  $6^{\circ}$  S, reported by WACOGNE and PITON (1992), which is conjectured to be fed from the southward turning South Equatorial Under Current (SEUC) and the Equatorial-Under-Current (EUC) as well.

The surface part of the Angola Current disappears at about  $15^{\circ}$  S and is separated from the Benguela upwelling area by a pronounced frontal system, MEEUWIS and LUTJEHARMS (1990). However, the undercurrent is believed to extend southward and advects tropical water into the Benguela ecosystem. In light of the presently available data, the seaward Ekman transport component removes mass from the Angola Current and plays a major role in its mass balance, LASS et al. (2000). It remains to be investigated, whether along

the front a westward recirculation into the South Equatorial Current (SEC) occurs, and whether filaments penetrate through the front pole-ward; symmetrically to the situation as along the Cape-Verde-Frontal-Zone, FIEKAS et al. (1992), JOHN and ZELCK (1997).

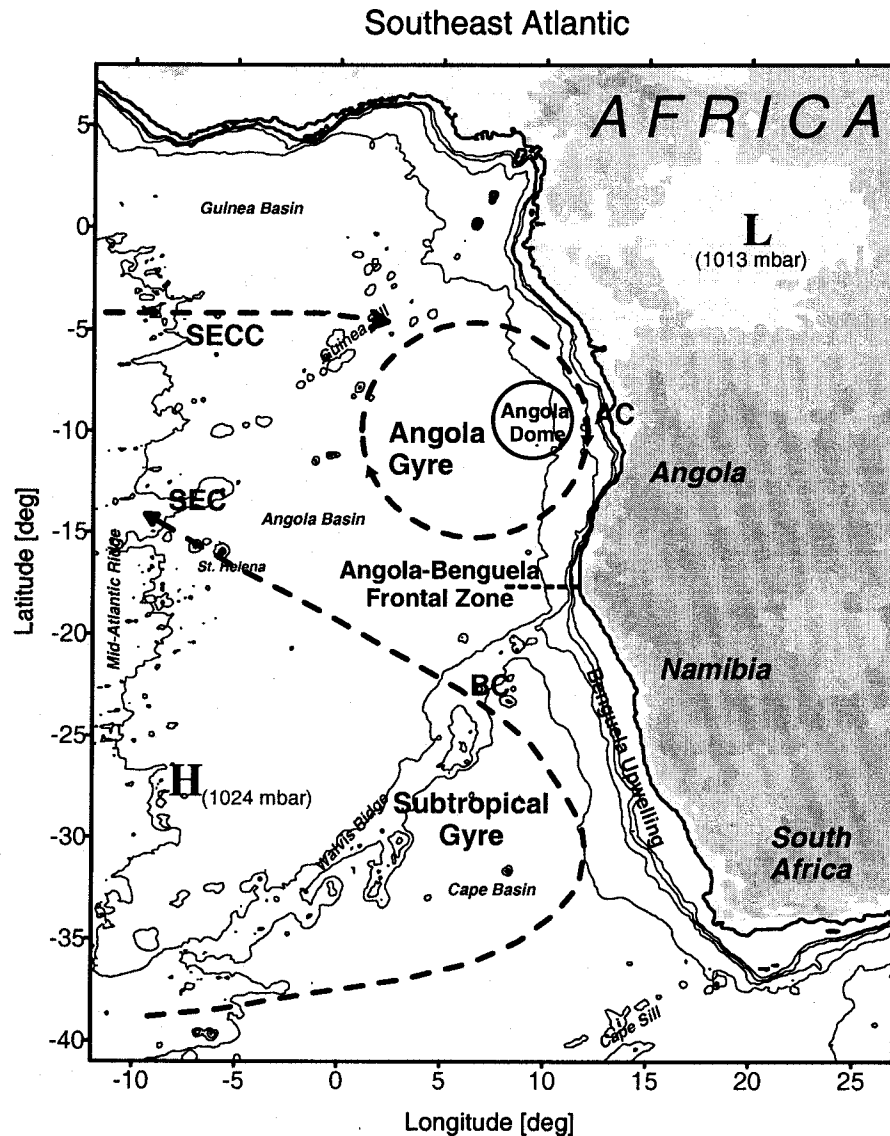


Figure 1.1: Principle circulation in the Southeast Atlantic

The Angola Dome is a rise of the thermocline within the Angola Gyre near 10° S and 8° E to 10° E which has been analyzed by MAZEIKA (1967) on basis of oceanographic data. It is undetectable in the sea surface temperature but can be clearly seen in the field data from 20 m to 150 m depth. It corresponds also to lower salinity (0.3 to 0.5) and lower oxygen (2 to 3 ml l<sup>-1</sup>). However, although appearing in the thermocline only seasonally from January to May, there is a permanent subthermoclinic doming of isotherms, VOITUREZ (1981), VOITUREZ and HERBLAND (1982).

The position of the Angola Dome determined from quasisynoptic field measurements varies considerably. So VOITUREZ and HERBLAND (1982) determined the Dome at about  $10^{\circ}$  S and  $10^{\circ}$  E but FILIPE (1998) reported a Dome structure at  $12^{\circ}$  S and  $12^{\circ}$  E. Several dome-like structures were detected during the cruise of the R/V Poseidon in April 1999. The most prominent one identified as Angola Dome was found at  $8^{\circ}$  S and  $8.5^{\circ}$  E (MOHRHOLZ et al., 2001).

The dynamics of the Angola Dome is still under discussion and leaves open many questions. The seasonal thermocline uplift suggests that it is linked with the seasonal cycle of the SECC. In turn SECC's variability is believed to be triggered by the seasonal cycle of the local wind stress curl, WACOGNE and PITON (1992). The minimum wind stress curl is two degrees south of the position of the Angola Dome and suggests upwelling in the open ocean due to horizontal Ekman transport divergence. However, in the light of numerical model simulation results the situation appears much more complex. Seasonally, warm saline water mass from the equatorial current system penetrate with a downwelling signal as baroclinic Kelvin waves southward and produce the eastern limb of the Dome. An interplay of horizontal and vertical convergence of the flux near the thermocline with the surface heat flux generates a seasonal cycle of the heat balance of the Angola Dome area, YAMAGATA and IIZUKA (1995).

The circulation of the upper layers of the South East Atlantic are governed in the open ocean by the Benguela Current as the eastern boundary current of the subtropical gyre in the South Atlantic. Details of this circulation are described in the review by STRAMMA and ENGLAND (1999). The Benguela Current emerges at the southern tip of Africa fed by parts of the South Atlantic Current, the Agulhas Current and the shelf circulation, GARZOLI and GORDON (1996). The formation of the water mass in the source region of the Benguela Current is a complicated process of mixing the central water masses of the South Atlantic and the Indian Ocean GORDON et al. (1992). Contributions of South Atlantic Water make the resulting water mass fresher and the partition of the Indian Ocean Water makes it saltier. Hence, the TS-characteristics of the resulting water mass depends on the details of the shedding of Agulhas eddies into the South Atlantic, GORDON et al. (1987). The Benguela Current transports according to the World Ocean Atlas 1998, CONKRIGHT et al. (1998), well oxygenated but poor in nutrients water, towards northwest and continues as South Equatorial current along the southern and western rim of the Angola Gyre. The eastern periphery of the Benguela Current is formed by an independent dynamical regime, characterised by the upwelling of cold water along the coast of South West Africa between the Angola-Benguela Front Zone and the southern tip of Africa. The first detailed description of this upwelling regime was given by HART and CURRIE (1960), the latest review on the large amount of research on this subject by SHANNON and NELSON (1996). The prevailing wind drives Ekman offshore transport with upwelling of cold, nutrient-rich water at the shelf associated with equatorward surface jets. The cross-shore circulation is closed by an onshore transport in the deep layer, BARANGE and PILLAR (1992). This circulation cell provides the link between the water masses of the Benguela Current, as eastern boundary current, and the upwelling regime on the shelf. A poleward undercurrent flows as continu-

ation of the Angola Current in the lower oxygen depleted layer. The nutrient flux into the surface layer sustains a high productivity of organic matter. The sinking organic material is decomposed rapidly, consuming oxygen and releasing nutrients in the lower layer.

In the Angola Gyre the water masses are sandwiched between the South Atlantic gyre and the equatorial current system. This forms a shadow zone with a residence time of 4 to 10 years, GORDON and BOSLEY (1991). In his analysis of the age of South Atlantic Central water, Tomczak has detected the oldest water mass in the area of the cyclonic gyre, TOMCZAK (1999). Consequently there is a significant minimum in the oxygen concentration ( $< 1 \text{ ml l}^{-1}$ ) and an accumulation of nutrients compared with the neighbouring water masses. This oxygen depleted and nutrient-rich water seems to propagate poleward into the Benguela current system and may have an important contribution to the oxygen and nutrient budget of the Benguela upwelling area.

## 2 Cruise Information

Cruise Number: M48/3 / IOW 130002

Chief Scientist: Hans Ulrich Lass  
Institute for Baltic Sea Research Warnemünde (IOW)  
Seestr.15, D 18119 Rostock - Warnemünde, Germany  
Tel: ++49 (0)381 5197 130, Fax: ++49 (0)381 5197 440  
Email: lass@io-warnemuende.de

Ship: R/V Meteor, length: 97.50 m width: 16.5 m , draft: 5.61 m,  
displacement: 4280 tons, Callsign DBBH

Port of calls: Namibe / Angola 28 to 29 August 2000

Cruise Dates: 26 August from Walvis Bay to 16 September 2000 Walvis Bay

### 2.1 Scientific programme

The objectives of the investigations during cruise M48/3 are to study the integration of the Angola and Benguela current into the circulation system of the South East Atlantic. Emphasis was given on the coupling of the different branches of the current system by the Angola gyre and the response to the wind field.

The aims of the oceanographic field measurements are:

- to understand the location and the structure of the south-eastern Angola gyre and their variability in response to the large scale wind field as well as to study the role of the Angola gyre in coupling of the equatorial currents and the Angola current.
- to estimate the location of the Angola-Benguela front in relation to the mass transport of the Angola current and the intensity of the meridional wind component along the shelf of South West Africa.
- to estimate the exchange of mass and dissolved and particulate matter between the area of the Angola and the Benguela current.
- to study the structure of the current off the shelf at the core depth of the Antarctic Intermediate Water (AAIW ) and to understand the integration of this current into the basin wide circulation.
- to confirm the elevated cadmium concentrations, which have been revealed in 1989 in the same area, and to find a possible source.

## 2.2 Strategy of measurements

Station work started with a CTD cast employing a SBE 911+ CTD and a HydroBios rosette mounted within a plastic covered stainless steel frame. Subsidiary instrumentation consisted in two oxygen sensors, a 2 channel fluorometer, an altimeter with a 200 m range for bottom finding, and a LADCP consisting of a coupled upward and downward looking 300 kHz Workhorse ADCP. The wire was a 11 mm single conductor steel cable of the W2 winch. After 5 minutes adjustment of the CTD in a depth of 10 m it was lowered with  $0.5 \text{ ms}^{-1}$  in the upper 150 m and  $1 \text{ ms}^{-1}$  below this depth. The cast went down from the surface to 1200 dbar or near the bottom. Bottles were closed automatically on the downward cast, except for the surface bottle, which was closed by hand at the end of the cast. During the CTD cast the ship was held on position with the bow into wind direction. After the cast the rosette was placed on deck without shelter and secured. The oxygen sensor was covered by a protective cap. Subsequently, water samples were drawn from the water bottles for oxygen, nutrient, salinity, phytoplankton analysis, and trace metal analysis. The rosette remained on deck between stations. The multiple opening-closing net (multinet) was operated with winch W3 via the aft deck crane on starboard side of the vessel. The multinet, consisting of 5 nets with  $200 \mu\text{m}$  meshsize, was lowered while towing with 1.5 kn in different depth levels between the sea surface and a maximum depth of 500 meter. After towing the nets were rinsed with seawater while hanging over the side. Placed on the main deck the cod-ends were cleaned and the samples were carried to the lab.

Additionally, throughout the cruise temperature and salinity were measured continuously in the surface layer by the thermosalinograph of the research vessel. Simultaneously, phosphate concentration of water in the surface layer was measured continuously by an autoanalyser. The current profile in the upper 500 m of the ocean was measured by the vessel mounted 75 kHz ADCP manufactured by RDI. To support the ADCP measurement heading of the ship was measured by ADU II manufactured by Ashtech Inc. and a fiber optical gyro manufactured by C. Plath GmbH which provided information superior to that of the ship's gyro. Bottom finding was mainly performed by the Hydro-Sweep and Parasound echo sounders manufactured by Atlas GmbH. Meteorological data were continuously measured by the ship's weather station.

Large scale properties of the circulation were detected by the launch of three WOCE type surface drifter. One was released in the coastal branch of the Benguela, one in the branch of the SECC, and one in the Angola current.

A detailed description of measurements, samples, sensor calibration and data analysis will be given subsequently.

### 2.3 List of cruise participants

Name	Group	Responsibility	Affiliation
H. U. Lass	Chief Scient.	Underway measurements	IOW <sup>1</sup>
M. Schmidt	Hydrography	CTD, LADCP	IOW <sup>1</sup>
V. Mohrholz	Hydrography	CTD, LADCP, ADCP	IOW <sup>1</sup>
St. Weinreben	Hydrography	CTD, LADCP, Salinity	IOW <sup>1</sup>
D. Rüß	Hydrography	CTD, LADCP, Drifter	IOW <sup>1</sup>
R. Kay	Zooplankton	Multinet operation, Mech. Engineer	IOW <sup>1</sup>
G. Nausch	Chemistry	Oxygen, Nutrients, Autoanalyser	IOW <sup>1</sup>
B. Wachs	Chemistry	Nutrients, Oxygen	IOW <sup>1</sup>
N. Wasmund	Phytoplankton	Chlorophylla, Phytoplankton analysis	IOW <sup>1</sup>
K. Kunert	Phytoplankton	Primary Production	IOW <sup>1</sup>
L. Postel	Zooplankton	Metabolic rates	IOW <sup>1</sup>
A. Postel	Zooplankton	Sample Treatment	IOW <sup>1</sup>
Chr. Pohl	Trace metals	Trace metal samples	IOW <sup>1</sup>
I. Kauvee	Chemistry	Nutrients, Oxygen	NMIRC <sup>2</sup>
B. Dundee	Chemistry	Nutrients, Oxygen	NMIRC <sup>2</sup>
A. Iita	Hydrography	CTD and LADCP Operation	NMIRC <sup>2</sup>
D. Mouton	Hydrography	CTD and LADCP Operation	NMIRC <sup>2</sup>
A. da Silva	Zooplankton	Multinet sampling, Data Analysis	IIP <sup>3</sup>
E. Vasco	Chemistry	Nutrients, Oxygen	IIP <sup>3</sup>
A. Chicunga	Zooplankton	Sample Treatment	IIP <sup>3</sup>
G. Kahl	DWD	Weather analysis and prediction	DWD <sup>4</sup>
W. Ochsenhirt	DWD	Weather observation	DWD <sup>4</sup>
T. Truscheit	DWD	Weather observations	DWD <sup>4</sup>

Crew of R/V 'Meteor' (33), Master N. Jakobi

Service and support of the crew is greatly acknowledged here.

- <sup>1</sup> IOW            Baltic Sea Research Institute Warnemünde  
Seestraße 15, D18119 Rostock-Warnemünde, Germany
- <sup>2</sup> NatMIRC       National Marine Information and Research Center  
PO Box 912, Swakopmund, Namibia
- <sup>3</sup> IIP             Fisheries Research Institute  
PO Box 2601, Luanda, Angola
- <sup>4</sup> DWD            Deutscher Wetterdienst

## 2.4 The extent of measurements

The investigations covered the area of the Angola Dome, the Angola-Benguela Front and the northern Benguela off southern Angola and northern Namibia from 9° S to 21° S. Six off shore sections and one longshore section at 8° E have been worked. The typical distance between the stations is 10 n.m. near the coast and up to 60 n.m. in the open ocean. The meridional distance between the sections is roughly 2° (see Figures 2.2 and 2.1). CTD casts have been carried out to the bottom in shallow water or to 1300 m in the open ocean.

### *Hydrographic stations*

A total number of 73 stations were worked using a CTD SBE 911+ with two IOW oxygen sensors, 2 channel Haardt fluorometer, Datasonics PSA-900 altimeter together with a HydroBios 12 bottle Kranzwasserschöpfer rosette equipped with 5 litre free flow water sample bottles of HydroBios. At the CTD frame a LADCP system was mounted, consisting of coupled upward and downward looking Workhorse ADCP in a 3000dbar pressure case. The station list is given in the Appendix (Table A.1).

### *Water Sampling*

843 water samples taken on all CTD stations were analysed for oxygen, phosphate, nitrate, nitrite, ammonia, and silicate. The sampling depths in meter were surface, 20, 40, 50, 60, 80, 100, 200, 400, 600, 800, 1000, 1200 or bottom. Moreover, on 53 stations, shown in Figure 2.3, 91 water samples have been taken for phytoplankton analysis and in 314 samples the potential and in 216 samples simulated in situ primary productivity has been estimated, respectively. Chlorophyll-a has been estimated on 54 stations in 799 samples. At selected stations and depths salinity of water samples was measured by Autosal for intercomparison with the CTD. 132 water samples have been taken from the mixed layer and different depths below for the determination of the Hg, Cd, Cu, and Ni.

### *Phyto- and Zooplankton sampling*

Phytoplankton samples were taken at 53 selected stations, listed in the Appendix (Table A.2) and Figure 2.3, 25 of them sampled also with a plankton net in the surface mixed layer. During day time on most of these stations depth profiles of light intensity and primary production were measured. Zooplankton hauls were carried out mainly with the HYDROBIOS-Multi Net on 17 stations shown in Figure 2.4. The station list of the Multi net hauls is given in the Appendix (Table A.3).

### *Underway measurements*

A total of 20 days meteorological, thermosalinograph, phosphate and vessel mounted ADCP measurements along the track of the ship have been collected on the cruise.

### *Drifter*

Three ARGOS surface drifter of WOCE-type have been deployed. One at the shelf break in the Benguela current area, one at the shelf break in the Angola current area and one offshore in the assumed area of the South Equatorial Countercurrent.



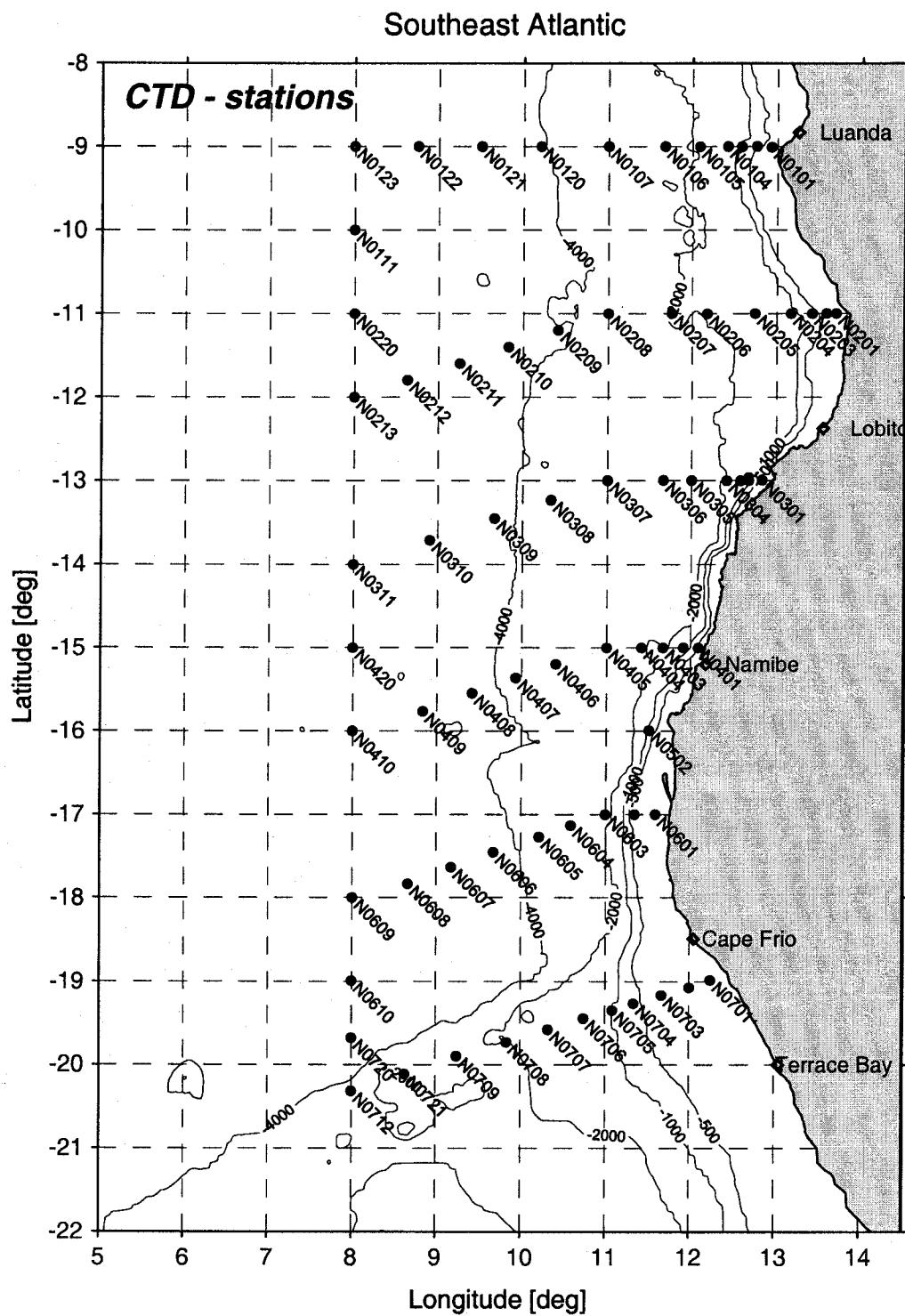


Figure 2.2: Map of hydrographical stations of the cruise M48/3 (26. August - 16. September 2000). Stations are labeled with station names.

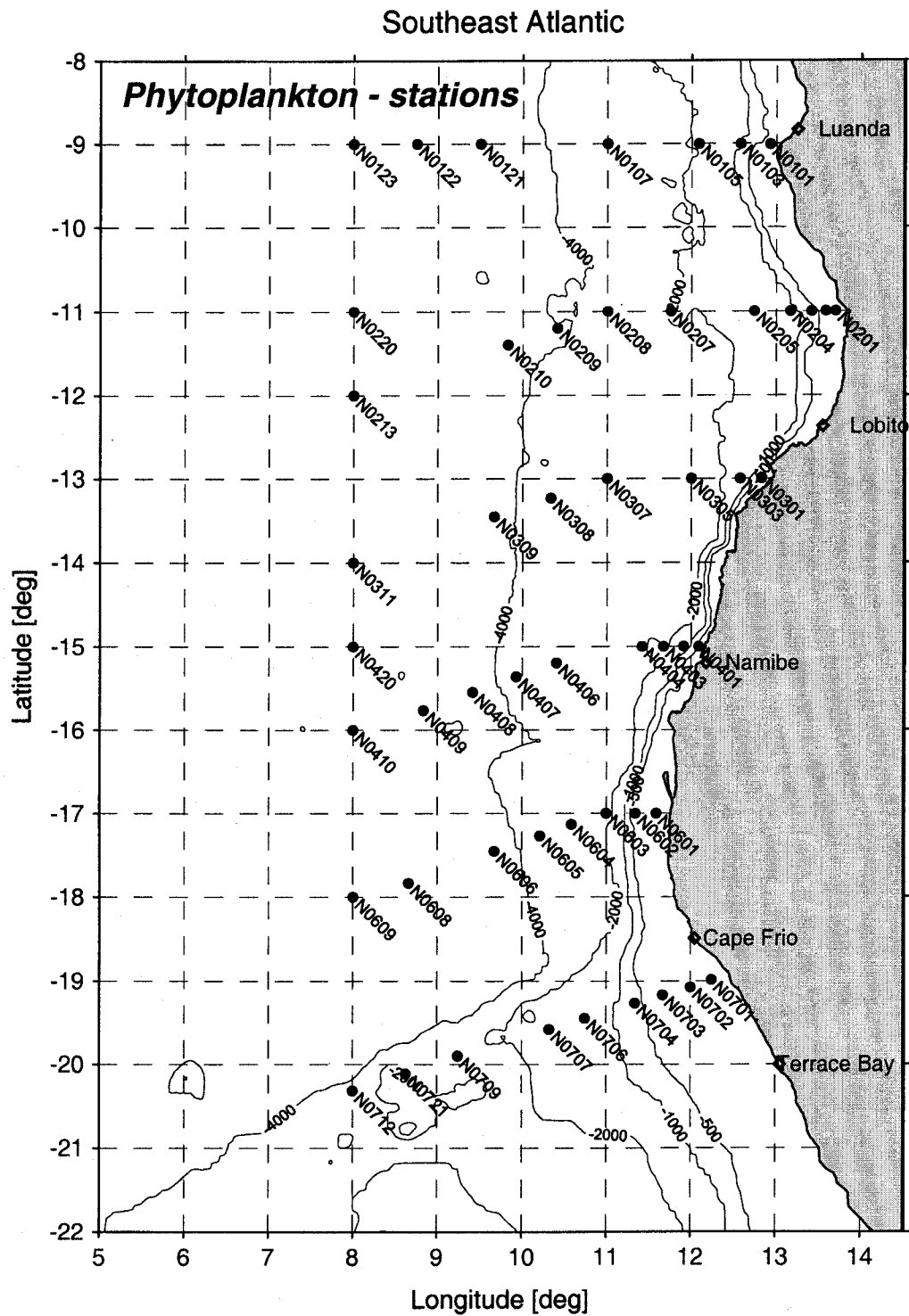


Figure 2.3: Map of phytoplankton stations of the cruise M48/3  
(26. August - 16. September 2000)

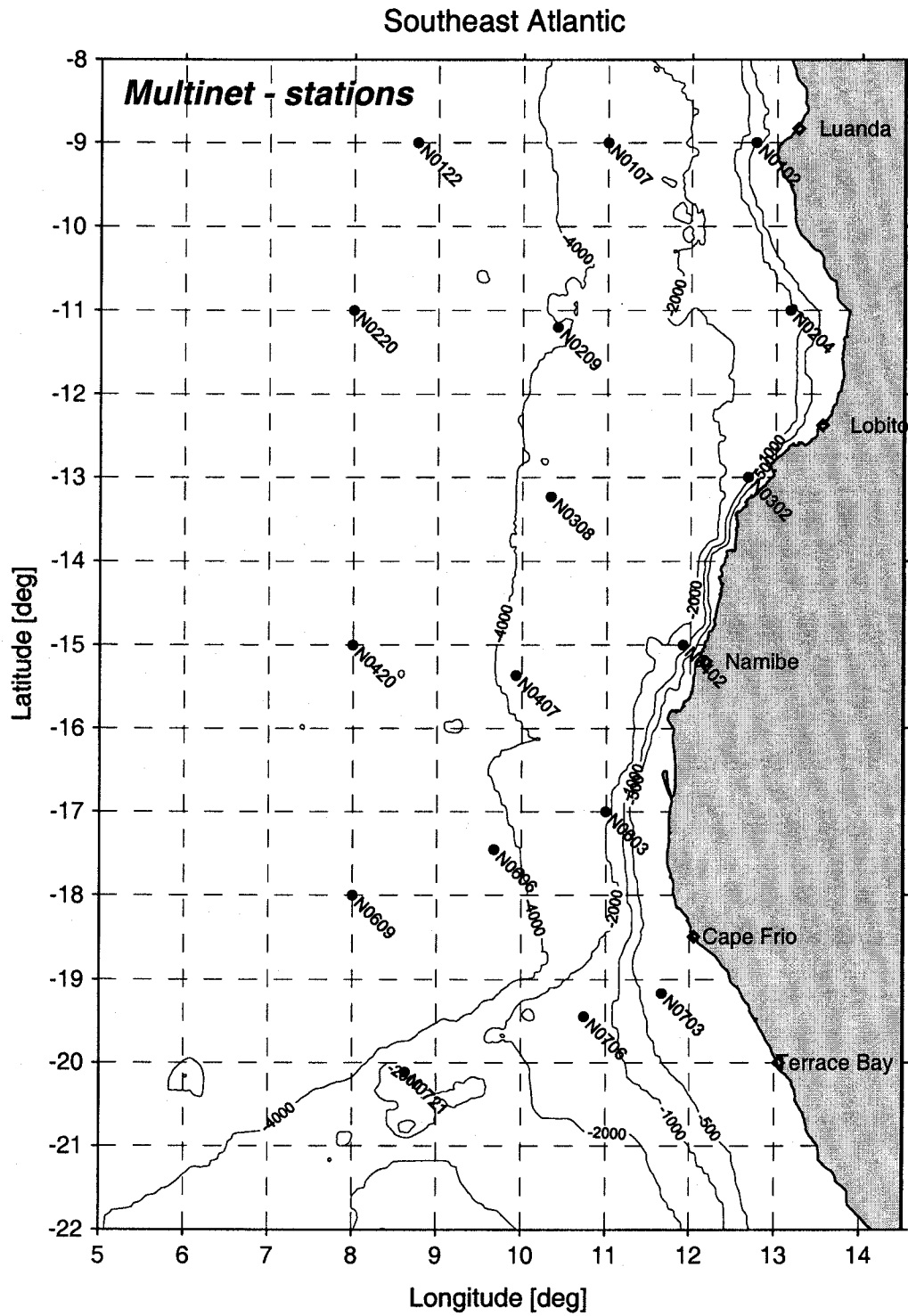


Figure 2.4: Map of Multinet stations of the cruise M48/3  
(26. August - 16. September 2000)

## 2.5 Survey Chronology

Activity	Date
Boarding in Walvis Bay	24th Aug 2000
Unloading container, installing and testing equipment	
Calibration of LADCP	25th Aug 2000
Embarking equipment for oceanographic station in Namibe	
Departure Walvis Bay	26th Aug 2000
Start longshore ADCP section 09	
Sailing to Namibe, test station, release first ARGOS surface drifter in Benguela current	
Arriving Namibe, disembarking equipment, reception on board of R/V Meteor	28th Aug 2000
Departure of Namibe, sailing along the shelf towards northern section, releasing second ARGOS drifter in the Angola current	29th Aug 2000
End longshore ADCP section 09	31st Aug 2000
Starting station work on northern section 01	
Releasing third ARGOS drifter, end of station work on northern section 01	1st Sep 2000
Start station work on section 02	2nd Sep 2000
End station work on section 02	4th Sep 2000
Begin station work on section 03	5th Sep 2000
End station work on section 03	7th Sep 2000
Begin station work on section 04	8th Sep 2000
End station work on section 04	9th Sep 2000
Begin station work on section 05	10th Sep 2000
End station work on section 05	11th Sep 2000
Begin station work on section 06	12th Sep 2000
End station work on section 06	14th Sep 2000
Station work on Section 07 cancelled due to stormy weather	15th Sep 2000
Arrival in Walvis Bay	16th Sep 2000

### Major problems encountered on the cruise

Strong winds up to 8 Bft. on 14 to 15 September 2000 prevent the work on the stations of the southernmost section.

## 2.6 List of principle Investigators

The principle investigators responsible for the major parameters measured on the cruise are listed below.

Parameter/Instrument	Sampling Group	Principal Investigator
CTDO / Rosette	IOW	M. Schmidt
LADCP	IOW	V. Mohrholz
ADCP	IOW	H. U. Lass
Salinity / Temperature	IOW	M. Schmidt
Oxygen / Nutrients <i>O<sub>2</sub>, NH<sub>4</sub>, NO<sub>3</sub>, NO<sub>2</sub>, PO<sub>4</sub>, SiO<sub>4</sub></i>	IOW	G. Nausch
Chlorophyll-a, Phytoplankton, Primary Productivity	IOW	N. Wasmund
Zooplankton, Species composition, Abundance, Metabolic Activity	IOW	L. Postel
Trace metals <i>Hg, Cd, Cu, Ni</i>	IOW	Ch. Pohl

## 3 Measurements and methods

### 3.1 Underway measurements

Navigation as well as information about winches together with surface meteorological and throughflow measurements was provided by a variety of sensors throughout the cruise. These data were fed into the Atlas-Navigations-und-Planungsanlage ANP 2000. The common time base of all data is generated in the ANP 2000 system from GPS time. In case of a GPS failure an internal time substitutes the GPS time. The data of the sensors are checked, formatted and distributed to the corresponding servers of the system. Flags are added to the sensor data according to the results of the checks. All horizontal position data are transformed into the WGS 84. The main server of the ANP 2000 provides a data string with a sampling rate of 1 s and distributes it over the navigation net towards the bridge and the laboratories. The main server of the ship routes the navigation net into the science net and stores the data in a data base.

#### 3.1.1 Navigation

Navigation, i.e., ship position and velocity over ground, ship heading, ship speed and bottom detecting was provided by several similar sensors and the ANP 2000 selected the most reliable value by comparing the different results.

#### GPS

Ship position was provided by a Trimble 4000 DS continuous satellite tracking GPS receiver with differential GPS capability. If DGPS is selected the 4000 DS will be provided with the signals of a SkyFix-decoder and a Multifix-PC. Since the Selective Availability of the GPS system is switched off since May 2000 DGPS was not used throughout the cruise. The mean number of satellites used for fixes was about 8 with a standard deviation of 1.3. Occasionally no satellites for GPS fixes were available. Then both latitude and longitude were set to zero. The standard deviation of fixes in the harbour Walvis Bay on 26 August 2000 was 2.5 m and in Namibe on 29 to 30 August was 2.2 m and 3.1 m for latitude and longitude, respectively.

#### ADU

Ship position, heading as well as pitch and roll was provided throughout the cruise also by an Ashtech ADU with a four GPS antenna array located near the top of the main mast. The antenna separation is 1.4 m. According to the manual the achievable accuracy of the heading is  $0.2^\circ$  without multipath effects. Typical multipath effects can reduce the accuracy to  $0.4^\circ$ . The accuracy of the ADU position measurement compares with conventional GPS.

## Gyrocompasses

Heading of the ship was measured by two Gyrocompasses Plath Navigat II and Navigat X. The Gyro error due to latitude and ship velocity is corrected by special processor. Heading, pitch and roll was also provided by a new fibre optical gyro platform Plath Navigat 2100. This system provides a very accurate heading measurement with an error independent of the velocity of the platform which is comparable with the error of the heading measurement of the ADU.

The heading measurements of the Gyro, the fibre optical gyro and the ADU were compared during 9 hours where the ship was moored in the harbour of Walvis Bay. Since the ship velocity is zero the heading of the gyro output should be unbiased. Mean values and standard deviations of the heading measurements are shown in Table 3.1.

Table 3.1: Mean values and standard deviation of heading measurements in Walvis Bay on 26.08.2000

Device	Mean	Standard Deviation
Gyro	45.9959°	0.1018°
Fibre Optical Gyro	45.9536°	0.0857°
ADU	47.3830°	0.1737°

The ADU has a misalignment of about 1.4° since the antenna array was reinstalled in Walvis Bay after a repair of the unit. The calibration was performed from the swimming ship. The variations of the heading measurements of both the classical and the fibre optical gyro agree quite well but the variation of the ADU is twice as large as the standard deviation of the fibre optical gyro. The heading measurements at sea have been analysed with spectral methods. The coherence between the gyro and the FOG is significant with values in excess of 0.9 throughout the whole spectrum until 3 cpm. The coherence between the gyro and the ADU is significant but reduced by noise between 0.5 to 2 cpm and is not significant above 2.5 cpm. The power spectrum of the difference between FOG and Gyro depicts a white noise level of  $3 \cdot 10^{-3}$  (Degree<sup>2</sup> cpm<sup>-1</sup>) for frequencies above  $3 \cdot 10^{-3}$  cpm, corresponding to a standard deviation of about 0.1°, whereas the power spectrum of the difference between ADU and gyro has a white noise level of  $1 \cdot 10^{-1}$  (Degree<sup>2</sup> cpm<sup>-1</sup>) for frequencies above  $1 \cdot 10^{-1}$  cpm, corresponding to a standard deviation of about 0.5°. Taking into account the observation that the failure of the fibre optical gyro is less frequent than that of the ADU the fibre optical gyro seems to be more suitable for the heading measurement to be used in accordance with the VMADCP measurements.

## Ship speed

Ship speed through the water was measured by an one component electromagnetic log Plath Naviknot II located at the keel of the ship. This log turned out to measure slightly enhanced speed. The reason for this error could not be detected. Ship speed was also measured by two component Acoustic Doppler Log of Atlas Elektronik GmbH DOLOG 23. The transmitter is working at 79 kHz and has a nominal range of 600 m. No interference

with the 75 kHz VMADCP was detected during this and earlier cruises. The instrument measures both in the bottom track mode if the depth is smaller than the nominal range and deeper than 40 m and in mode referenced to the water layer within this range. The DOLOG 23 compares well with the speed estimated from the GPS in regions with weak currents.

### Echo sounding

Depth was measured during the cruise by a variety of bottom finding devices which are implemented on the ship according to the different requirements of the users. On this cruise no particular emphasis was given on echo sounding. Hence, the depth measurement was used which was selected by the DVS system operator. Throughout this cruise this was either the Atlas Elektronik GmbH Hydrosweep, a combined sideward and forward-backward looking acoustic 15.5 kHz transmitter array, or the Atlas Elektronik GmbH Parasound 18 kHz narrow beam deep sea echo sounder. The echo sounders were corrected with respect to pitch, roll and heave of the ship. The performance of the hydrosweep was spoiled by air bubbles passing the transmitters below the ship which were generated by pitching of the ship even in moderate swell conditions.

### 3.1.2 Meteorology

Standard meteorological parameters were measured by the ship weather station implemented and serviced by the German Weather Service (DWD). The signals of the individual sensors will be transmitted either in an A/D transformer, a data logger of type COMBILOG or directly into the server METCO II of the Bordwetterwarte. The sensor signals are resolved by 12 bit with an error of  $\pm 1.5$  LSB. The physical values of the basic parameters are calculated by applying the calibration coefficients. These comprise the parameters measured at positions given in Table 3.2.

Table 3.2: Table of basic meteorological sensors

Sensor	Type	Height above sea surface
Apparent wind speed	Cup anemometer	40.1 m on port and starb.
Apparent wind direction	Wind vane	40.1 m on port and starb.
Air temperature	Ventilated Pt 100	28.3 m on port and starb.
Humidity	Rotronic capacitive sensor	28.3 m on port and starb.
Visibility	AEG visibility sensor	33 m on starb.
Sea surface temperature	Pt 100 in ships hull	-2.1 m on port and starb.
Air pressure	AIR barometer DB-1A	10.6 m
Precipitation	Sensor according Prof. Hasse	33 m
Global radiation	Pyranometer CM21, by Kipp and Zonen	40.1 m on starboard
Atmospheric long wave radiation	Pyrradiometer according to Schulze/Däke, by Lange	40.1 m on portside

The following meteorological parameters are calculated by the server from the basic parameters:

- True wind velocity for port and starboard sensors by vectorial addition of the apparent wind velocity (gyro heading + apparent wind direction) and the ship velocity over bottom. The true wind direction is the direction where the wind comes from.
- Dew point temperature is calculated from air temperature and humidity according to the psychrometer formula according to Magnus and Sprung for port and starboard side.
- Long wave heat radiation of the atmosphere is calculated from the output of the pyrriometer and its body temperature together with the global radiation according to the so called pyrriometer equation.

The sampling rate of the basic sensors 1 second and 0.5 second of the wind sensors, respectively. Derived parameters have the same sampling rate. The meteorological server calculates arithmetic mean values over ten second from every parameter from which mean values over 1 and 10 minutes are calculated and stored. Identified wrong values are filled with '999'. The meteorological server is linked to the DVS server via the ANP and provided the meteorological parameters as mean values over 10 s. These values are imbedded into the data string of the DVS. The sensors of the Bordwetterwarte are exchanged by serviced and recently calibrated sensors by the DWD in case of failure of a sensor or more generally during a stay of the ship in the harbour for repair. During the cruise all sensors of the Bordwetterwarte performed well.

### 3.1.3 Thermosalinograph Measurements

Continuous underway measurements of surface temperature and salinity were made throughout the cruise. Seawater was pumped from a sea chest located at the bow in 4 m depth on starboard side into the Lab 18 at the Zwischendeck located in the bow section. The seawater flow was conducted through the cell of a Seacat SBE 21 instrument serial Nr. 2114061-2156 with an external temperature sensor located directly in the sea water inlet. Water temperature and conductivity is measured in the measuring cell of the Seacat together with the water flow through the cell located in Lab 18. The sampling rate is 6 seconds. The instrument is interfaced to the ANP 2000 and the DVS via an interface box located in the CTD-Lab 9. Data are stored at 1 s sampling interval by the DVS and by 1 min sampling rate the by 'Reise' software (WLOST, 1999) in \*.ddm files. Unfortunately, the cell temperature was linked to the 'Reise' software as SST measured by the thermosalinograph. Hence, this temperature is usually several 0.1 K to great compared with the SST.

The Seacat was calibrated by the manufacturer in May 1996. Six water samples have been taken 14 times during the cruise for calibration purpose from the through flow box. The salinity of the samples have been estimated by an Autosal salinometer. The mean difference between the salinity of the samples and the thermosalinograph was 0.01 with a standard

deviation of 0.03. The residuals of the calibration procedure were about 0.001 K for both the external and internal temperature sensors and  $0.00001 \text{ S m}^{-1}$  for conductivity. Hence, no correction of the thermosalinograph can be recommended with respect to salinity. The corresponding uncertainty of the salinity measurements is 0.03. The calibration of the thermosalinograph with respect to temperature was made at shore. The seawater flow through the thermosalinograph was maintained at sea only and was stopped by closing the valves when entering a harbour.

### 3.1.4 Continuous determination of phosphate in the surface water

The phosphate content of the surface water has been measured quasi continuously during the cruise by pumping of surface sea water (4 m depth) through an autoanalyzer. The sample was taken from a plastic container of around 4 l. The exchange rate of the seawater was  $2 \text{ l min}^{-1}$ . The system worked reliable throughout the cruise.

#### Method

The determination of the phosphate content is based on the classical colorimetric reaction of phosphate ions with an acidified molybdate reagent to yield a phosphormolybdate complex which is then reduced to a blue coloured compound (GRASSHOFF et al. 1983). This method is transferred to an automatic process using an Automatic Analyser APP 4002 (ME Meerestechnik-Elektronik GmbH, Trappenkamp, FRG). In the first step the stagnant volume of the filter and the hoses is changed in order to take a representative sample. The cuvette is flushed by the sample, a special amount of the sample is taken and the extinction is measured. After adding the reagents and passing the reaction time at  $25^\circ\text{C}$ , the extinction of the formed blue dye is measured. The two values will be subtracted in order to eliminate the colour and turbidity of the sample and calculated with the calibration coefficients. The measurement is completed after 9 min. Using the continuous mode, the next measurement follows directly.

#### Accuracy

The accuracy given by the company is  $\pm 2\%$  in the lower calibration range (4 mM). Intercalibrations were performed 9 times during the cruise by taking water samples of the trough flow system and determination of its phosphate content by the standard manual method. The mean difference between manually determined phosphate and autoanalyzer measurements (correction) is  $-0.03 \mu\text{mol l}^{-1}$  with a standard deviation of  $0.03 \mu\text{mol l}^{-1}$ . The mean error of the correction is then  $0.02 \mu\text{mol l}^{-1}$  ( $n = 16$ ).

#### Archiving

The data have been recorded on a separate Laptop PC with a software of the supplier. Every record contains date, time and phosphate content in  $\mu\text{mol l}^{-1}$ .

## 3.2 Vessel mounted Acoustic Doppler Current Profiler

### Equipment

A 75 kHz vessel mounted narrow band Acoustic Doppler Current Profiler (VMADCP) (Manufacturer RDInstruments) was mounted in 5 m depth in a sea chest located just on the starboard side of the centre line of the ships hull about 55 m from the bow of the ship which is about 90 m long. The signal of the Gyrocompass was included in the VMADCP record and in the permanent datalog as well.

An ASHTECH Attitude Determination Unit ADU 2 was available on the cruise. The antenna array was installed on ships RADAR mast. The ADU 2 provides additional information on ships heading without the typical gyrocompass deviations. Additionally, heading information was provided by a fibre optical gyro. All the instrumentation providing heading of the ship which is relevant for the accuracy of the ADCP measurements is described more detailed in Section 3.1.1.

### Mode of Operation

The VMADCP was used during the cruise with the configuration given in Table 3.3. The vessel mounted ADCP was used during the whole cruise in the water tracked mode. Data were averaged over a period of 5 minutes online. An increased averaging period did not improve the statistical significance of the mean value.

Table 3.3: Configuration of the vessel mounted ADCP

Parameter	Value
Average interval	300 s
Bin number	60
Transducer depth	5 m
Bin length	16 m
Pulse length	16 m
Blank after transmit	8 m
Ping interval	as soon as possible
Ping per ensemble	1
En threshold	2500 mm s <sup>-1</sup>
Heading offset	180 deg
Pitch offset	0 deg
Roll offset	0 deg
Frequency transmit	75 kHz
Band width	narrow band
Bottom tracking	auto
Top reference bin	12
Bottom reference bin	18
Heading bias	0 deg

## Calibration

The calibration of the ADCP in bottom track and water track mode was performed after the cruise. In areas with a water depth up to 800 m bottom track data are available for calibration purposes.

## Performance

A first check of the VMADCP data supplied reasonable results. Sometimes at the begin of cruise the ADU 2 was out of work for about some (30) minutes. The problems were fixed imediatly by the instrumentation group of the ship.

## Data Processing

During the cruise preliminary checks were performed with CODAS3 software (FIRING et al., 1995) - the final processing was carried out after the cruise.

## Data storage

The data output of the ADCP was merged on-line with the corresponding navigation data (Gyro Compass, ADU 2, GPS data) and stored on the hard disc of a PC using the storage system DAS.

## 3.3 CTD measurements

### Winch arrangements

During the cruise a 11 mm one wire coaxial cable on winches W2 and W3 and a hydraulic frame were used in combination with the crane on the aft deck of the ship for:

- deployment of the vertical profiling CTD with rosette sampler (11 mm cable winch and hydraulic frame)
- deployment of the towed Multinet

The performance of the used facilities was well throughout the cruise.

### CTD Description

The CTD-system "SBE 911plus" (SEABIRD-ELECTRONICS, USA) was used to measure the parameters:

- pressure, temperature, conductivity
- bottom distance
- fluorescence chlorophyll, backscattering turbidity by a Dr. Haardt BackScat II-Fluorometer.

- oxygen with two IOW-oxygen sensors. Only one sensor was included in the SBE-pumping-system.

The IOW-Oxygen sensor uses a fast response Clarck sensor (12 mm-Teflon membrane;  $t_{90\%} = 7$  s) with a platinum electrode and a thermodynamically matched Pt-1000- temperature sensor. The sensor is equipped with two outputs for the oxygen-current and the temperature. The computation of the dissolved oxygen in  $\text{ml l}^{-1}$  is made by the Seasave-software including the temperature correction for the changes of the permeability of the membrane. An altimeter was used for bottom finding.

Additionally the CTD-probe was equipped, with a HYDROBIOS-Rosette water sampler with 12 free flow bottles of 5 l volume. Almost all metal-parts of the CTD were covered with a thin plastic-layer to avoid disturbance of the metallic tracer measurements.

The CTD case was mounted vertically at the center of a modified SBE guard cage. Both the inlet and outlet of the TC-duct were located a few centimeter above the bottom of the cage. This guard cage carries the main SBE 9 body, all SBE- and additional sensors and the altimeter. The sea-cable is directly plugged into the main body and other cables connect the main body to sensors and trigger mechanism of the HYDROBIOS- Rosette.

Two Free-Flow Water-bottles were replaced by two cages for a LADCP and a battery pack. Outside the racks 2 water-bottles were attached.

A special attachment of the CTD-probe to the sea-cable was implemented to minimize the tilt during deployment. The package was weighted by a lead weight in order to avoid looping during lowering.

### CTD-Configuration

For each station a configuration file (*stationnumber.con*) is written which contains the complete parameter set, especially sensor coefficients used for the conversion of raw data (frequencies and voltages) to standard output format.

### Mode of Operation

The CTD is located midship on the open main deck on starboard side of R/V Meteor. The probe is lowered 2 m off the vessel on an 11 mm steel armored cable linked with the CTD. The ship was positioned on station with the bow into the direction of the wind, so the maximum angle of the cable was less than  $5^\circ$ .

The CTD was always put for 3 minutes at 10 m depth into the water before the cast started in order to remove air bubbles from the rosette- and the pumping system. The CTD was lowered with  $0.5 \text{ m s}^{-1}$  to 200 m, afterwards the speed was increased to  $1.0 \text{ m s}^{-1}$ . The maximum depth of the deployments was 1250 m. Water bottles were closed during downcast automatically, only the surface-bottle was triggered by hand during upcast.

At the end of each station the CTD was taken back to the deck. The oxygen sensor was

Table 3.4: Configuration of the CTD SBE 911+

Parameter	Value
SBE-911plus Underwater Unit	SN 09P7807-0306
Depth capability (CTD and sensor housings)	6 800 m
Pressure sensor range	0 - 10 000 psia (0 - 6 885 dbar)
Digiquartz pressure sensor (with temperature comp.)	SN 51392
Modulo 12P	SN MOD12P-0448
Temperature sensor (SBE 3-02/F)	SN 1458
Conductivity sensor (SBE 4-02/0)	SN 1144
Oxygen sensor (IOW) included in the duct	SN OX9903
Oxygen sensor (IOW)	SN OX9904
Dr. Haardt BackScat II-Fluorometer (model 1101.1)	SN 2070
Pump (SBE 5T)	SN 05076
HYDRO-BIOS / IOW Rosette water sampler	
Altimeter (Datasonics PSA-900D)	SN 584
Logic Board EPROM	Version 1.0
Modem Interface	Installed
Modem Board Micro-controller	Vers. 2.0 IOW
HYDRO-BIOS Rosette Interface	Installed

Table 3.5: Configuration of the CTD SBE 911+ Software

Software	Version
Seasoft (SBE)	4.243 (2000)
presscor, do_om, depth (IOW)	3.5 (11.05.1997)
Reise für WINDOWS (IOW)	6.44 (2000)

covered by a protection cap filled with sea-water. Power was left on to the CTD and the conductivity cell was left open when the next station was expected to be in less than 12 hours. Otherwise the CTD power was switched off and the TC-duct was filled with triton solution.

### CTD data processing and storage

Every cast is started after an adjustment time of 3 minutes. During this time the CTD was lowered to 10 m depth. Then the cast was started from the sea surface.

The CTD data were passed from the SBE Deck Unit Model 911+ to the CTD client, where data are stored with 24 scans per second. It also permits an on line data visualisation. Over a local net the actual GPS position, UTC date and time, echo sounding depth and station number have been provided and were added automatically to the CTD header data. During one cast three files were generated:

- one file with the extension \*.dat consisting of a header and a data section. The header summarises information on date, time, GPS position, echo sounding, air pressure, thermosalinograph measurements and station number. The data section contains 24 scans per second for each sensor channel,
- one file with the extension .con containing the actual configuration of the CTD, i.e. the relevant information on the mounted sensors and the corresponding sensor coefficients
- one header file with extension .hdr which repeats the header section of the .dat file as an ASCII formatted file.

The file names are formed from the CTD deployment number and the CTD series number. These numbers are generated automatically by the Reise program (see section 9) and are delivered to the Seabird software over the local network.

After the CTD cast the raw data have been processed using Seabird post processing routines (CTD DATA ACQUISITION SOFTWARE, SEASOFT version 4.323, SEA-BIRD ELECTRONICS, INC.):

- conversion of the binary coded raw data (frequencies) to engineering units,
- subtracting the actual air pressure from the pressure measurements,
- removal of the conductivity cell temperature thermal mass effects by a recursive filter,
- minimising salinity spiking errors by aligning temperature and conductivity measurements with respect to time by 0.07 s to each other (is done online by the deck unit).
- removing bad scans and loops if pressure slow-downs and reversals occur, applying the temperature and salinity correction according to Weiß to the oxygen data.
- averaging the bins to 1 dbar steps and to 5 dbar steps.

As a result of the post processing two files are generated:

- a data file with extension '.cnv' which consists of a header and a data section. The header summarises information on the station as date, time, GPS position, station number, echo sounding depth, air pressure, temperature ( Attention, it is the cell temperature on this cruise) and salinity measured by the thermosalinograph, a protocol of the post processing procedures applied to the data and a description of the format of the subsequent data section.
- a file with extension '.bt1' which contains the CTD-data, date and time according to each bottle closed.

Additional by means of the software chbottle.exe the water sample in each closed bottle was assigned to an unique consecutive ID-Number during the cruise.

An immediate printout of the vertical profile of temperature, salinity and oxygen as well as the fluorometer data and a T-S diagram as well as a O<sub>2</sub>-S diagram was used for operational purposes.

All files resulting from a CTD deployment are kept on hard disk and are saved to the archive directory of the server together with the CTD cast diaries. Additionally the data are burned to CD-ROM.

## **Performance**

73 CTD casts were taken. The reliability of the CTD was well during the whole cruise. At the first station sometimes it happened that the return message from the closing unit to the deck unit failed, nevertheless the bottles of the HYDROBIOS-water sampler were closed correctly. After exchanging of the HYDROBIOS-unit the problem was fixed. The oxygen-sensor OX9903 produced pressure-dependent spikes. The problem could not be solved. The other oxygen sensor OX9904 was reliable. The 'Reise' program in the CTD client mode was not able to edit the list of water bottle closing depths. This problem was solved by writing this list with a text editor and copying it from there into the corresponding input window of the 'Reise' program. The system date of the CTD client was temporally wrong and caused corresponding errors of the system upload time in the CTD '\*.dat' and '\*.hdr' files. The wrong entries in the '\*.hdr' files were corrected manually.

## **CTD calibration and standards**

### **CTD temperature calibration**

The temperature sensor was calibrated at 12.05.2000 in the laboratory of the IOW. The International Temperature Scale of 1990, ITS-90, was realised with a platinum resistance thermometer calibrated by the PTB. During the sensor calibration the stability of the platinum thermometer was observed with the water triple point and the gallium melting point. The residuals of the calibration process are below  $4 \cdot 10^{-4}$  K.

The sensor was checked once a day (when hydrographic conditions allowed it) by mercury- and an electronic reversing thermometers. No significant deviation between the SIS reversing thermometer and the temperature sensor of the CTD was observed. The standard deviation of the difference was 0.003 K.

### **CTD salinity calibration**

The conductivity sensor was calibrated at 12.05.2000 in the calibration laboratory of the IOW. An Autosal 8400 salinometer was used as reference instrument. The residual of the conductivity calibration was below  $0.3 \text{ mS m}^{-1}$ .

Water samples have been collected to determine the accuracy of salinity measurements. The mean difference between sample conductivity at temperature measured by the CTD and the conductivity measured by the CTD was  $-0.473 \text{ mS m}^{-1}$  with a standard deviation

of  $0.12 \text{ mS m}^{-1}$ .

### Oxygen sensor calibration

The oxygen sensors were calibrated at 15.06.2000 in the calibration laboratory of the IOW. Because of the lower stability of the Oxygen sensors the sensor slope was estimated continuously by comparison with discrete water samples, determined after WINKLER (1888), see 3.8.2. The free oxygen sensor OX9904 was selected for the CTD oxygen measurements. The calibration of this sensor with the oxygen content of the water samples resulted in a piecewise correction of the slope of the sensor according to Table 3.6.

Table 3.6: Slope correction factor of oxygen sensor OX9904 for different station ranges

Since SBE *.dat file	SBE config file	Slope correction
0387f01.dat	mit 130002_a.CON	1.1274971
0389f01.dat	mit 130002_b.con	0.9798496
0393f01.dat	mit 130002_c.con	0.9973926
0404f01.dat	mit 130002_d.con	0.9931245
0432f01.dat	mit 130002_e.con	1.004777
0450f01.dat	mit 130002_f.con	0.9646722

### Pressure sensor calibration

The pressure sensor has been calibrated by the manufacturer on 27.05.1993 and has the following performance:

resolution	0.01 ppm
repeatability	0.005 % FS
hysteresis	0.005 % FS
pressure conformance	0.005 % FS
acceleration sensitivity	0.008 % FS

The full scale (FS) is 69 MPa. (see the Sea-Bird manual.)

At least once a day before the deployment a registration of the CTD on deck was performed to determine the offset of the pressure-sensor. The mean deviation between air pressure and pressure measured by the CTD was -1.00 dbar with a standard deviation of 0.02 dbar.

### Fluorometer calibration

An inter-comparison measurement for the fluorometer data has not been done. The Dr. Haardt BackScat II-Fluorometer (Dr. Haardt, Germany, Model 1303 MP/Chla/Phy/2R/MO, SN 7091) is calibrated by the manufacturer (valid from 27.04.1998). Backscatter (turbidity) is given in reflectance units (percent). 100 % reflectance is defined by a white reflectance standard (Lambertian) and 1 %, 0.1 % and 0.01 % scales are realised by calibrated optical attenuators.

### 3.4 Salinometer

A salinometer "AUTOSAL Model-8400B" (GUILDLINE INSTRUMENTS LTD., Canada, Serial No. 59593) was used as reference for conductivity measured by the CTD and the thermosalinograph.

The salinometer was installed in an air conditioned lab. Twice a week the measurements were performed. No problems occurred. Characteristic calibration of the salinometer data are shown in Table 3.7.

Table 3.7: Calibration data of the salinometer

Date	Normal water	Bath-temp.	Room-temp.	SBY-value	Zero-value	Stand. Res.
26.08.2001	P136	24	22.9	5669	..3	536
27.08.2001	P136	24	23.3	5668	..3	536
31.08.2001	P136	24	24.8	5670	..2	540
03.09.2001	P136	24	24.6	5667	..3	534
06.09.2001	P136	24	23.3	5671	..2	540
10.09.2001	P136	24	23.3	5664	..2	530

### 3.5 Reversing Thermometers

A set of three Mercury Reversing Thermometers (THERMOMETERWERK GERABERG) manufactured for temperature ranges of -2 to 30 °C, protected, numbers 2, 3 and 4, and an Electric Reversing Thermometer Typ SIS RTM 4002 Number T788 served as check for the CTD-temperature sensor.

To attach the thermometers on the CTD-Probe it was always necessary to remove three water bottles. The thermometers were turned always after an adjustment time of 10 minutes in a homogeneous layer. The readout was performed in an air conditioned lab.

The thermometers are calibrated in the laboratory of the IOW. Characteristic data of the thermometers are shown in Table 3.8.

Table 3.8: Calibration data of reversing thermometer

Nr.	Calibrated	Resolution
2	2/1999	0.1 °C
3	2/1999	0.1 °C
4	2/1997	0.1 °C
RTM	4/2000	0.001 °C below 20 °C, 0.01 °C above 20 °C

### 3.6 Lowered Acoustic Doppler Current Profiler (LADCP)

#### Description of Equipment

During the cruise a LADCP-2 system was used to obtain full depth velocity profiles at each CTD-station. Two ADCP WH-300 were mounted in the frame of the CTD-probe. The LADCP-system was equipped with an external battery case for elimination of magnetic disturbances by battery packs. One LADCP was used in upward looking mode (SN 1129) and one in downward looking mode (SN 0586) in order to get the vertical range as large as possible. The Workhorse LADCP produce two profiles, one for velocity and one for echo intensity. Additionally, the temperature inside the ADCP case is recorded.

#### Mode of Operation

The LADCP-system attached to the CTD probe was used at every CTD station (73 stations). Before deployment, the deck unit PC-clock of the ADCP was synchronised with the CTD deck unit PC clock. This allows for later correction of the sound velocity profile with CTD temperature and salinity data as well as the correction of LADCP depth. GPS position and time were recorded as fixpoints for the calculation of the ADCP path, when the CTD passed the 30 dBar horizon during both down and upcast, as well as the lowest point of the profile. The LADCP configuration is given in Table 3.9. The selected parameters result in a mean ensemble time of 1.8 s. The maximum range of each LADCP amounts to 120 m using an 8 m depth cell size. This results in a total range of 240 m. The standard deviation of velocity is  $2 \text{ cm s}^{-1}$  for a single ping.

#### Calibration

Prior to the cruise the LADCP compass was calibrated at the IOW on 08.07. 2000. An residual compass error after the calibration of 0.3 deg was obtained. Just before the cruise started, this calibration was controlled at the beach of Walvis Bay. Before this calibration an compass error of 18.6 deg for the master LADCP and 12.7 deg for the slave LADCP were detected, respectively. After recalibration for downward (master) and upward looking mode (slave) with an external battery case residual errors were 0.5 deg for master and 1.1 deg for slave LADCP, respectively. Local magnetic variation was corrected during the post processing of the current data.

#### Performance

During the whole cruise the LADCP-system worked without any problems.

#### Data pre-processing

Pre-processing of LADCP data were carried out with MATLAB Version 5 and the LADCP-V5 software by Martin Visbeck. First the velocity profiles were differentiated with respect to depth to eliminate the CTD-package's motion. Then a depth record was obtained by integrating the vertical velocity in time. Now the shear profiles were averaged within depth

Table 3.9: Configuration of the lowered ADCP

Command	Parameter	Value
	frequency transmit	300 kHz
ED0000	depth of Transducer	0 m
ES35	salinity	35
EX11111	co-ordinates	use earth co-ordinates
SA001	synchronising pulse	before each ping
SI0	synchronising pulse	sent on every ping
SW75	wait step	75 ms
TE00:00:01.00	time per ensemble	1 s
TP00:00.00	time between pings	as soon as possible
LD111100000	data output	vel, corr, intensity, percent good
LF0400	blank after transmit	4 m
LP00003	ping per ensemble	3
LJ1	receiver gain	1
LN020	number of depth cells	20
LS0800	bin length	8 m
LV250	correlation velocity	$2.5 \text{ m s}^{-1}$
LW1	band width	narrow band
LZ30,220	amplitude, Cor. Thresh	
EZ1111111	sensor source	use all
EA00000	heading alignment	0 deg
EB00000	heading bias	0 deg magnetic deviation

bins. The average shear profile was integrated vertically to obtain a baroclinic velocity profile. The barotropic correction was calculated from the start and end positions measured by from GPS, which were recorded while the CTD-probe passed the 30 dbar depth level during downcast and upcast, respectively. A more detailed description is given by VISBECK (2000). Data of local magnetic variation were taken from German nautical maps (release BSH-1991). The yearly change of the magnetic variation was taken into consideration.

### Data Storage

The LADCP raw data and pre-processed data and figures were stored on Zip-Disk as well as on CD-ROM for back up purposes. After the final processing the validated data will be distributed on a CD-ROM.

### 3.7 ARGOS Drifter

Three ARGOS surface drifters have been deployed in order to get information of the surface circulation in the South East Atlantic on longer time scales. One drifter has been released

at the shelf edge in the Benguela Current regime, one drifter at the shelf edge in the Angola Current regime and one drifter offshore in the expected area of the South Equatorial Counter Current. The specifications of the start positions of the drifters are given in Table 3.10.

Table 3.10: Specifications of ARGOS surface drifter released by R/V Meteor

Drifter ID	Start Date	Time UTC	Latitude	Longitude	Comment
19205	27.08.00	11:44	19° 42.23' S	11° 40.82' E	Benguela Current
19204	29.08.00	22:06	12° 58.50' S	12° 40.49' E	Angola Current
19206	01.09.00	19:12	09° 00.31' S	08° 00.00' E	SECC

### Description

The SVP Drifting Buoy is used to track ocean currents at shallow depths as well as to collect environmental data at or near the sea surface. The buoys conform to design specifications developed in the World Ocean Circulation Experiment, Surface Velocity Program (WOCE/SVP). Basic components include a spherical surface float containing system electronics and a 'Holey Sock' drogue. The drogue is designed to track a given parcel of water at a given depth. In its standard configuration, the drogue is approximately 92 cm in diameter and 550 cm long providing a drag ratio of approximately 40:1 between the surface float and the drag elements beneath the surface. The centre of the drogue is located in a depth of 15 m. The float contains an Argos-certified PTT which transmits nominally every 90 seconds according to user-specified duty cycles. Battery power is sufficient for approximately 2 years of continuous operation in normal sea conditions. The standard SVP drifting buoy reports:

- Identification number
- Sea water temperature to  $\pm 0.1$  °C.
- Time that the float is submerged during each 1/2 hr. (an indication of whether the drogue is still attached and operational).
- Battery voltage.

The SVP is now widely accepted throughout the world as an effective and economical tool for measuring surface currents while at the same time collecting key environmental parameters.

### Deployment

The drifters have been deployed according to the deployment instructions of the manufacturer after they were tested on the deck of R/V Meteor before deployment. Just before the release the plastic shrink-wrap was removed. Then the magnet was removed manually. Finally the unpacked drifter was thrown from the stern about 5 m above the sea surface

while the ship was travelling between 2-4 kn. The date, time (GMT) and location of deployment as well as the five digit ID were recorded and mailed to the Global Drifter Center (Pazos@aoml.noaa.gov).

### **Calibration**

The ARGOS Service was instructed prior to the cruise on the calibration coefficients according to the recommendations of the manufacturer Technocean, Inc. in Cape Coral, Florida, USA.

### **Performance**

The drifter provided positions and sea surface temperature during the cruise.

## **3.8 Hydrographic measurements**

### **3.8.1 Sample salinity measurements**

#### **Sample collection**

For the quality check of both the conductivity measurement with the CTD and the underway salinity measurement salinity samples have been taken. For the CTD check two bottles are closed at the same depth in a water body with small vertical gradients and three samples are taken from each bottle. If possible this procedure has been carried out daily but especially in the Angola current water the water is highly stratified and suitable conditions for a CTD check are found rarely. For the check of the underway salinity measurement three water samples have been taken twice a day.

#### **Equipment, technique and calibration**

For the sampling quartz glass bottles with a screw cap and a teflon inlet have been used. The samples have been measured with an Autosal 8400B described in section 3.4.

#### **Quality control**

Rough errors could be detected from the deviation between the different samples. The deviation between the three samples used for the check of the underway salinity measurements is always smaller than 0.002 PSU. The standard deviation of the six samples taken for each CTD check was smaller than 0.003 PSU.

#### **Data Archiving**

The results of the underway salinity measurement checks are written on standard protocol sheets of the IOW. The CTD checks are processed using the IOW program Valid, version 2.25. This program extracts the necessary CTD data from the \*.bt1-files and provides an input for the Autosal results. The data are combined to a \*.vgl file which may also

include temperature, oxygen and pressure sensor check results. The \*.vgl files contain the running number of the CTD checks in their filename. They are stored together with the CTD data. The program Valid provides both tools for a statistical analysis of the CTD checks and recommendations for the validation of the CTD data.

### 3.8.2 Sample oxygen measurements

#### Sampling

Bottle oxygen samples were taken in calibrated clear glass bottles for the determination of dissolved oxygen immediately after the rosette sampler had been recovered before all other sub-samplings. Strong attention was paid to this step and the subsequent fixation because this step is one of the main sources of error in the oxygen determination. The analysis of the fixed oxygen sample was carried out in the lab within 2 hours after the CTD-cast.

#### Method

The determination of oxygen is based on the classical WINKLER procedure (WINKLER, 1888) after the following principle: The physically dissolved oxygen in an amount of water is chemically bound by manganese (II) hydroxide in a strongly alkaline medium, which is oxidised to manganese (III) quantitatively. Any contact with atmospheric oxygen was strictly avoided during this step of analysis. After complete fixation of the dissolved oxygen and precipitation the sample is acidified to a pH between 2.5 and 1. The precipitated hydroxides dissolve and manganese (III) ions are liberated. Manganese (III) is a strong oxidising reagent in acidic media and react with an equivalent amount of iodide. The iodide ions are oxidised to iodine, which in turn forms a complex with surplus iodide. This complex formation is desirable because of the fact that dissolved iodine has a relatively high vapour pressure and tends to escape during the subsequent steps of analysis. Finally, the iodine is titrated with thiosulphate. The iodine is reduced to iodide and the thiosulphate in turn is oxidised to tetrathionate ion. Because thiosulphate is not a primary standard the precise concentration of the solution must be determined prior to analysis with a potassium iodate solution.

#### Titration

Titration was performed with an DMS Titrino 702, METHROM AG CH-9101 Herisau (Switzerland), whereby the endpoint of the titration is determined potentiometrically. The oxygen content of the water sample is calculated according to the following relation:

$$O_2 = \frac{111.96 BT}{(V - 1)} - 0.03 \text{ ml l}^{-1} \quad (3.1)$$

where

- B - is the volume of thiosulphate in *ml* used for the titration of the sample
- T - is the titer
- V - is the volume of the sample bottle in *ml*

### Accuracy

The accuracy of the determination is at least  $\pm 0.02 \text{ ml l}^{-1}$ .

### 3.8.3 Nutrient measurements

The following inorganic nutrients were determined in every CTD cast from every water sample, except ammonium where the reaction time limits the number of analysis: phosphate, silicate, ammonium, nitrite and nitrate. Standard depths were 1, 10, 20, 30, 40, 60, 80, 100, 200, 400, 800, 1200 m.

### Sampling

The subsampling for nutrients was performed immediately after oxygen sampling using  $500 \text{ cm}^3$  plastic bottles which were rinsed with seawater before and are used for these investigations exclusively. Before filling the bottles they were washed with the respective sample vigorously. Each water sample taken by the bottles of the rosette sampler was identified in a unique manner by combining the cruise number and the number of bottles closed so far since the beginning of the cruise. The analysis were performed immediately after sampling and were finalised latest after two hours, again with the exception of ammonium (6 hours).

### Methods

For the determination of nutrients the manual standard colorimetric methods have been used which are described in detail by GRASSHOFF et al. (1983) and ROHDE and NEHRING (1979).

### Calibration

The calibration was performed in regular intervals during the cruise and compared with experienced calibration factors (Stewart-charts).

### Accuracy

Ammonium:	$\pm 0.05 \mu\text{mol l}^{-1}$ (in the range under discussion)
Nitrite:	$\pm 0.02 \mu\text{mol l}^{-1}$
Nitrate:	$\pm 0.05 \mu\text{mol l}^{-1}$ (low concentration range) $\pm 0.10 \mu\text{mol l}^{-1}$ (high concentration range)
Phosphate:	$\pm 0.02 \mu\text{mol l}^{-1}$
Silicate:	$\pm 0.10 \mu\text{mol l}^{-1}$

### Quality Control

The methods are used over long periods within the HELCOM Monitoring Programme. Beside the above mentioned internal quality control, the methods are cross-checked biannually since 1993 within QUASIMEME (general good: overall performance).

## Data Archiving

The results of the analysis are calculated directly after the measurements using an internal programme of the IOW and are stored as ASCII-files together with the oxygen data and sample ID-number. The assignment to the hydrographic and biological observations is made via the sample ID-Number by using the routine Connect.exe.

### 3.8.4 Trace Metals

#### Sampling

Water samples for the determination of trace metals (Cd, Ni, Cu, Hg) were collected from surface and deep waters by 5 l teflon coated samplers (HYDROBIOS), fitted on an polyethylene-coated CTD-rosette. The zinc anodes were preserved with polyethylene and polyethylene coated lead was used as bottom weight. To avoid contamination from the ship, the samplers were conditioned by up and down movement after the surface sample was taken in the 20 m depth horizon. Unfiltered seawater samples (Cd, Ni, Cu) were directly filled in pre-cleaned polyethylene bottles (500 ml) and acidified with 1 ml sub-boiled HNO<sub>3</sub> of supra-pure quality. For mercury analysis, 500 ml unfiltered water samples were preserved with 3 ml sub-boiled HNO<sub>3</sub> of supra-pure quality directly after sampling and stored in silica bottles.

#### Filtration

To separate the particulate matter, the samples from the coastal stations were pressure filtered (0.5-0.8 bar) with N<sub>2</sub> through 0.4 µm pre-cleaned and pre-weighed Nuclepore filters. All water samples were acidified immediately after filtration by adding sub-boiled HNO<sub>3</sub> to a final pH < 2. The filtered samples (0.8-1.5 l) include dissolved metal species plus metal leached during storage from particulate matter < 0.4 µm. The filters were then rinsed twice with 5 ml high purity water to remove sea salt residues before being stored in cleaned plastic dishes at -20 °C. The preparation of the bottles, the filtration procedures, and the acidification of the samples were carried out in the clean laboratory of the RV Meteor. All teflon bottles, Nuclepore filters, samplers, and reagents were pre-cleaned, using the methods of PATTERSON and SETTLE, (1976).

#### Analysing

The unfiltered samples were analysed for Cd, Cu, Ni and Hg in the Institute for Baltic Sea Research Warnemünde. For the determination of Cd, Cu and Ni the freon-dithiocarbamate extraction back-extraction method of DANIELSSON et al. (1978) was used. Final measurements have been carried out by using a Perkin-Elmer AA spectrophotometer (ZL 4100 with Zeeman correction) in combination with a HGA 600 graphite furnace and an autosampler (model AS 60). For analysis of trace metals in suspended particulate matter, the samples will be digested by pressure wet ashing with 2 ml HNO<sub>3</sub> (sub-boiled) and 100 µl HF (supra-pure) for two hours at 180 °C, evaporated to dryness and dissolved in 1 ml HNO<sub>3</sub> (1 mol). The final acidic solutions will be analysed using a Perkin-Elmer AA spectro-photometer

(model ZL 4100 with Zeeman correction) in combination with a HGA 600 graphite furnace and an autosampler (model AS 60) (POHL, 1997).

The reactive mercury HgR, a methodically defined fraction, which consists mostly of inorganic Hg (II) (COSSA et al., 1997) were analysed using AFS (Atomic Fluorescence Spectrometry, Merlin system of PS Analytical Ltd.) after reduction with SnCl<sub>2</sub> and amalgamation on a gold net (HATCH and OTT, 1968). When the determination of HgR was finished, 1 ml of KMnO<sub>4</sub> was added to the same seawater sample for the determination of total Hg (Hg<sub>tot</sub>). The sample was stored again 24 hours, then the surplus of KMnO<sub>4</sub> was reduced with hydroxyl ammonium chloride, and Hg<sub>tot</sub> was determined as mentioned above.

### 3.8.5 Sample phytoplankton measurements

#### Sample collection

Water samples from 0, 10, 20, 30, 40 and 60 m depth were taken from the rosette samplers. From the sample water, sub-samples for the different phytoplankton parameters were gathered. These parameters were:

- phytoplankton biomass
- chlorophyll-a
- potential primary production (incubator method)
- primary production (simulated *in situ* method).

#### Phytoplankton biomass

250 ml of water were filled into glass bottles. They were immediately preserved by the addition of 1 ml of alkaline Lugol solution (KI/I<sub>2</sub>). The microscopical counting and biomass determination of the different phytoplankton species were made after the cruise, see 4.5.

#### Chlorophyll-a

500 to 1000 ml (depending on the seston concentration of the water) were filtered onto Whatman GF/F filters. Adhering moisture was removed by putting the filters on filter paper (for some minutes in the dark). The filters were stored for not longer than 24 hours at a temperature of -20 °C in well stoppered tubes and afterwards extracted by filling 10 ml of 90 % acetone into these tubes. After 3 hours of extraction in the dark, the extract is measured in a TURNER fluorometer 10-AU-005. For phaeopigment correction, the extract is measured again after acidification with 100 µl 1N HCl in 8 ml extract.

#### Potential primary production

Water from the surface and one or two additional depths was filled into clear plastic bottles of 70 ml content (1 light and 1 dark bottle from each depth). Into each bottle, 100 µl of a

$\text{NaH}^{14}\text{CO}_3$  solution ( $2\ \mu\text{Ci} = 74\ \text{kBq}$ ) were injected. The bottles were attached to a rotating wheel in an incubator at *in situ* surface temperature and constant light of  $560\ \mu\text{E m}^{-2}\ \text{s}^{-1}$  for 2 hours. After incubation time, the contents of the bottles were filtered onto Whatman GF/F filters. The filters were fumed with concentrated HCl for 15 minutes and then placed into scintillation vials. The further processing was made according to 4.6.

### Primary production (simulated *in situ*)

To reflect the natural conditions of primary production, a simulated *in situ* technique was applied. In contrast to the "potential" primary production, it uses the natural light. Therefore, these experiments could be carried out only during daytime at sufficient light intensities (7:00 to 17:00 local time). The extinction of light with water depth was simulated by the use of 5 different grey filters, which reduced the light intensity to 50 %, 30 %, 15 %, 7 % and 4 % of the incident light, respectively. The standard sampling depths (0, 10, 20, ...m) were roughly related to the different light intensities on the basis of measured underwater depth profiles of light. For instance, the surface water sample was considered to be representative for the upper 5 metres and therefore used for the 100 %, 50 % and 30 % light intensity; the sample from 10 m depth was taken for the 15 % and 7 % light intensity and that from 20 m depth for the 4 % incubation.

Water from the different standard depths was filled into the appropriate number of 280 ml polycarbonate bottles (one bottle per light intensity). Into each bottle, 200  $\mu\text{l}$  of a  $\text{NaH}^{14}\text{CO}_3$  solution ( $4\ \mu\text{Ci} = 148\ \text{kBq}$ ) were added. Then the bottles were put into Plexiglas tubes, each of them was coated with the above mentioned grey foils (only one was left clear for the 100 % light intensity). The tubes were placed into a shallow bath which was flushed with surface water for cooling. The bath was installed on deck at an unshaded place. After 2 hours of incubation, the whole content of each bottle was filtered onto Whatman GF/F filters, then fumed with HCl, put into vials and stored at room temperature until further processing after the cruise.

### Calibration

The fluorometer was calibrated with a dilution series of pure chlorophyll-a (SIGMA) against spectrophotometric determinations (SHIMADZU UV-1201V Spectrophotometer). There was no possibility for calibration of the other biological methods during the cruise. However, according to different quality checks the expected accuracy of the used methods are as follows: According to the HELCOM manual (<http://www.helcom.fi/ec.html>), at least 400 individuals will be counted to give a precision of  $\pm 10\%$  (LUND et al., 1958) for the phytoplankton biomass estimation.

The precision of chlorophyll a measurements was evaluated at the "Second Workshop on Quality Assurance of Pelagic Biological Measurements in the Baltic Sea", Warnemünde, 16. - 20.09. 1995, resulting in a standard error of 1.2 to 5.2 % (our method 3.2 %).

According to a HELCOM intercalibration, the coefficient of variation for the estimated potential primary production by the incubator method of different institutes was 16.6 %

(HELCOM, 1991). This is similar to the relative standard deviation < 15 %, reported by GARGAS et al. (1978).

For an *in situ* method primary production, KELL and BÖRNER (1980) found a mean standard error of 15 % in a coastal water of the Baltic Sea.

### Data Archiving

The results of the analysis are stored as ASCII-files together with the sample ID-number. The assignment to the hydrographic and chemical observations is made by the sample ID-Number with the routine Connect.exe.

## 3.9 Net sampling

### 3.9.1 Phytoplankton net

For the qualitative analysis of the microphytoplankton, a plankton net of 10  $\mu\text{m}$  mesh size and an opening of 17 cm diameter was used. It was lowered on station to 20 m depth and then hauled slowly to get a sample of about 30 ml. Few drops of that sample were immediately observed under the microscope at a magnification of 160 x and 400 x. Afterwards, some of the samples were preserved with formaldehyde to a final concentration of 1 % to enable further examination in the institute.

### 3.9.2 Zooplankton sampling

#### Sample collection

Zooplankton studies were focused on differences between water masses in terms of biomass, taxonomy, production and metabolic activity.

One stock of samples comprises all aspects on the basis of size fractions (55 - 100  $\mu\text{m}$ , 100 - 200  $\mu\text{m}$ , 200 - 500  $\mu\text{m}$ , 500 - 1000  $\mu\text{m}$ , and > 1000  $\mu\text{m}$ ). They were collected at 17 stations with oblique haul by HYDROBIOS Multiplankton sampler (Multinet), equipped with 2 different mesh sizes (55  $\mu\text{m}$  and 200  $\mu\text{m}$ ). The smaller size fractions have been collected by the 55  $\mu\text{m}$  mesh, the larger with the 200  $\mu\text{m}$  net. We performed stratified hauls from 200 to 75 m, 75 to 25 m and 25 m to the sea surface. An additional level had been introduced down to 500 m at three stations: north and south the Angola Benguela Frontal Zone and one within the transition area.

The Multi net (Multi Plankton Sampler MPS, HYDRO-BIOS Apparatebau GmbH, Kiel, Germany) consists of a net frame with an opening area of 0.25 m<sup>2</sup>, a pressure capsulated motor unit (3000 dbar) with external battery housing, 5 nets (L = 2.5 m, diameter at the end = 0.11 m) with zip fasteners, 5 plastic net buckets with side windows, covered with sieve gauze, a V-fin depressor, and a deck unit.

Depth was recorded online by a pressure sensor. Flow velocities in and outside the net and

the amount of water filtered had been also available online by two flow-meter, mounted in and outside the frame. The data had been viewed by OCEAN LAB Software (Hydrobios). Parallel, the R/V "Meteor" data collecting and distribution system made it possible to follow both the ship speed through water (kn) and the velocity of the winch during oblique hauls. The opening device enabled us to collect plankton in five different depth levels during one oblique haul.

In order to collect a sufficient amount of plankton for the different purposes as mentioned, the net had been towed and lowered in the certain depth stratum several times. For example, the 200 to 75 m level was collected by the 200  $\mu\text{m}$  mesh in the "M" manner (up, down, up, down), followed by the 55  $\mu\text{m}$  mesh in the "N" manner (up, down, up) at station 457 at 13. September 2000. The same principle had been repeated in the 75 to 25 m level (Figure 3.1).

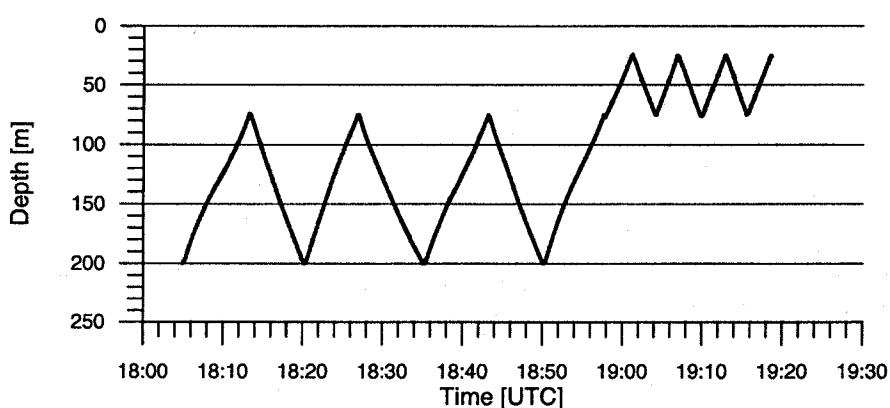


Figure 3.1: Multinet sampling performance in the depth levels 200 - 75 m and 75 - 25 m on station 457 (N0703) at 13-9-2001

The ships velocity amounted 1.5 kn, the winch speed was  $0.3 \text{ m s}^{-1}$ . It resulted in a total speed of about  $1 \text{ m s}^{-1}$  during the towing phase and  $0.5 \text{ m s}^{-1}$  during lowering the net. The collection had been stopped according to the amount of plankton being expected to be caught and the amount of water filtered. Nets were rinsed by sea water from outside.

The determination of zooplankton respiration- and excretion rates by enzymatic methods, which were generally used, requires a calibration by the classical incubation techniques (IKEDA et al., 2000). For that purpose we collected plankton very carefully, towing an WP-2-net (UNESCO, 1968) by ships drift during station work in the upper 5 m. The organisms had been kept in a totally closed cod-end containing a water volume of 5 l. Besides the modified cod-end, the net was constructed in the original manner, with an opening area of  $0.25 \text{ m}^2$ , a total length of 2.61 m and a mesh size of  $200 \mu\text{m}$ .

#### Sample conservation and archiving

The samples had been stored in an air conditioned room at  $4^\circ\text{C}$  until processing. The process of splitting, fractionation and storing started immediately. Samples for enzymatic activity had been processed first.

Samples had been prepared in the following way:

- Splitting, one half for enzymatic activity measurements, gentle size fractionation, storage in liquid nitrogen
- one quarter for biomass determination, gentle size fractionation, concentrating on pre-weighed glass fibre filters (Whatman GF/C), storage in a deep freezer
- another quarter for taxonomy, gentle size fractionation, storage in buffered formalin (4 % final concentration).

Consequently, 45 samples had been collected at each station which covered the upper 200 m, and 60 samples at stations with four depth levels.

### 3.10 Light measurements

The vertical attenuation of the underwater light was measured on station by the LI-COR Data Logger LI-1000, equipped with a spherical underwater light sensor. The extinction of the light with water depth can be used to characterise a water body. In addition, the Secchi depth was measured by means of a Secchi disk of 30 cm diameter. The reading was always done by the same two persons.

## 4 Data postprocessing

### 4.1 Underway measurements

For the purpose of validation raw data, logged by the DVS system of the ship, were converted into matlab files. Reasonable physical thresholds were used to clip outliers and to remove bad data. The validated date from the quasi-continuous phosphate measurements in the surface water were added to the data set. The validated data were averaged over intervals of 1, 10 and 60 minutes and stored in Matlab files and ASCII formatted files as well.

During the periods listed below no data from the DVS system were available:

begin	end	comment
28.08.2000 18:24:50	29.08.2000 09:23:00	Namibe habor
11.09.2000 13:37:50	11.09.2000 14:27:00	DVS problems

#### 4.1.1 Navigation

The navigation data (ship position, ship speed, ship heading and echo sounding depth) were scanned for outliers and bad values. A median filter has been applied. The detected bad data were removed from the data set.

#### 4.1.2 Meteorology

The meteorological data set consists of starbord and portside sensor groups. Because the sensor group at the lee side is shaded by the ship we used only data from the luv side. The luv side was detected from the relative wind direction. In case of transition between both sides we used a mean value. Outliers have been removed by a median filter.

##### **Air pressure, global radiation, long wave radiation**

The MATLAB procedure *outmedi(-,9,3)* was applied to remove outliers. Values below zero in the global radiation during the night time were set to zero.

##### **Air temperature and humidity**

The air temperature and relative air humidity were processed with the MATLAB procedure *outmedi(-,9,3)*. On 27. and 29.08. the temperature data was disturbed by exhaust gas from the ships chimney. These data were removed.

##### **Wind**

The vector components of wind were calculated from the unvalidated true wind. The MATLAB procedure *outmedi(-,13,3)* was applied to remove outliers from the wind components.

### 4.1.3 Thermosalinograph

In order to calibrate the salinity-measurements of the thermosalinograph, a set of six sample bottles was filled with water taken from the cage of the thermosalinograph inside the ships hull. The salinity of the 6 samples was determined by means of the Autosal salinometer.

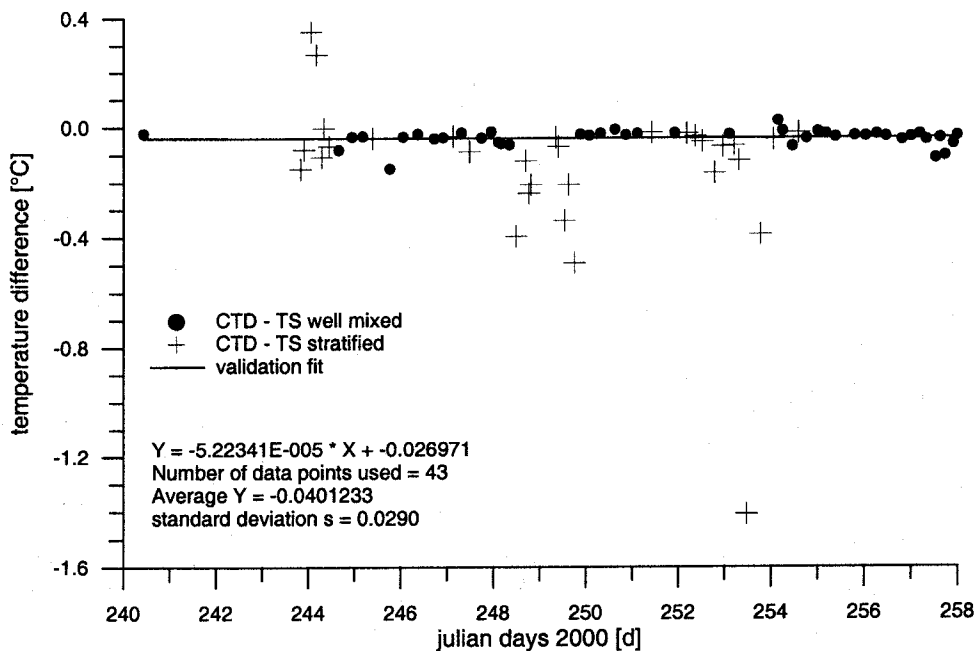


Figure 4.1: Calibration of the thermosalinograph - temperature

Additionally, on each station the salinity and the temperature have been compared with the values of the CTD. For this check stations with a well mixed surface layer have been selected and thermosalinograph data and the CTD data have been tested for a drift with time. Figures 4.1 and 4.2 show the difference between the SeaBird CTD data and thermosalinograph data. For temperature the statistical analysis gives:

$$\begin{aligned}
 T_{CTD} - T_{TS} &= -0.0000522 \text{ K } d^{-1} \cdot t - 0.02697 \text{ } ^\circ\text{C} \\
 \text{time range} &: \text{ day 238 to day 258} \\
 N &= 43 \\
 r^2 &= 0.000073 \\
 \sigma &= 0.029,
 \end{aligned}$$

where  $T_{TS}$  and  $T_{CTD}$  denote thermosalinograph temperature and SeaBird CTD temperature.  $t$  is the time since 1th January 00:00,  $N$  is the number of points,  $r^2$  describes the statistical significance of the linear trend. So, the negligible trend is of no statistical significance and a constant correction of  $\Delta T_{TS} = -0.04 \text{ K}$  is used.  $\sigma$  is the residual error of regression.

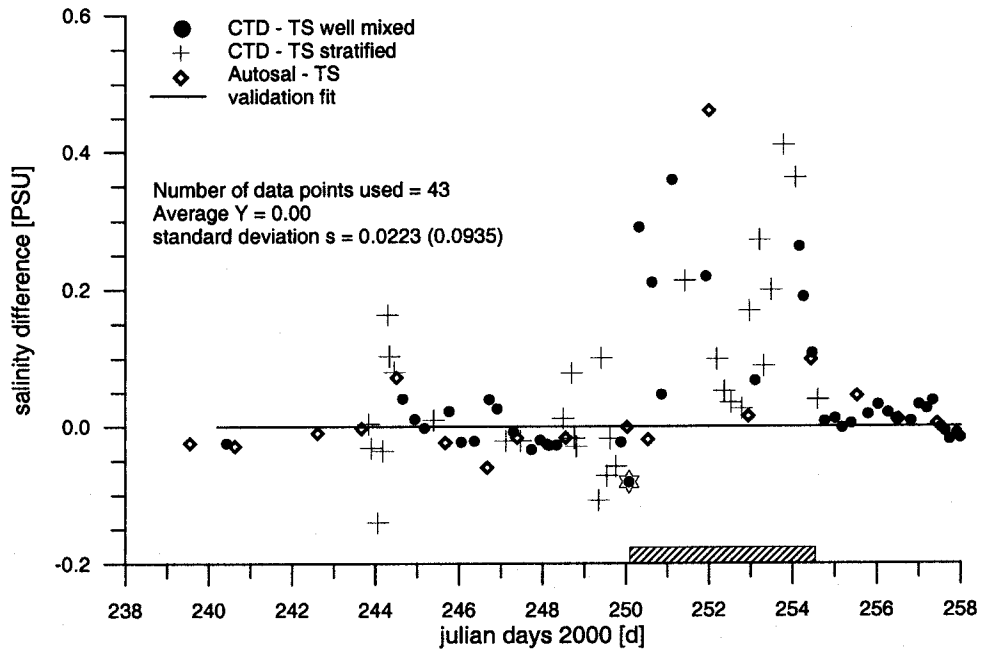


Figure 4.2: Calibration of the therosalinograph - salinity

Salinity requires no correction, since the large standard deviation exceed the mean difference considerably and no significant trend was found (see Figure 4.2).

After applying the corrections outliers have been eliminated with a median filter (MATLAB procedure *outmedi(-,19,3)*).

#### 4.1.4 Surface phosphate measurements

After applying the phosphate measurements to the DVS data set outliers have been eliminated.

#### 4.1.5 Output file format

Table 4.1 lists all parameters and the residual errors of the validated meta data and under-way measurements. The data are stored in Matlab- and ASCII-format.

### 4.2 Vessel mounted ADCP

The validation and postprocessing of vessel mounted ADCP data was carried out with the CODAS3 software package written by FIRING et. al (1995).

Prior uploading into the CODAS database the data were checked for time errors. Some single point errors were found and corrected. During creation of the CODAS database 10 ensembles with a short ensemble time were excluded. As the next step the cruise track was

Table 4.1: File format of validated DVS meta data

parameter	unit	residual error
time	[d]	0.000012 (5 s)
latitude	[deg]	0.00018 (3.5 m)
longitude	[deg]	0.00018
ship-heading Fiber Optical Gyro	[deg]	0.1
ship-heading Gyro	[deg]	0.1
heading difference FOG-Gyro	[deg]	-
ship course	[deg]	-
ship speed	[m s <sup>-1</sup> ]	-
depth - echo sounder	[m]	-
air pressure	[hPa]	0.5
air temperature (10 m)	[°C]	-
humidity (10 m)	[%]	3.0
wind vector east (10 m)	[m s <sup>-1</sup> ]	0.5
wind vector north (10 m)	[m s <sup>-1</sup> ]	0.5
wind direction	[deg]	-
wind speed	[m s <sup>-1</sup> ]	-
global radiation	[W m <sup>-2</sup> ]	-
long wave radiation	[mW m <sup>-2</sup> ]	-
salinity (4 m depth)	[PSU]	0.023
water temperature (4 m depth)	[°C]	0.029
phosphate (4 m depth)	[μmol l <sup>-1</sup> ]	0.06

calculated and the outliers were eliminated.

The transducer temperature was compared with the validated thermosalinograph temperature. A correction of  $T_{ADCP} - T_{TS} = -1.0822 K (\pm 0.1421 K)$  was applied. The constant soundspeed of  $1500 \text{ m s}^{-1}$  was corrected with the surface salinity measured by the thermosalinograph.

Some periods with low percent good rate were found. They are correlated with high wind speeds.

The statistical data analysis with the CODAS software gives the following values of error thresholds for the identification of bad data (Table 4.2).

These parameters were used to flag the outliers and bad data values in the profiles. The error of relative velocities amounts roughly  $1 \text{ cm s}^{-1}$ .

The ship velocity was removed from the data using both the water tracking method and the bottom tracking method. Both methods show a temporal trend in the amplitude and phase. The calibration was repeated after the ADCP heading was corrected by a time depend polynomial. Considering amplitude and phase of the calibration coefficients the water track method and the bottom track method give consistent results (see Table 4.3).

Table 4.2: Error thresholds for bad VMADCP data

parameter	threshold
reference layer bins	5-15
w variance	2000.0
w 2nd derivation	85.0
uv 2nd derivation	110.0
error velocity	70.0
amplitude	30.0

Table 4.3: VMADCP calibration coefficients

parameter	Bottom tracking	Water tracking
amplitude	1.0047	0.9947
ampl. standard dev.	0.0046	0.0077
phase	-1.1759	-1.1337
ph. standard dev.	0.2020	0.2698

The calibration coefficients for amplitude (1.00) and phase (-1.15) were added to the database. The residual heading error of roughly 0.3 deg results in an error of  $2.6 \text{ cm s}^{-1}$  at the absolute current velocities. The absolute reference layer velocity was calculated and the navigation data were scanned for outliers. After elimination of bad values the navigation data were smoothed. The residual error of validated current data was estimated as 3 to  $5 \text{ cm s}^{-1}$ . Contour and vector plots of all data completed the post processing (Figures 5.27 and 5.28).

### 4.3 CTD data validation

Table 4.4 list the corrections which were used in the CTD data post processing. The corrections was derived from the particular reference measurements described in Section 3.3. For the backscattering no reference measurements were carried out. The data of fluorescence 683 nm (Chlorophyll-a) and backscattering are given in arbitrary units.

### 4.4 LADCP

Post-processing of LADCP data were carried out with MATLAB LADCP-2 software by VISBECK, which was used for the pre-processing also. Now the validated bottom depth of the CTD/LADCP package was used instead of the raw pressure values. The LADCP-2 software was modified in order to get an additional output of backscatter intensity. The Blueprint export procedure v5blue.m was added. Table 4.5 lists the used post processing parameter.

Local magnetic variation was corrected by using the rotation parameter (*p.drot*) of the LADCP processing configuration file. Data of local magnetic deviation are captured from

Table 4.4: CTD sensor calibration coefficients

parameter	stations	correction
conductivity	all	-0.00473 mS cm <sup>-1</sup>
temperature	all	not necessary
pressure	all	1.0057 dBar
oxygen	387	SOC = 1.5054 BOC = -0.0068
	389 - 392	SOC = 1.3083 BOC = -0.0059
	393 - 403	SOC = 1.3317 BOC = -0.0060
	404 - 431	SOC = 1.3260 BOC = -0.0060
	432 - 449	SOC = 1.3416 BOC = -0.0060
	450 - 459	SOC = 1.2880 BOC = -0.0058
fluorescence	all	not validated
backcattering	all	no reference measurements

Table 4.5: LADCP post processing parameter

parameter	value	description
p.pglim	0.0	minimum percent good
p.elim	0.2	maximum error velocity [m s <sup>-1</sup> ]
p.wlim	0.08	maximum difference between W per profile [m s <sup>-1</sup> ]
ps.down_up	1	solve down and up individually
ps.dz	8	velocity profile vertical resolution [m]

German resp. British charts (release BSH-1991 resp. 1992). The yearly change of the magnetic deviation was taken into consideration. The applied magnetic deviation is given in Table A.1.

The validated data are stored in Blueprint format and as matlab \*.mat file. The plots of vertical sections were created using Surfer 6. The horizontal vector-plots were processed with Matlab 6.

#### 4.5 Phytoplankton

The microscopical counting and biomass determination of the different phytoplankton species is being done in the institute by the Utermöhl method using an inverted microscope LEICA Fluovert. While counting, the specimens are assigned to species or higher taxa and to size classes as well. Biomass is calculated using the appropriate stereometric formula (EDLER, 1979).

#### 4.6 Primary production

The filters resulting from the ship based experiments are measured in the institute at a PACKARD Tri-Carb Liquid Scintillation Analyser 2560 TR/XL for assimilated  $^{14}\text{C}$ . The "simulated in situ" primary production data, given per  $\text{m}^3$  and hour, were converted to daily primary production in the water column by the following algorithm:

- determination of the water depths corresponding to the experimental light intensities (5 grey filters per experiment) using the depth profiles of light,
- determination of the lower boundary of the euphotic zone, assumed at the 1% light depth,
- drawing the depth profiles of primary production which is used for the calculation of the depth-integrated primary production,
- extrapolation from this 2 hours depth-integrated primary production to daily primary production using the measured daily curve of global radiation and assuming a correlation between global radiation and primary production during the course of the day.

#### 4.7 Zooplankton

The zooplankton biomass of net samples was determined as ash free dry mass (AFDM) in the size fractions and depth levels mentioned above (see 3.9.2). The method, including preparation of glass fibre filters (Whatman GF/C), has been performed according to POSTEL et al. (2000), using oven drying at  $60^\circ\text{C}$  for 24 h and the subsequently combustion of samples in a muffle furnace at  $500^\circ\text{C}$  for at least 12 h.

The dry mass (DM) and ash free dry mass (AFDM) data are significantly correlated ( $p < 0.001$ ). The regression functions are shown in Figure 4.3 which allows an actual conversion of AFDM into DM in order to compare the results with earlier DM data from the region.

The stock of biomass data had been increased using ADCP profiles on all CTD-stations (Table A.1, Figure 2.2). Particles of a spherical diameter of the order of the wavelength (5 mm) should be ideally reflected by the back scattering signals of the 300 kHz LADCP system according to  $\lambda = c/f$  where  $\lambda$  stands for wave length [m],  $c$  for sound velocity (in water approximately  $1500 \text{ m s}^{-1}$ ) and  $f$  for frequency [Hz]. Nevertheless, the correlation between the AFDM [ $\text{mg m}^{-3}$ ] and the backscattering signal [dB] had been performed for all size categories and for the total of them. For that purpose, the acoustic signals were averaged over the depth ranges which were integrated by the net tows. The above 25 m were neglected because of the low amount of acceptable ADCP data. Consequently, the number of measurements depend on the number of biomass determinations between 25 to 75 and 75 to 200 m at 17 stations, which is an amount of 34. Table 4.6 includes the results

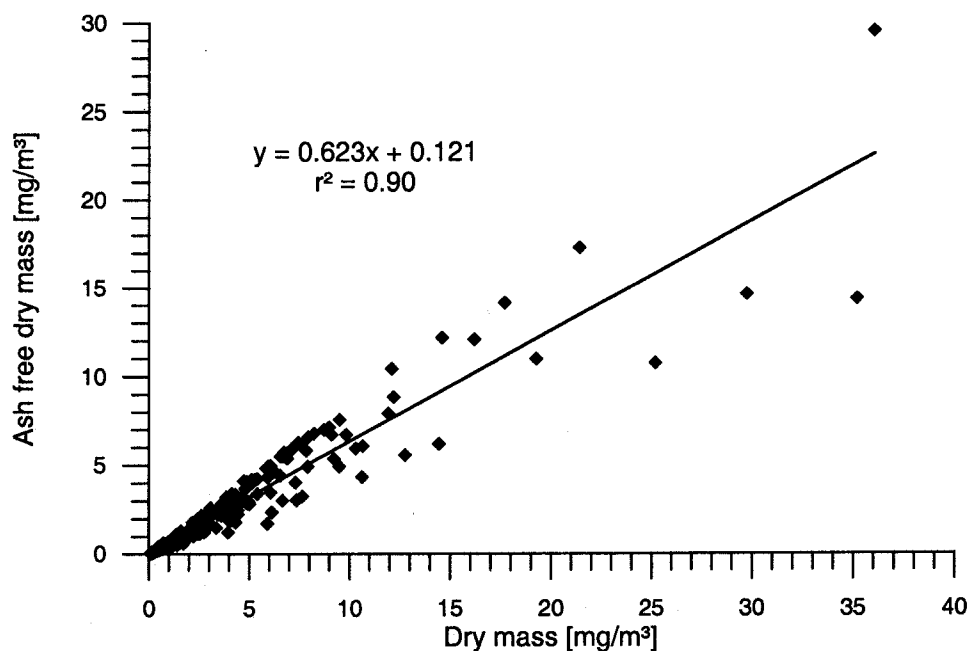


Figure 4.3: Relationship between dry mass (DM) and ash free dry mass (AFDM) of the total zooplankton of all size categories ( $N = 54$ ,  $r = 0.9485$ ;  $p < 0.001$ )

of the high degree significance for the correlations in most of the size classes, except for the 100 to 200  $\mu\text{m}$  category.

Table 4.6: Correlation between the vertical integrated Ash Free Dry Mass concentration of five zooplankton size classes and the LADCP backscattering signal averaged according to the integration depth of the plankton nets ( $N$  number of observation,  $r$  correlation coefficient,  $p$  probability level according to the STUDENT distribution). The lowest panel shows the back scattering signal if the  $\text{AFDM} = 0 \text{ mg m}^{-3}$ , which probably corresponds with the back scattering properties of sea water with no particles or other than within the mentioned size classes. (depth 25 - 200 m)

plankton size classes	> 1000 [ $\mu\text{m}$ ]	1000 - 500 [ $\mu\text{m}$ ]	500 - 200 [ $\mu\text{m}$ ]	200 - 100 [ $\mu\text{m}$ ]	100 - 55 [ $\mu\text{m}$ ]	Total [ $\mu\text{m}$ ]
$N$	34	34	34	34	34	34
$r$	0.753	0.606	0.519	0.494	0.522	0.674
$p$	< 0.001	< 0.001	< 0.001	< 0.01	< 0.001	< 0.001
dB if AFDM = 0	67.19	66.73	64.44	66.91	63.42	66.28

#### 4.8 Data storage and distribution

The following table list the current state of data processing and storage as well as the persons who are responsible for the particular data sets.

Data set	status	Format	responsible
CTD	validated	Seabird cnv-files (ASCII)	H.U. Lass
LADCP	validated	BluePrint, Matlab binary files	V. Mohrholz
VMADCP	validated	CODAS 3 data base	V. Mohrholz
Meteorology	validated	ASCII ,Matlab binary files	V. Mohrholz
Navigation	validated	ASCII ,Matlab binary files	V. Mohrholz
Oxygen	validated	ASCII-File	G. Nausch
Nutrients	validated	ASCII-File	G. Nausch
Phytoplankton	processed	ASCII-File	N. Wasmund
Zooplankton			L. Postel
Trace metals			C. Pohl

The raw data are available on CD-ROM for the cruise participants. A new edition with validated data is in progress.

## 5 Preliminary Results

### 5.1 Meteorological conditions

The entire investigation area is located within the latitudes of southeastern trade winds. The meteorological conditions during the cruise coincides well with climatological data.

The zonal wind component was generally weak, mostly below  $5 \text{ m s}^{-1}$  (Figure 5.1). The meridional wind component was positive (from south) and reflecting mostly the trade winds. The meridional wind component is generally low except for the strong winds at the end of the cruise from 10th September to 15th September, when the wind speed was about  $15 \text{ m s}^{-1}$ . The spatial wind distribution shows an area with weak wind speed north of  $16^\circ \text{ S}$  whereas south of this latitude the wind speed is much higher (see ERS-2 wind in Figure 5.4).

The air pressure was permanently between 1009 and 1021 hPa and shows a well developed semidiurnal cycle.

Figure 5.2 shows the air temperature, the relative humidity, the global solar radiation and the long wave radiation. The air temperature was about  $12-15^\circ \text{ C}$  in the south and increased up to  $23^\circ \text{ C}$  in the northern part of the investigation area. The humidity was between 90 and 100 % in the beginning of the cruise when the cloud coverage was nearly 100 %. After the 1st of September the humidity decrease slightly to 70-90 %.

The global radiation reflects the cloud coverage during the cruise. Until the 1st of September the global radiation was on a low level. After the 1st of September it increased considerably, except on 6th September.

One should keep in mind that the figures 5.1 to 5.2 show neither a time series nor a synoptic view. Thus for a better orientation with the plots figure 5.3 shows ships latitude and longitude as function of time.

### 5.2 Hydrographical measurements

#### 5.2.1 Surface water masses

The large scale properties of the water masses in the surface layer are maintained by the equatorial surface water, diluted by excess of precipitation and river discharge, the saline subtropical surface water off Angola and the Benguela upwelling zone in the south which injects water from deeper layers with a lower salinity into the surface layer at the coast. From there it is advected into the open ocean by the Ekman surface current. Figure 5.4 shows a quasisynoptic view of sea surface salinity (SSS), the sea surface temperature (SST) measured with the thermosalinograph, the sea surface phosphate concentration and the mean ERS-2 wind. The warm subtropical surface water with temperature higher than  $20^\circ \text{ C}$  observed in the north is separated by a cooler boundary layer from the Angolan

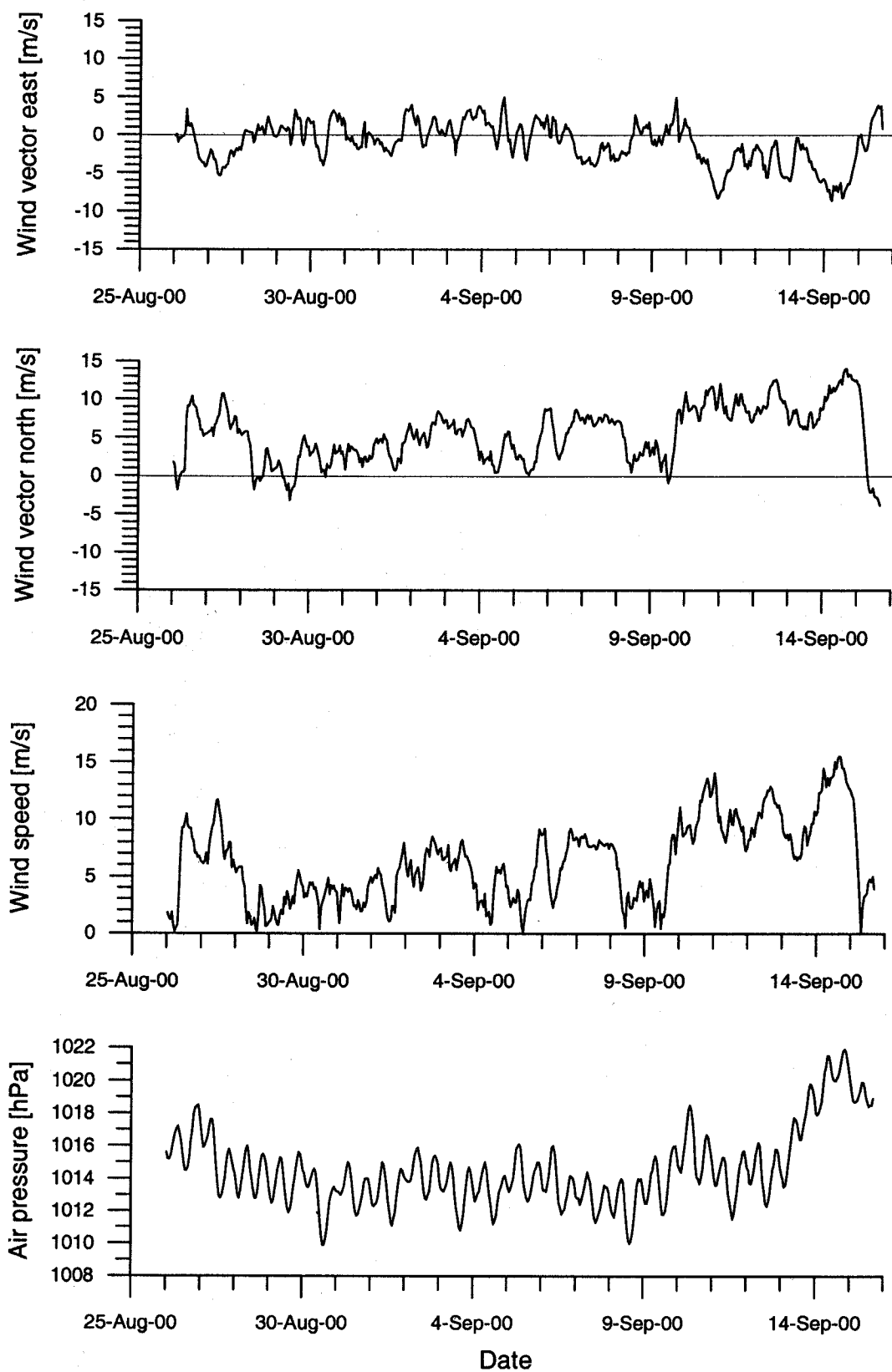


Figure 5.1: Time series of wind and air pressure

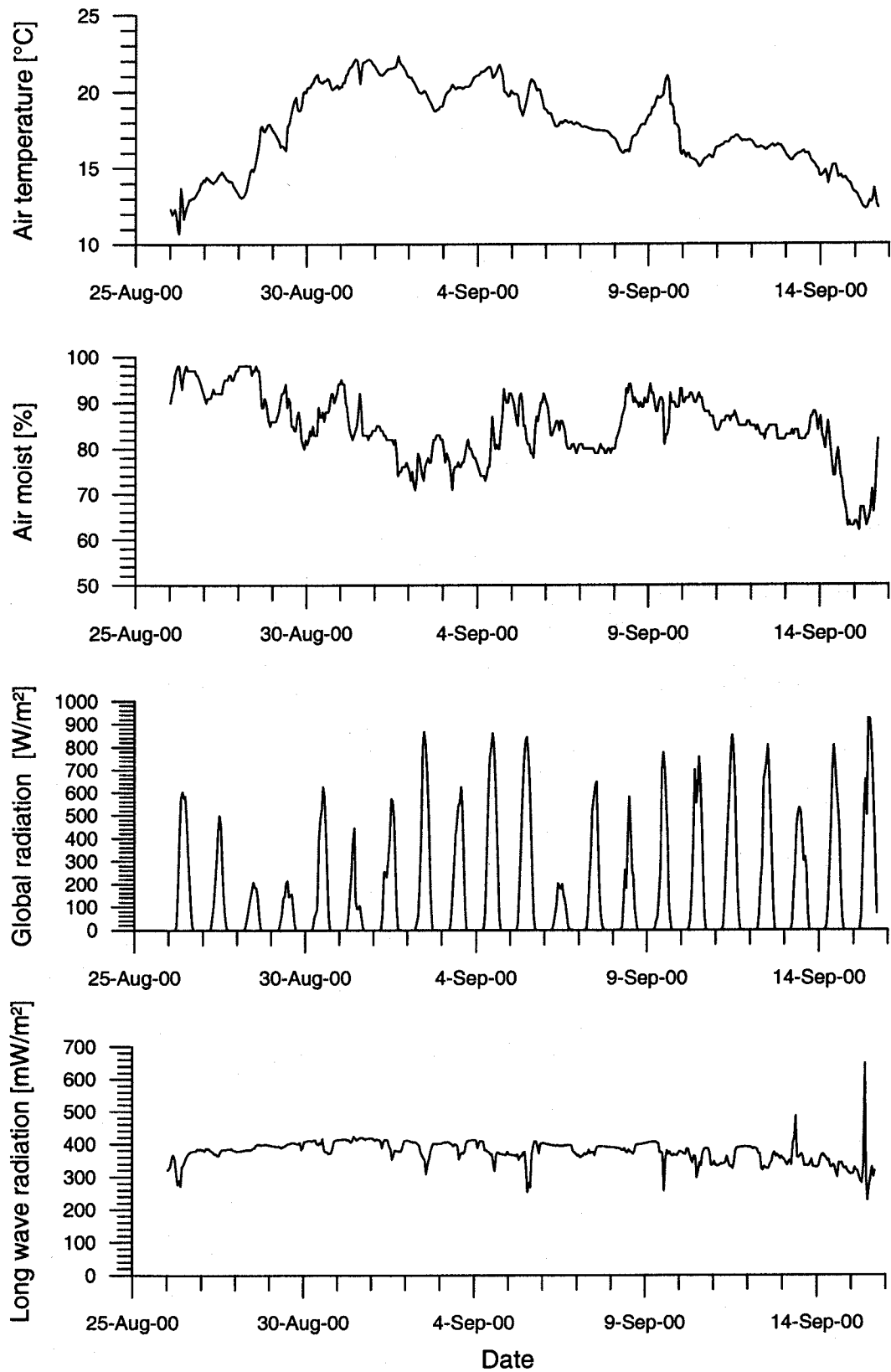


Figure 5.2: Time series of air temperature and moist, global- and long wave radiation

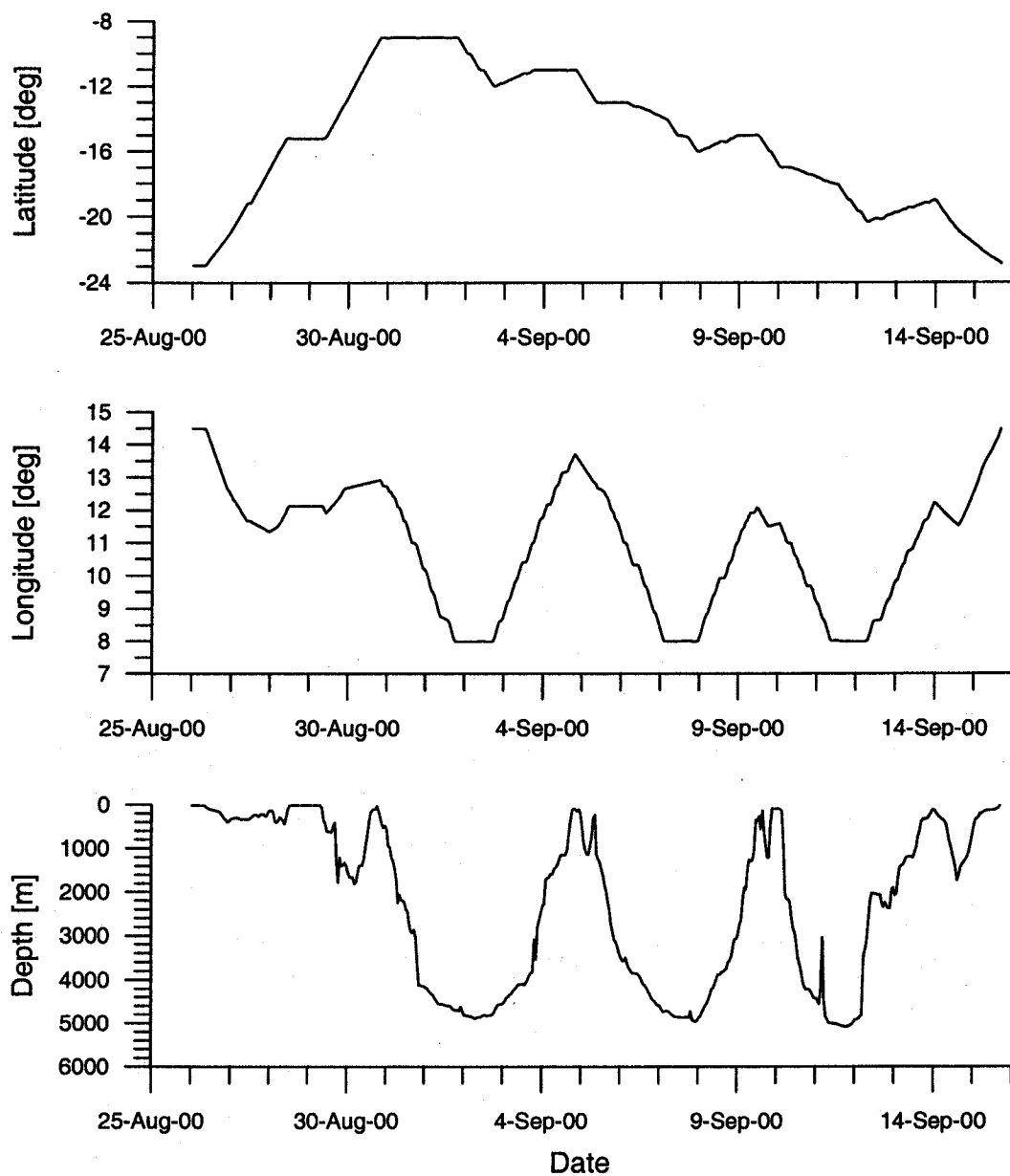


Figure 5.3: Time series of ship position and echo sounding depth

coast. This water extends to  $14^{\circ}$  S at the coast and nearly to  $12.5^{\circ}$  S offshore at  $8^{\circ}$  E. The subtropical surface water is separated by the ABFZ, characterised by a relatively weak thermal gradient at  $16^{\circ}$  S centered around the  $18^{\circ}$  C isotherm and the salinity of 35.8. South of  $16^{\circ}$  S cold Benguela upwelling water with temperature lower than  $16^{\circ}$  C cover the surface off the Namibian coast.

Compared with the SST the salinity distribution shows a high patchiness. The general structure in SSS is characterised by a salinity of more than 35.8 in the subtropical surface water in the north and salinity of less than 35.6 for the Benguela upwelling water. The

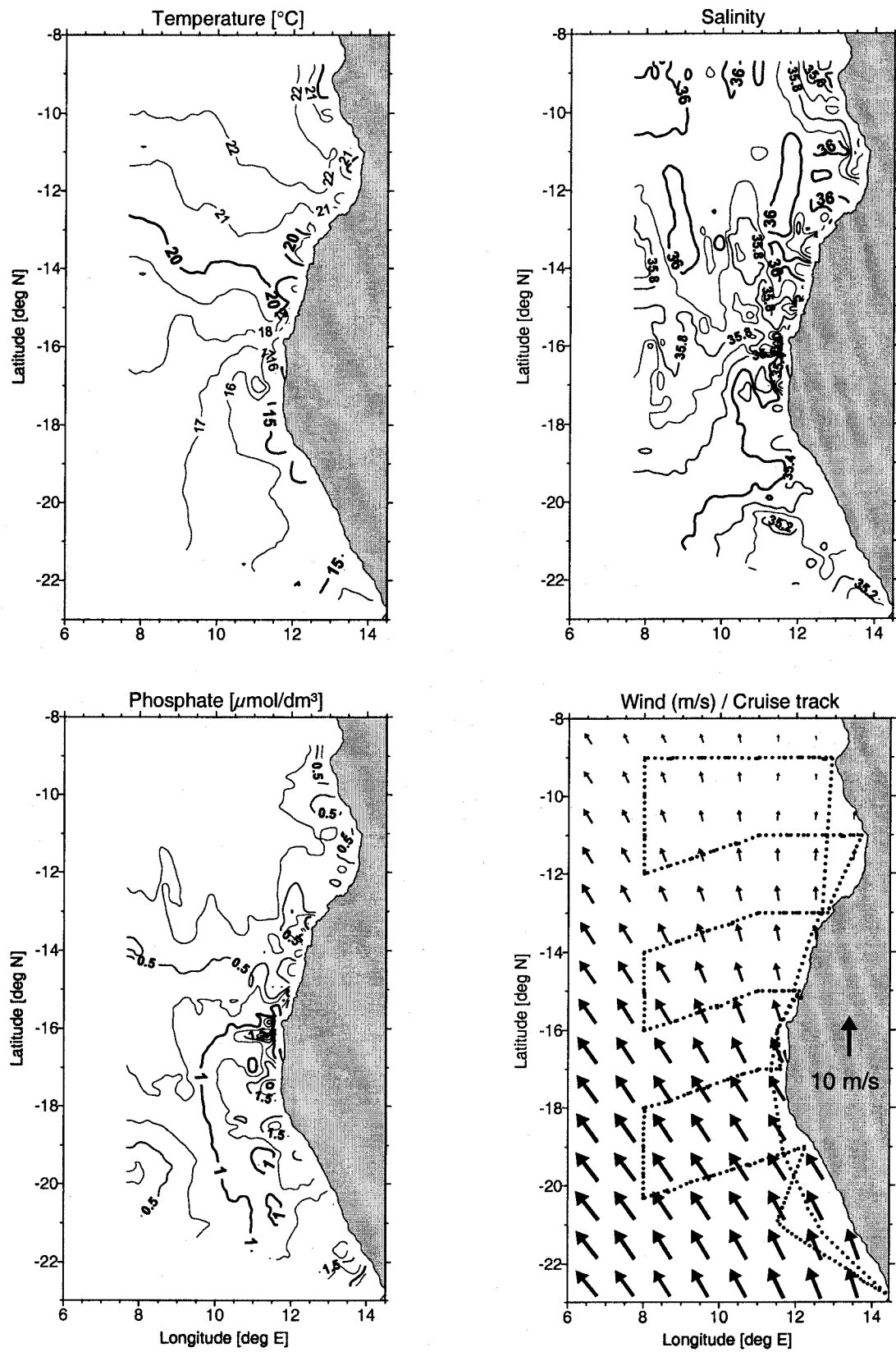


Figure 5.4: Sea surface temperature, salinity, phosphate and ERS-2 wind.

highest gradient was found in the ABFZ near 16° S. North of the front the salinity minima at the coast correspond to the observed local upwelling plumes which are visible in both the surface temperature and phosphate content. The total salinity minimum north of the ABFZ of 35.6 was observed in the coastal boundary layer off Luanda. At this location maximum values of silicate and cadmium were observed. This might be an indication of a water mass formed by mixing of subtropical surface water with upwelled SACW and Zaire river plume water. In the south the salinity distribution corresponds to the temperature signal with the lowest values in the upwelling area at the coast.

Additionally to the nutrient measurements with discrete CTD casts the phosphate content of the surface water has been measured quasi-continuously over the whole survey area with a temporal resolution of eight minutes concurrently with records of the thermosalinograph. The phosphate surface plot (Figure 5.4) points out clearly the frontal area. North of the ABFZ, the subtropical surface water masses were characterised by relative low phosphate concentrations ( $0.2 \mu\text{mol dm}^{-3}$ ). In the coastal areas north of the front smaller upwelling cells can be observed with concentrations of around  $0.5 \mu\text{mol dm}^{-3}$ , whereas the Benguela upwelling waters have phosphate concentrations higher than  $1.0 \mu\text{mol dm}^{-3}$ . It is worth to mention that phosphate concentrations never fall down to the detection limit. The phosphate patterns were well correlated with patterns of temperature and salinity (Figure 5.4).

The ERS-2 wind vectors averaged over the time of the cruise, correspond to the south east trade encountered in the whole area covered by the cruise. However, in the area of the ABFZ a separation occurs between low wind speeds in the north from higher wind speeds in the south. A map of the wind vectors extended towards the west reveals that the boundary zone between the low wind speeds in the Gulf of Guinea and the stronger south east trade winds stretches from the coast at about 16° S to the equator at about 10° W. Along this boundary zone the divergence of the Ekman transport in the surface layer drives open ocean upwelling.

### 5.2.2 The South Atlantic Central Water

The SACW is approximately found in the layer between the thermocline and about 600 m depth. In this layer downwelling is observed in a coastal boundary layer stretching between 9° S and 20.5° S. The width of the downwelling belt amounts to about 200 km and decreases gradually towards south, see Figure 5.7. Strongest downwelling is observed in the depth range of 100–300 m depth and is decreasing below. A broad band of upwelling is observed in the same depth range off the coast. The centre of this band is found at about 10° E on the southernmost section, from there it is gradually bending towards north west, and is crossing the western edge of the station grid at about 14° S, see Figure 5.24. The width of this upwelling band is about 400 km. There are several dome like elevations of isotherms (and isohalines) with horizontal scales of about 100 n.m in the SACW.

The SACW in the depth range between the lower rim of the thermocline and 600 m depth is characterised by oxygen depleted water. This water has oxygen concentrations of less than  $2 \text{ ml l}^{-1}$ . Water with oxygen concentrations below  $1 \text{ ml l}^{-1}$  was found between 500 m depth

and 200 m depth. The depth of the oxygen minimum was observed at 400 m north of the ABFZ and at about 250 m depth south of the front. Here patches of water were observed on the shelf containing oxygen concentration below  $0.5 \text{ ml l}^{-1}$ . Whereas the oxygen depleted water north of the ABFZ extended offshore beyond  $8^\circ\text{E}$ , the offshore extension of this water mass south of the ABFZ was confined to a coastal boundary layer of about 200 km width. The same, but inversed, pattern was observed for the distribution of the nutrients in this depth range, see section 5.3.1.

The observed oxygen and nutrient distribution in the SACW suggests that oxygen consumption and conversion of nutrients by remineralization of sinking particulate organic matter is important in the whole area. Ventilation of the water by cross shore circulation, consisting of the deep compensation current of the Ekman offshore current in the surface layer, causes the narrowing of the oxygen depleted water mass south of the ABFZ. Simultaneously, this advection transports water of lower nutrient concentration from the open ocean into the coastal boundary zone. Moreover, a great supply of nutrients and a weak ventilation of the deep water on the shelf south of the ABFZ is caused by the poleward advection associated with the upwelling undercurrent from the pool of nutrient enriched and of oxygen depleted SACW located north of the front.

The westmost stations of each section are aligned at  $8^\circ\text{E}$  along a meridional section from  $9^\circ\text{S}$  to  $20.5^\circ\text{S}$ . It represents the offshore conditions at the western edge of the investigated area. The temperature in the surface layer shows there a weak north-south gradient between the subtropical surface water with  $23^\circ\text{C}$  off Angola and the warmed Benguela upwelling water of  $17^\circ\text{C}$  at  $20.5^\circ\text{S}$ . At this longitude there is no clear indication of the Angola-Benguela Frontal Zone. Below the thermocline no well defined meridional temperature gradient is found in the South Atlantic Central Water. However, the low oxygen content of the SACW ends abruptly at about  $18^\circ\text{S}$  and higher oxygen content is found in the same depth range south of  $19^\circ\text{S}$ . Here, a meridional gradient of temperature and salinity is observed as well in the depth range between the thermocline and at least 200m depth. There are several dome like elevations of isotherms (and isohalines) with horizontal scales of about 100 n.m in the SACW. The most prominent one is located at  $14^\circ\text{S}$ . The VMADCP data show an eddy like current pattern in this area. The comparison with climatological data sets will show whether these features are transient phenomena or are found repeatedly at similar positions. The only large scale signal in the temperature below the thermocline is a southward decreasing temperature in the AAIW.

### 5.2.3 The Antarctic Intermediate Water

The core of AAIW, represented by the salinity minimum, is found in the whole investigated area at 800 m depth. The salinity of the core of the AAIW is slightly decreasing southward. Simultaneously, the oxygen content of the core water is increasing toward the south. Downwelling is observed in a 200 km wide coastal boundary layer between  $16^\circ\text{S}$  and  $9^\circ\text{S}$ .

### 5.2.4 The North Atlantic Deep Water

The upper rim of the NADW is found in 1200 m depth. Here the pattern of the distribution of temperature, salinity, and oxygen are characterised by gradients aligned roughly parallel to topography. Temperature and salinity both are decreasing from north to south whereas oxygen is increasing into this direction.

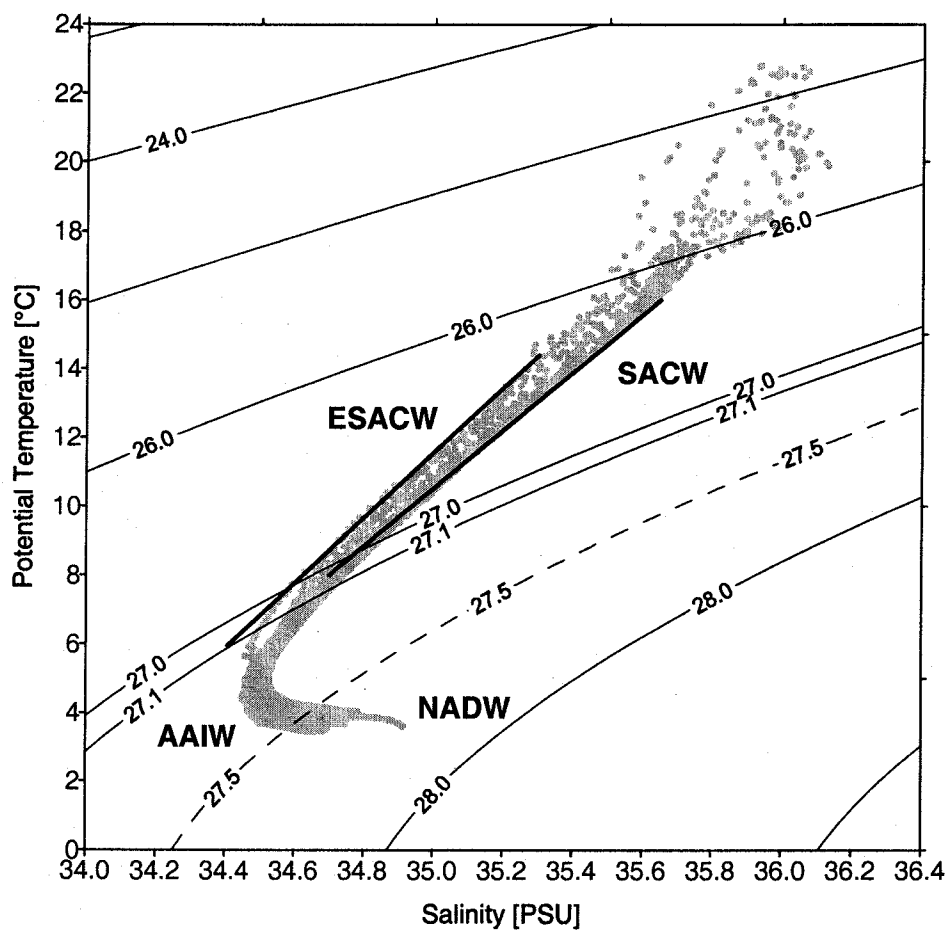


Figure 5.5: T - S diagram of all CTD measurements.

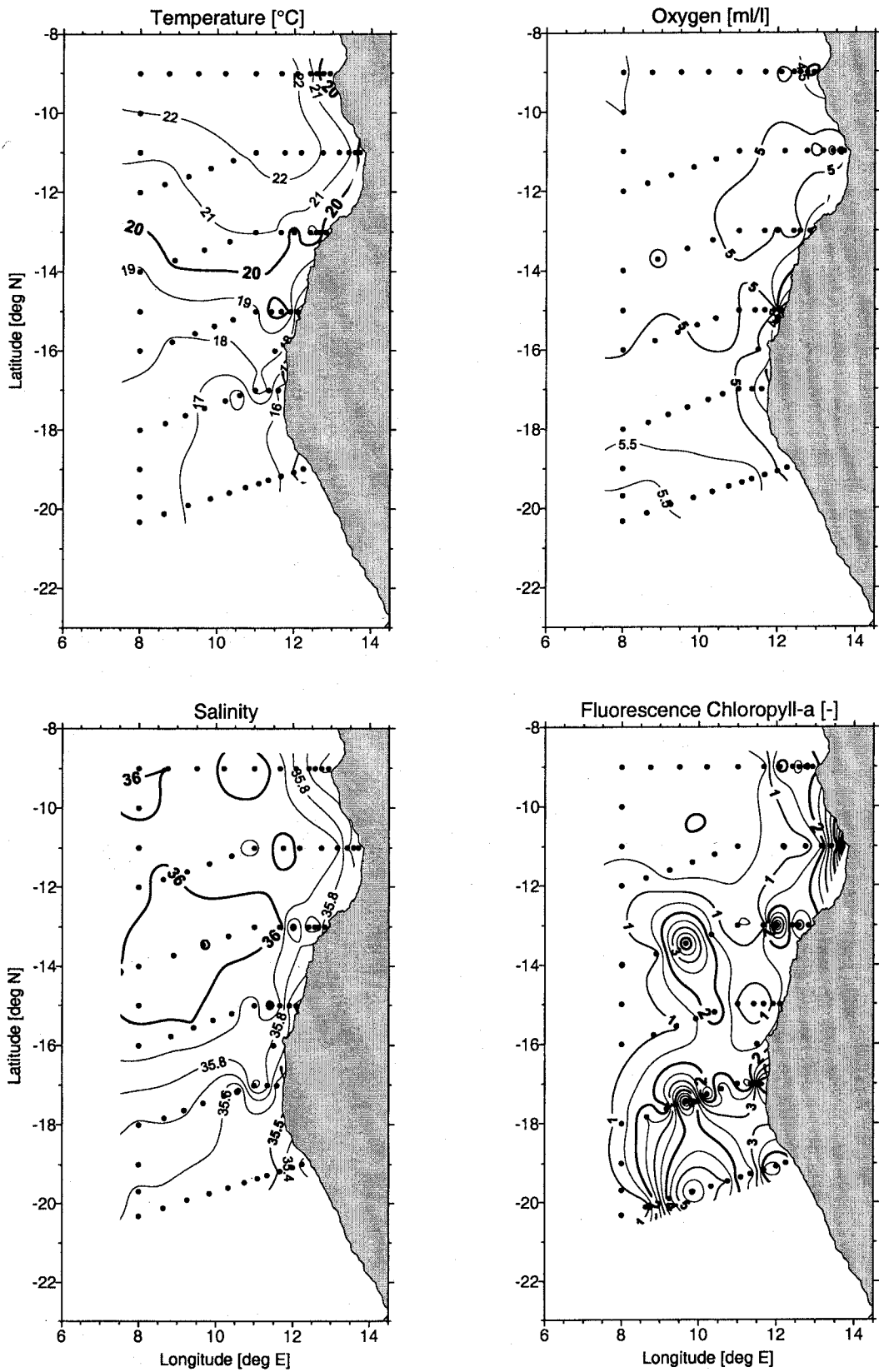


Figure 5.6: Horizontal distribution of T, S, O<sub>2</sub> and Chl.a-fluorescence at 0 m depth.

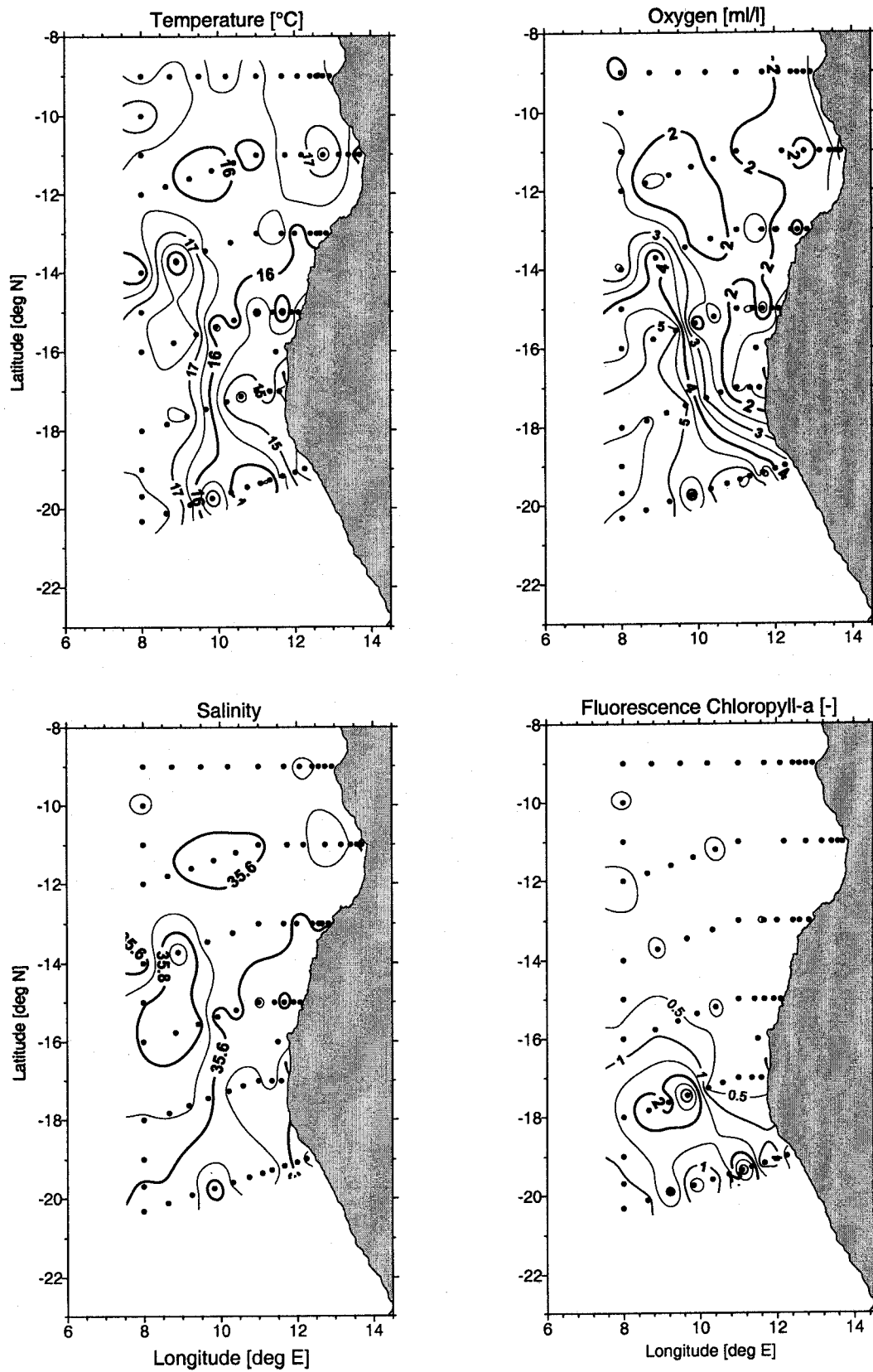


Figure 5.7: Horizontal distribution of T, S, O<sub>2</sub> and Chl.a-fluorescence at 50 m depth.

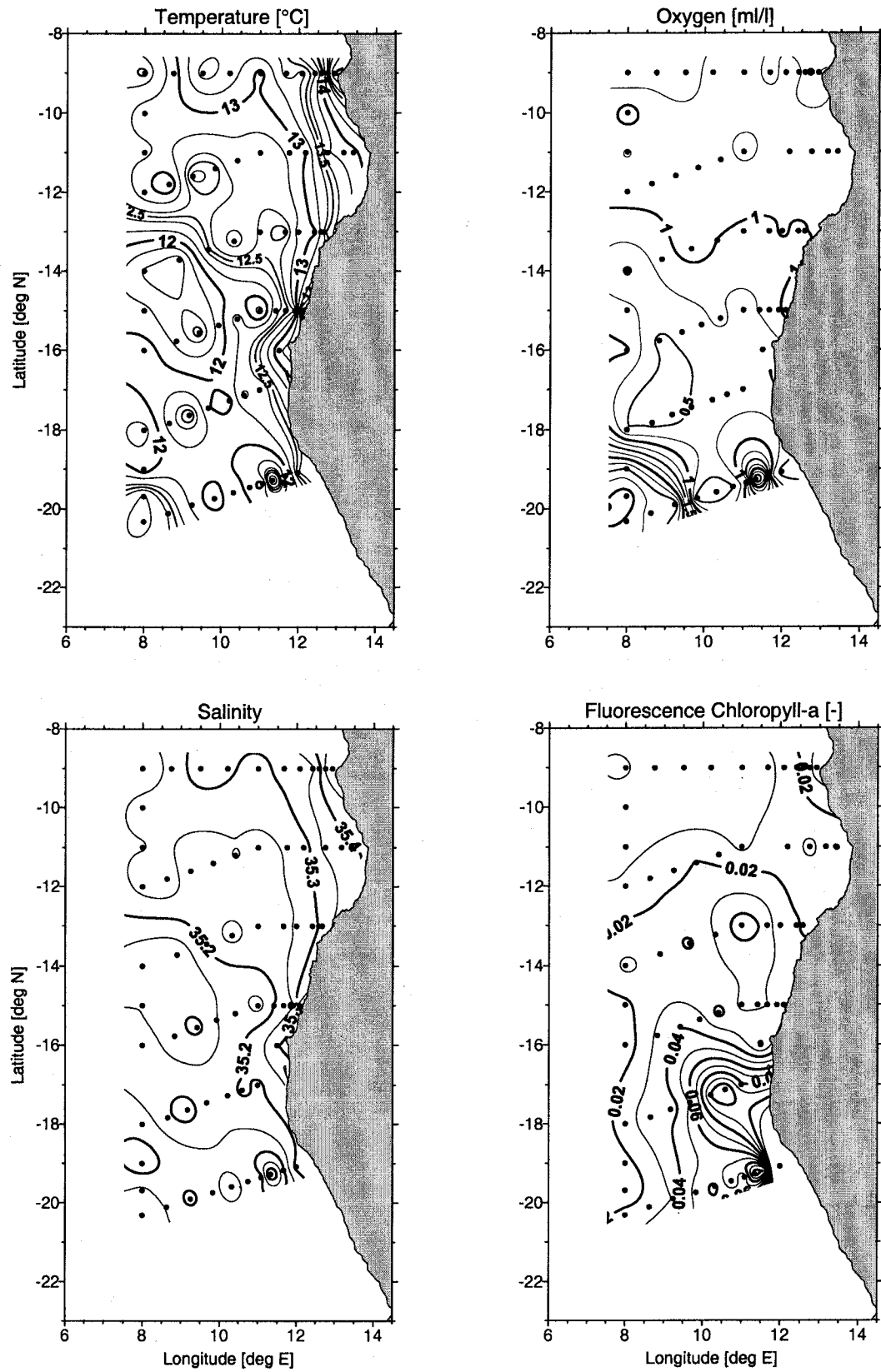


Figure 5.8: Horizontal distribution of T, S,  $O_2$  and Chl.a-fluorescence at 200 m depth.

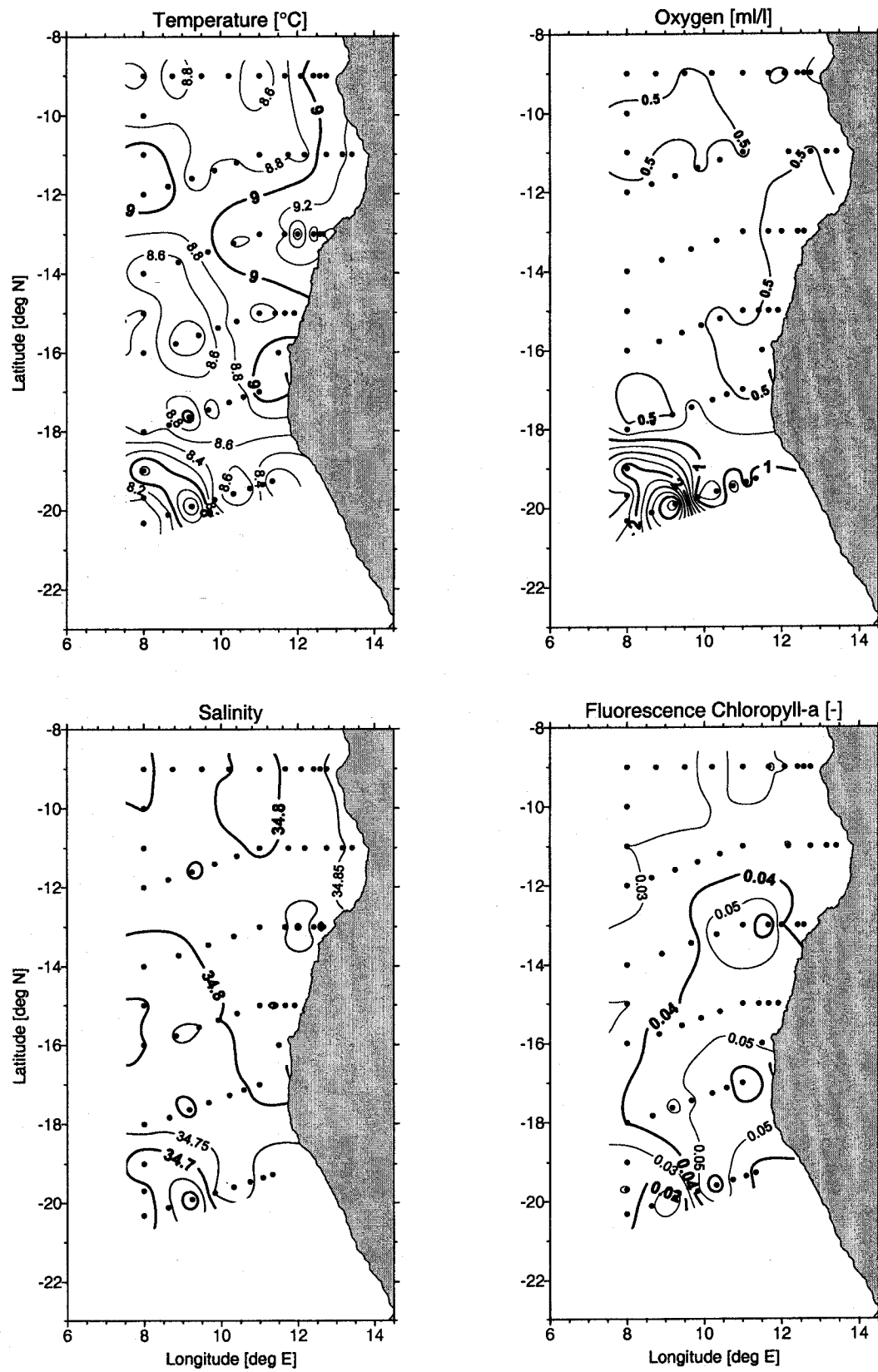


Figure 5.9: Horizontal distribution of T, S, O<sub>2</sub> and Chl.a-fluorescence at 400 m depth.

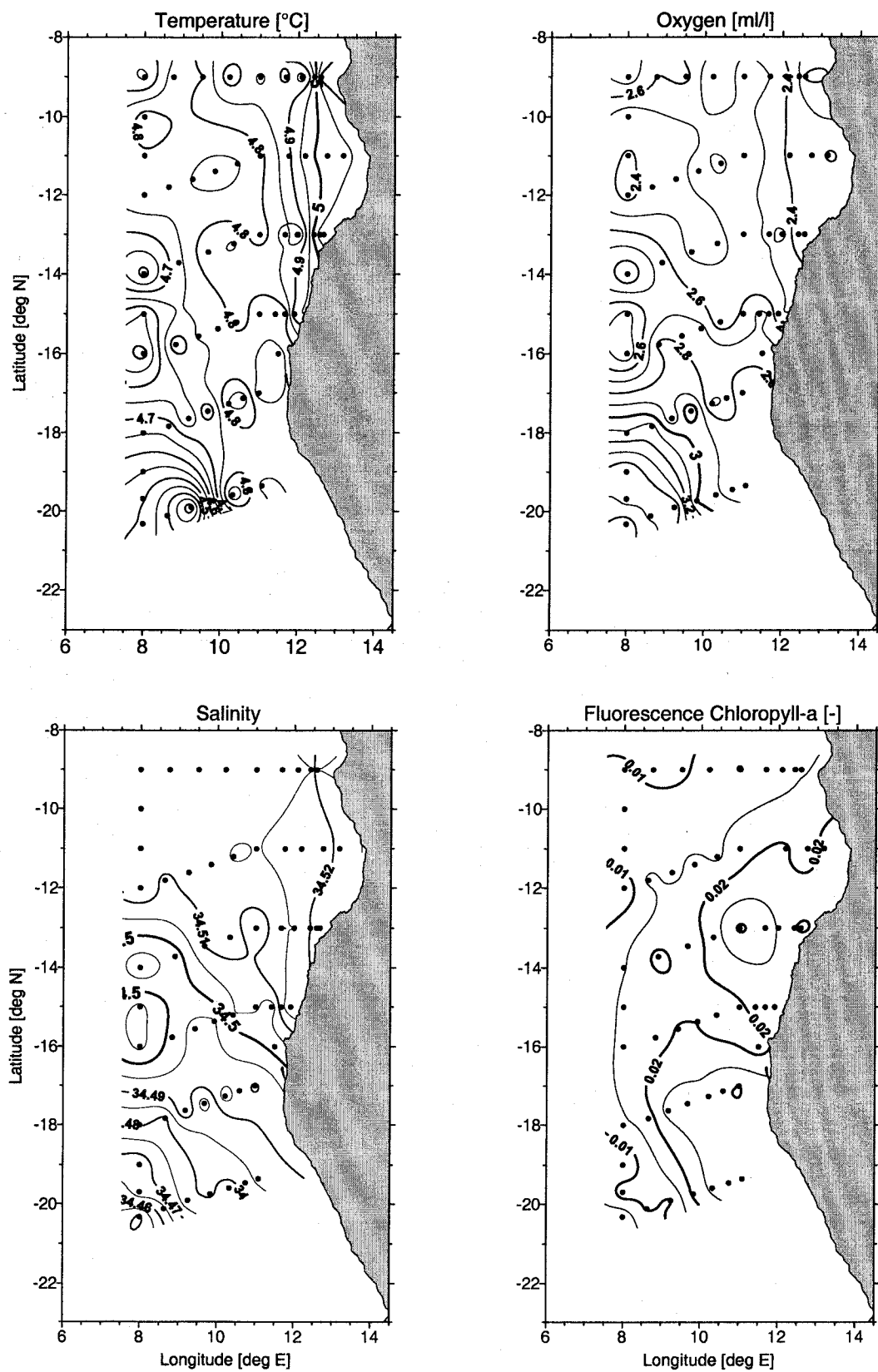


Figure 5.10: Horizontal distribution of T, S, O<sub>2</sub> and Chl.a-fluorescence at 800 m depth.

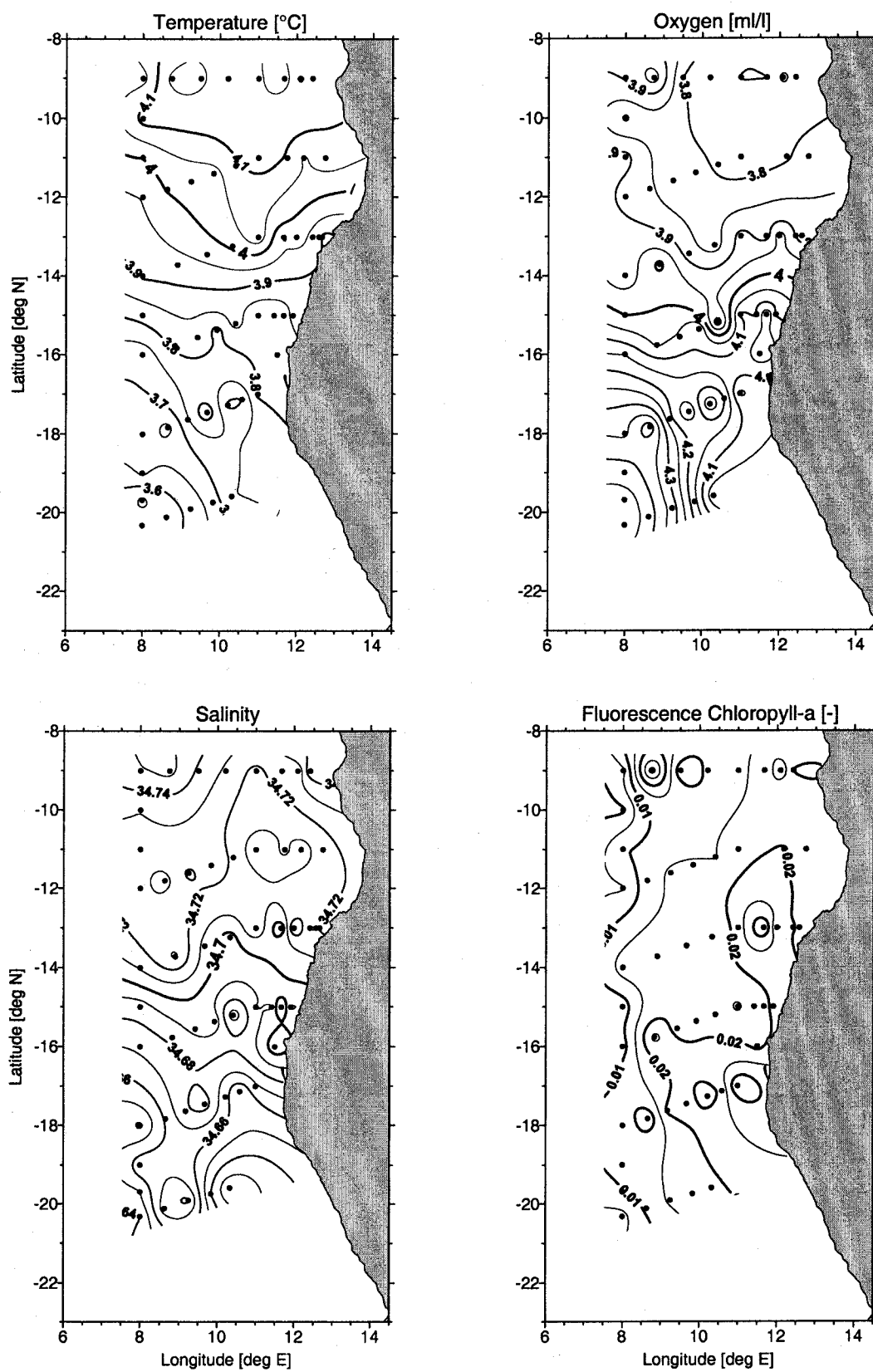


Figure 5.11: Horizontal distribution of T, S, O<sub>2</sub> and Chl.a-fluorescence at 1200 m depth.

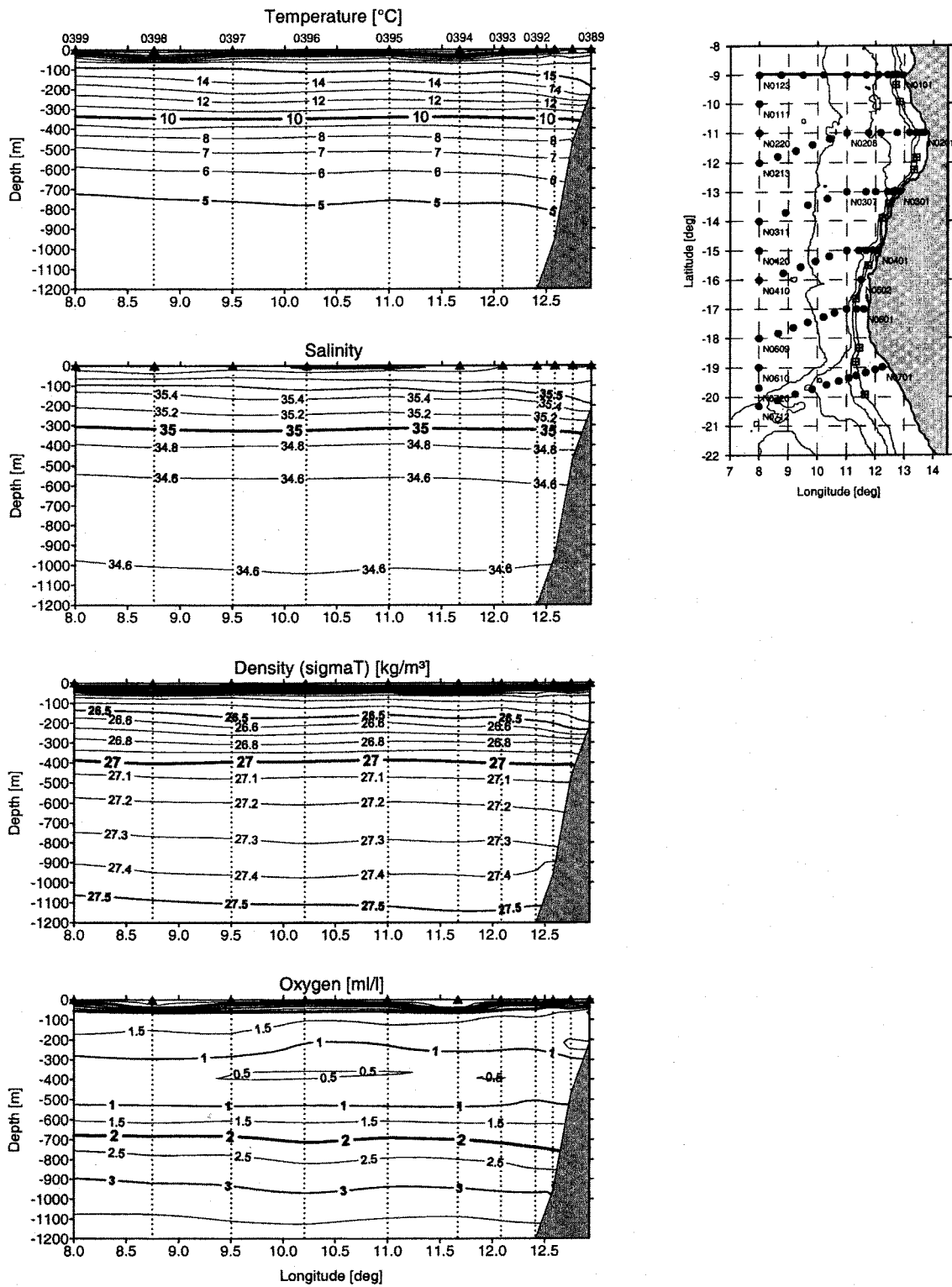


Figure 5.12: Section 01 vertical distribution of T, S,  $\sigma$  and  $O_2$  (0-1200 m).

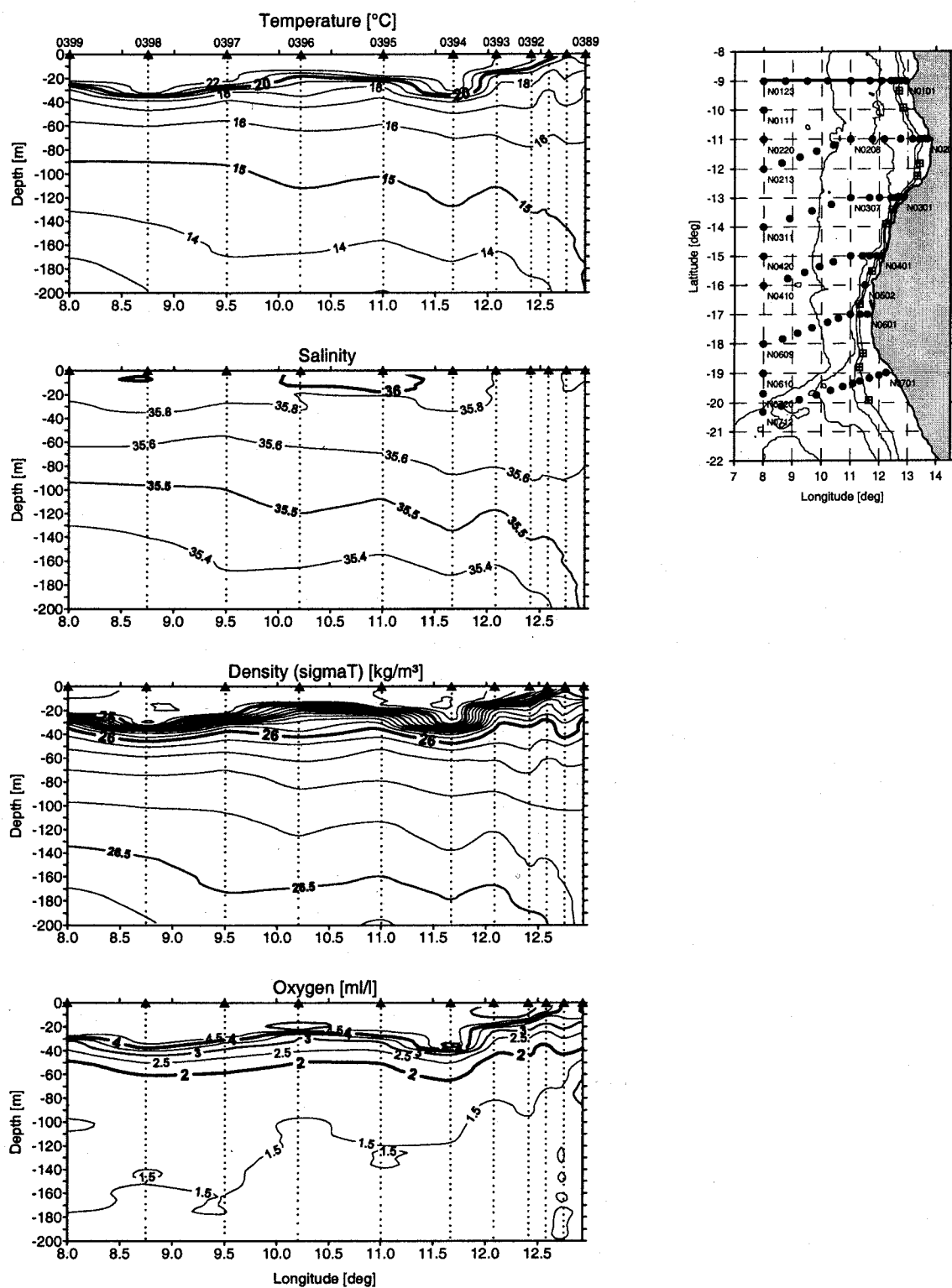


Figure 5.13: Section 01 vertical distribution of T, S,  $\sigma$  and  $O_2$  (0-200 m)

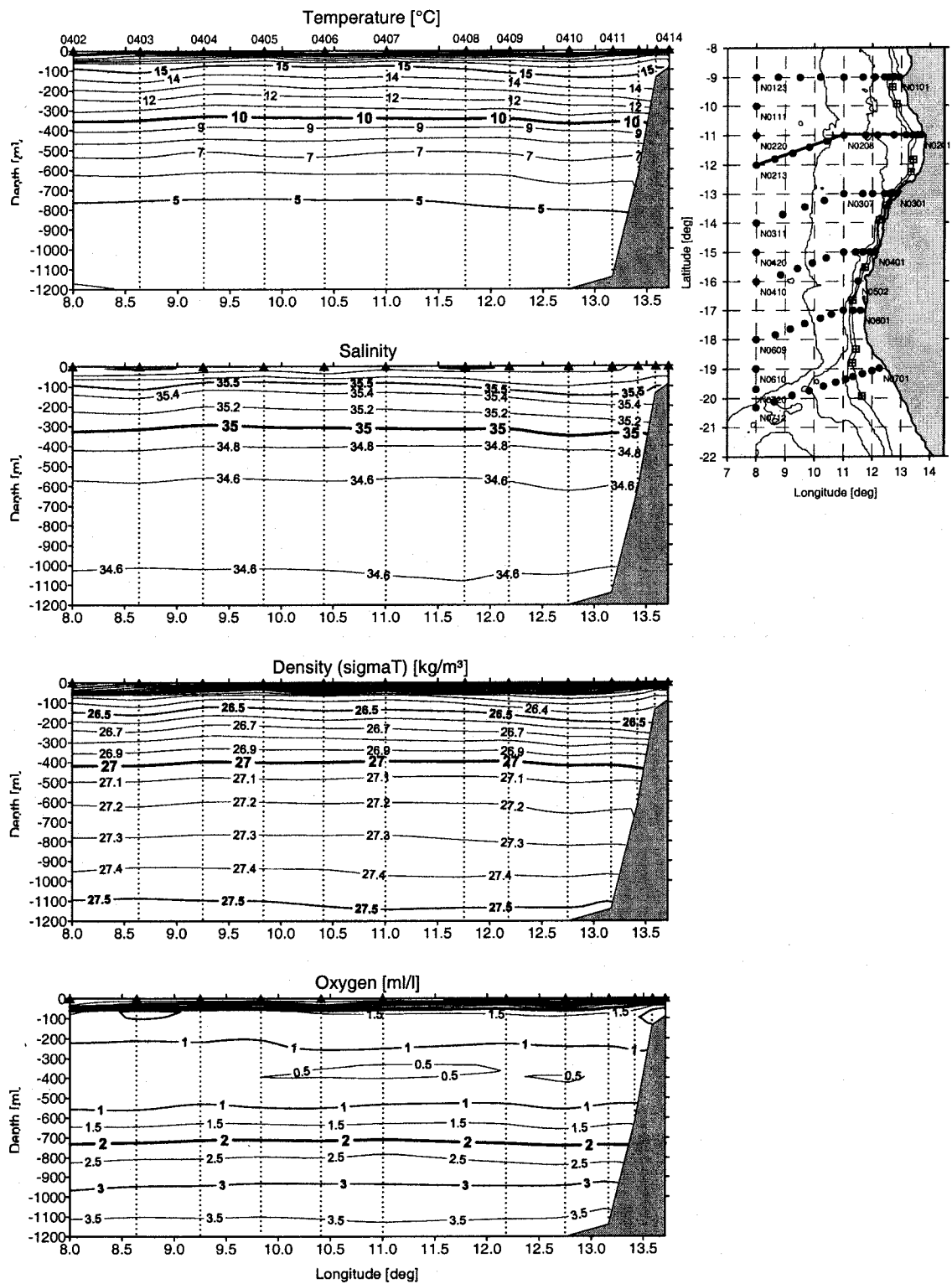


Figure 5.14: Section O2 vertical distribution of T, S,  $\sigma$  and  $O_2$  (0-1200 m):



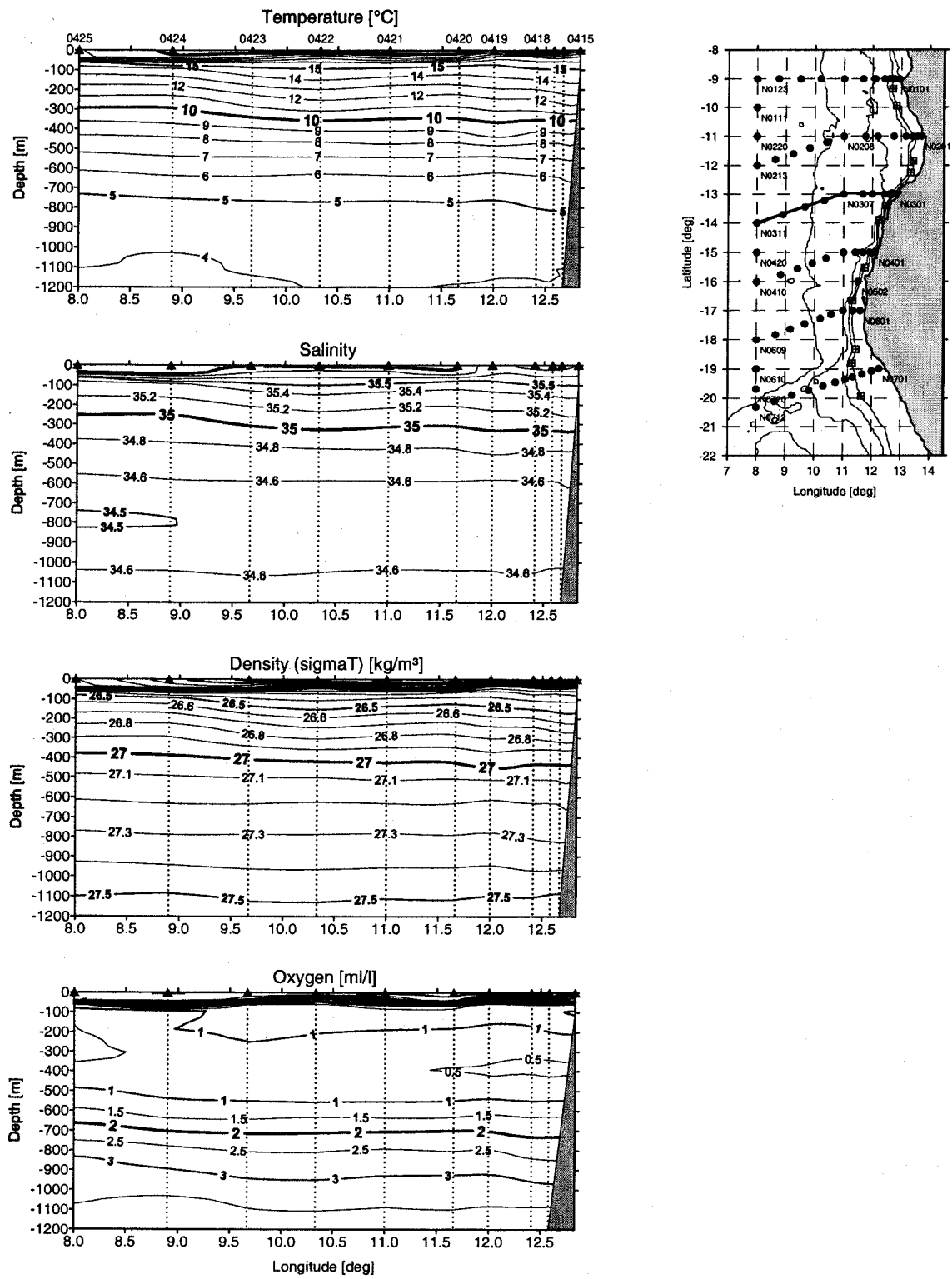


Figure 5.16: Section 03 vertical distribution of T, S,  $\sigma$  and O<sub>2</sub> (0-1200 m).

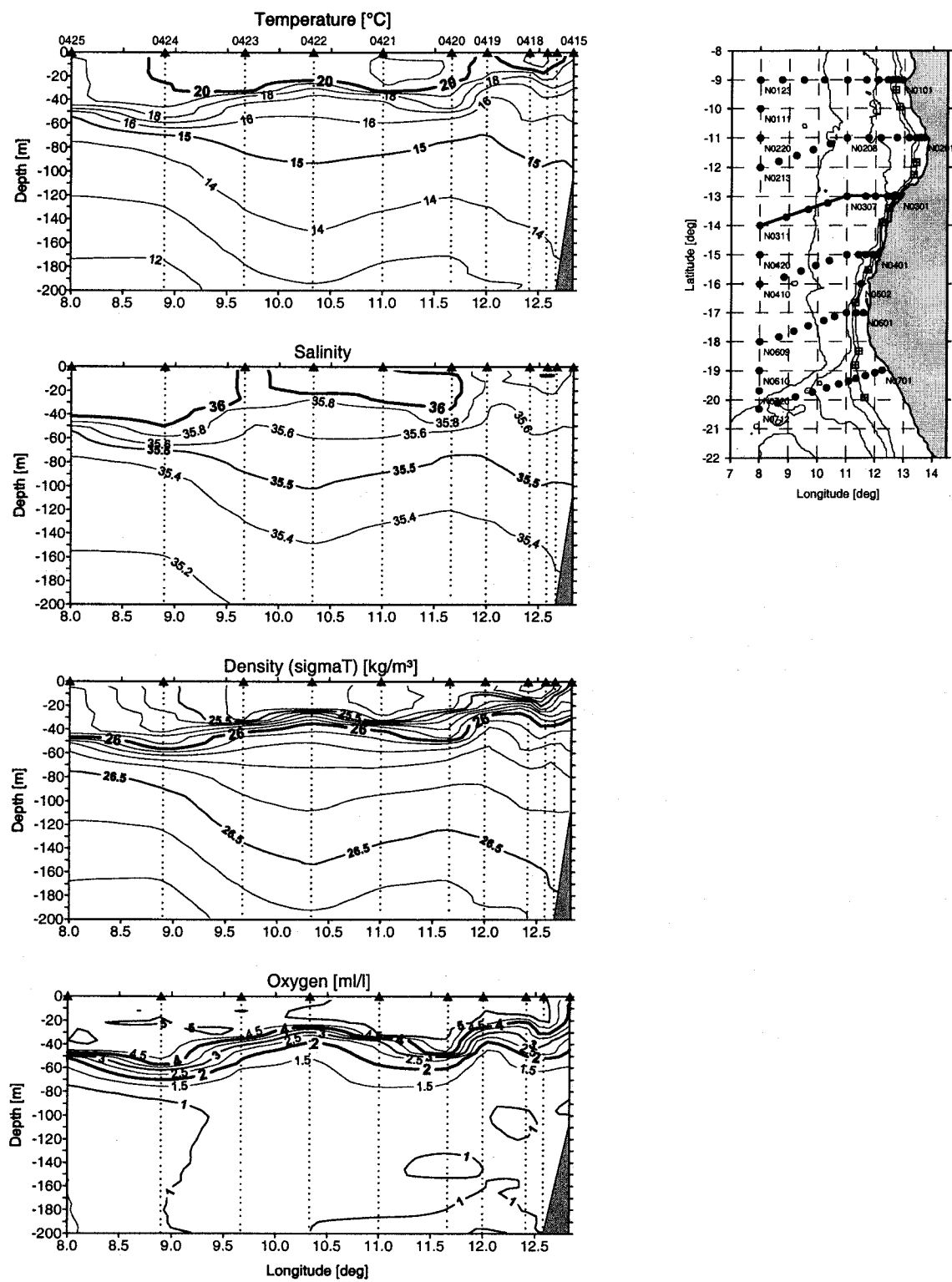


Figure 5.17: Section 03 vertical distribution of T, S,  $\sigma$  and O<sub>2</sub> (0-200 m)

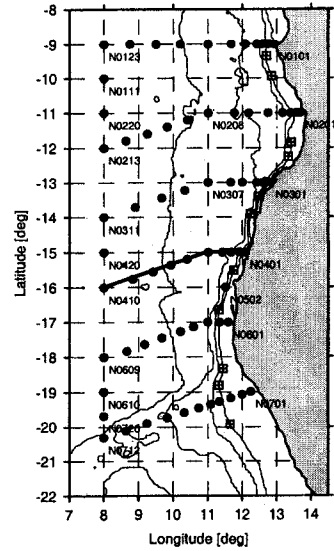
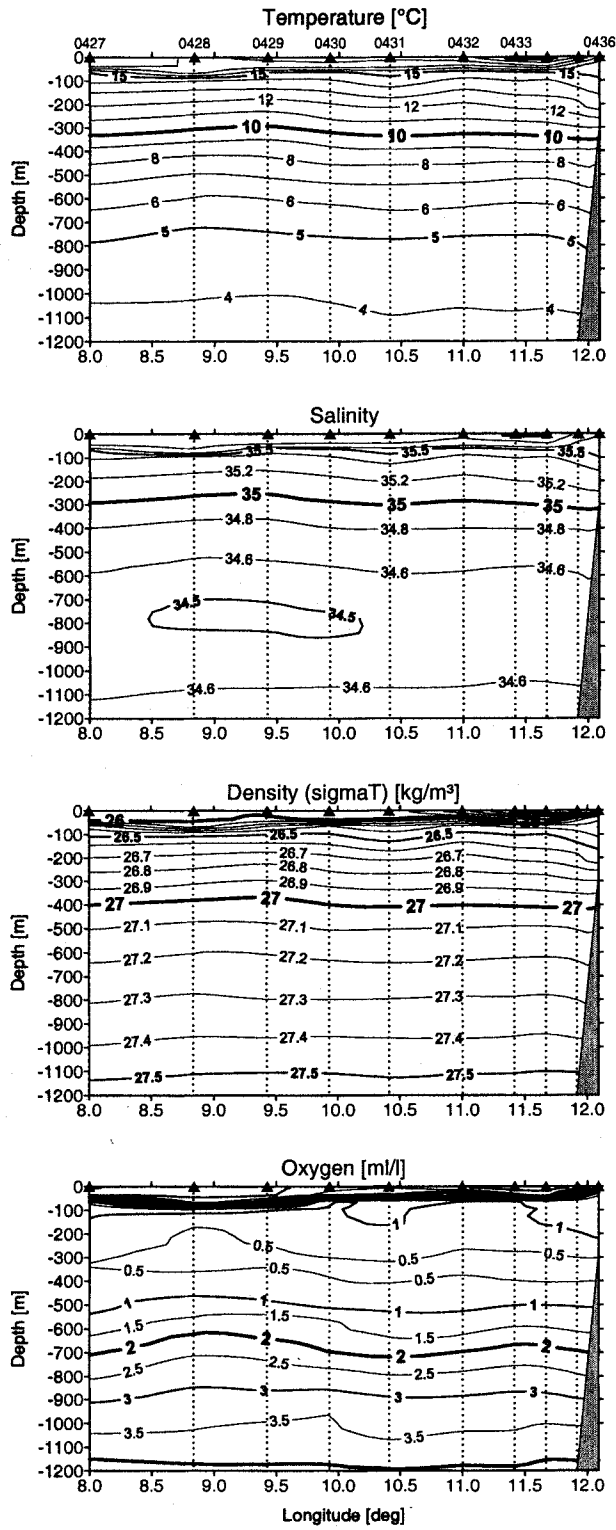


Figure 5.18: Section 04 vertical distribution of T, S,  $\sigma$  and O<sub>2</sub> (0-1200 m).

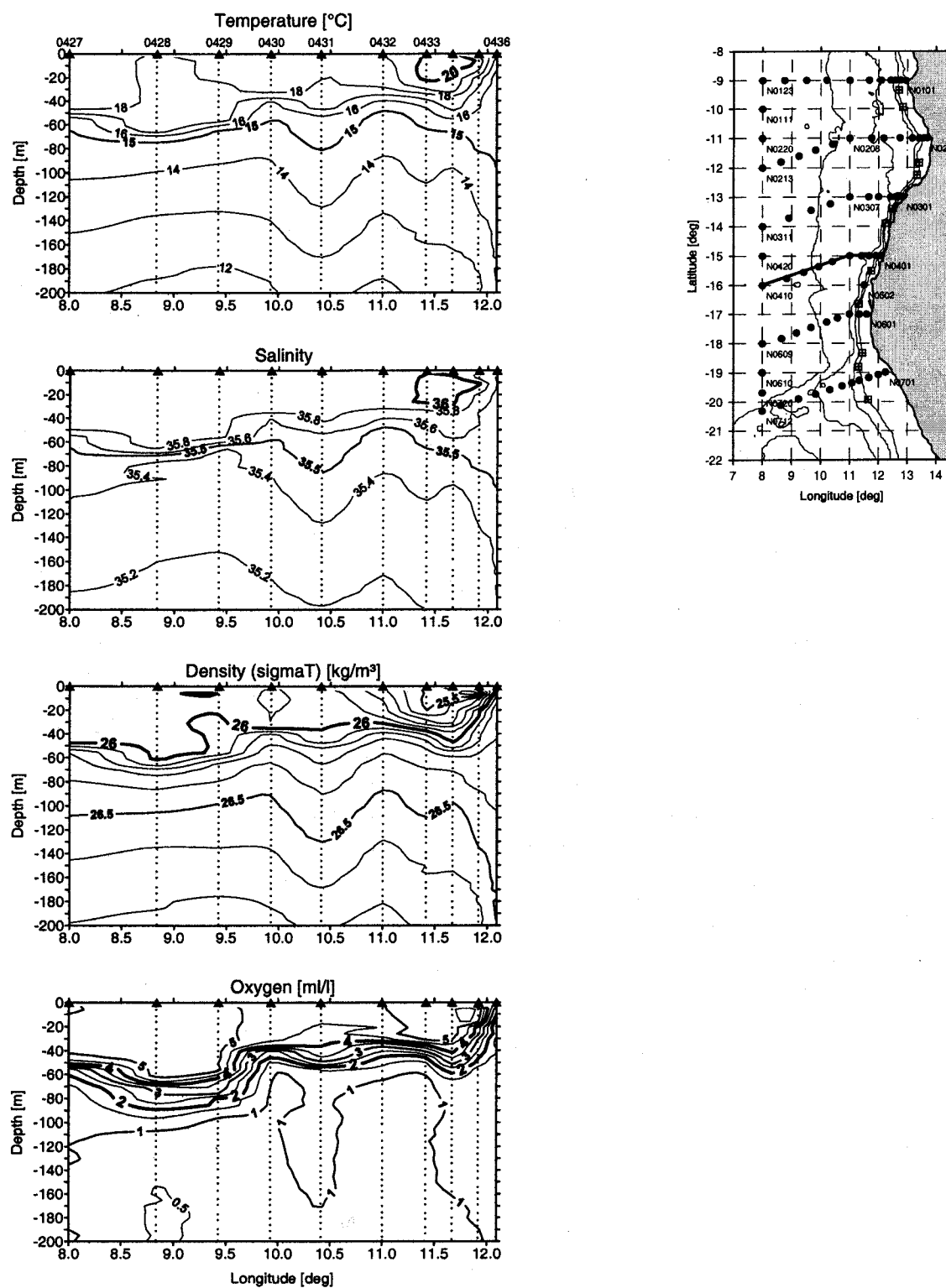


Figure 5.19: Section 04 vertical distribution of T, S,  $\sigma$  and O<sub>2</sub> (0-200 m)

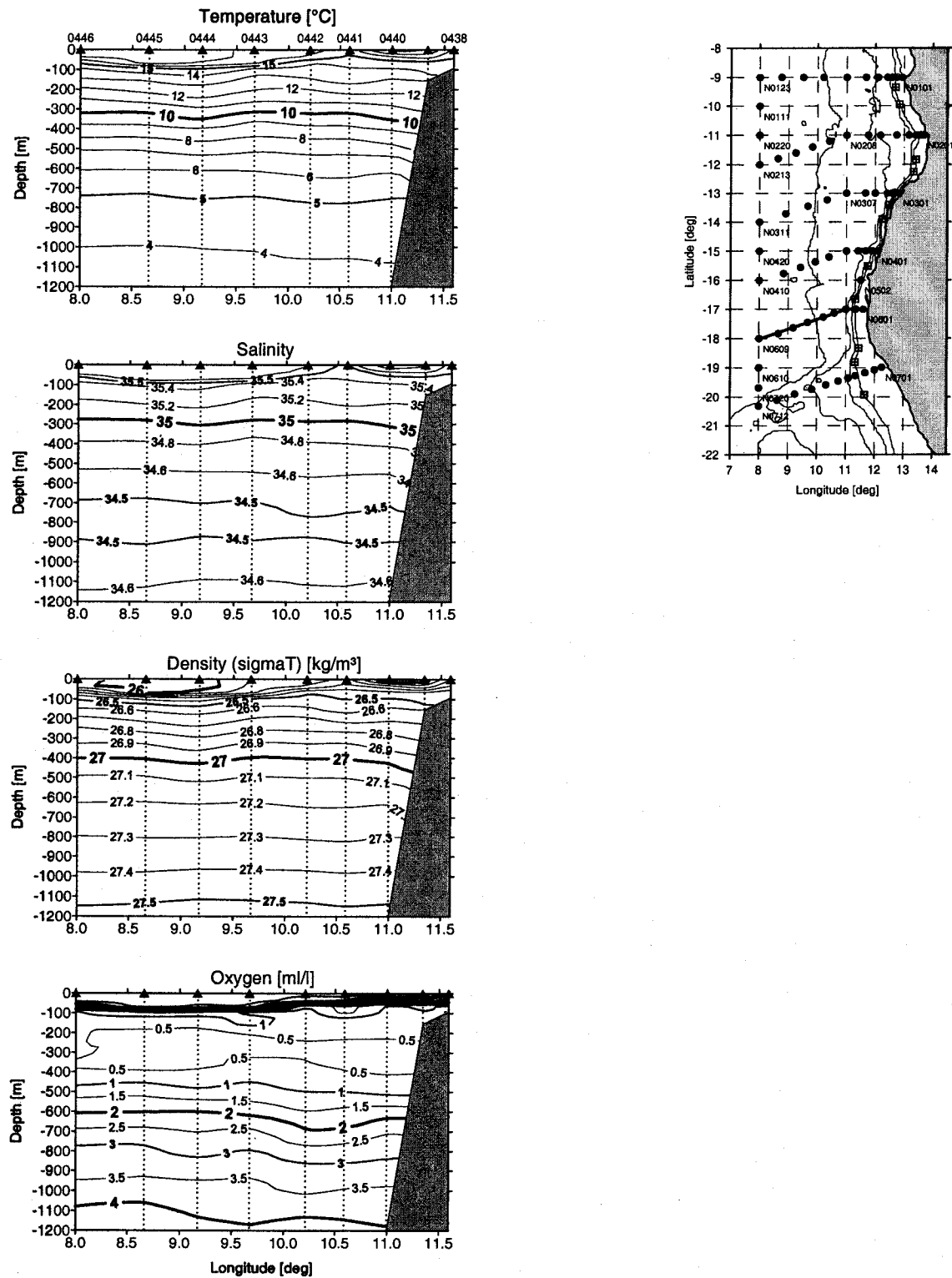


Figure 5.20: Section 05 vertical distribution of T, S,  $\sigma$  and  $O_2$  (0-1200 m).

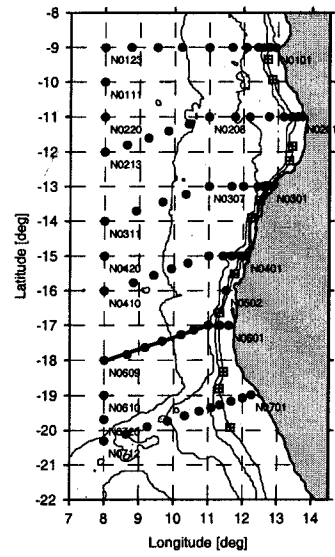
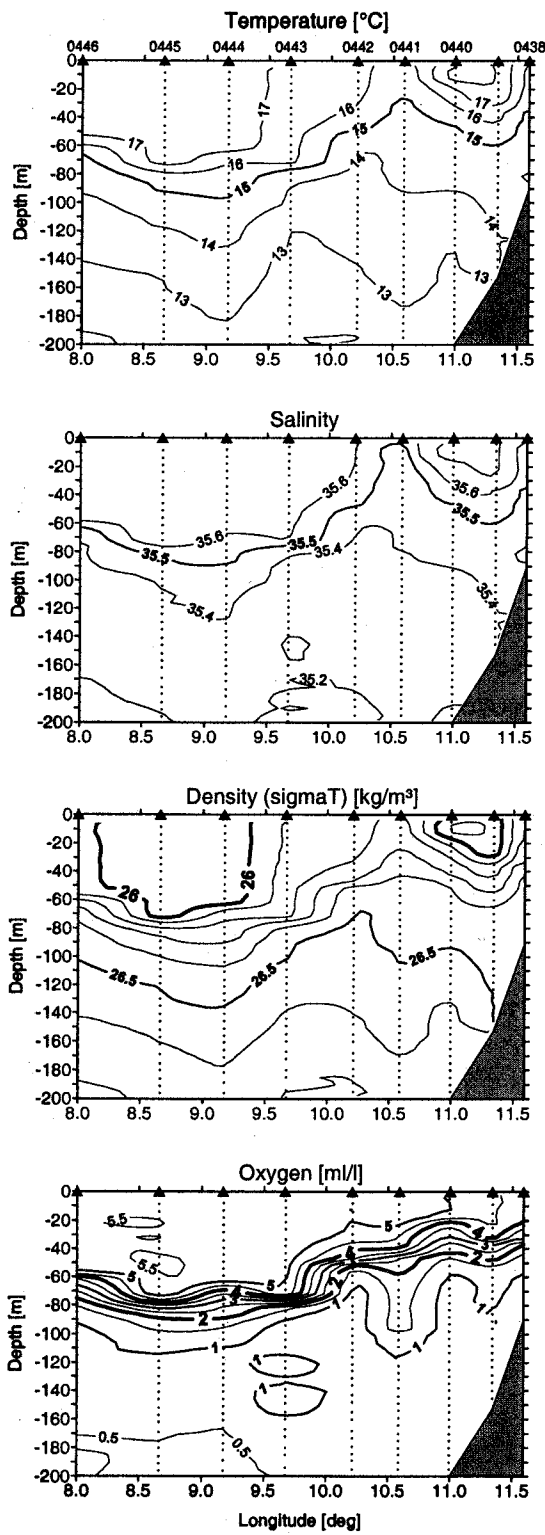


Figure 5.21: Section 05 vertical distribution of T, S,  $\sigma$  and O<sub>2</sub> (0-200 m)

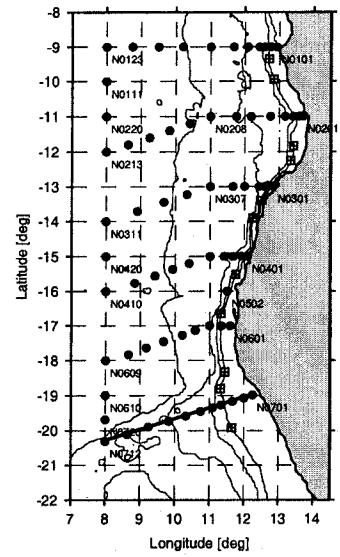
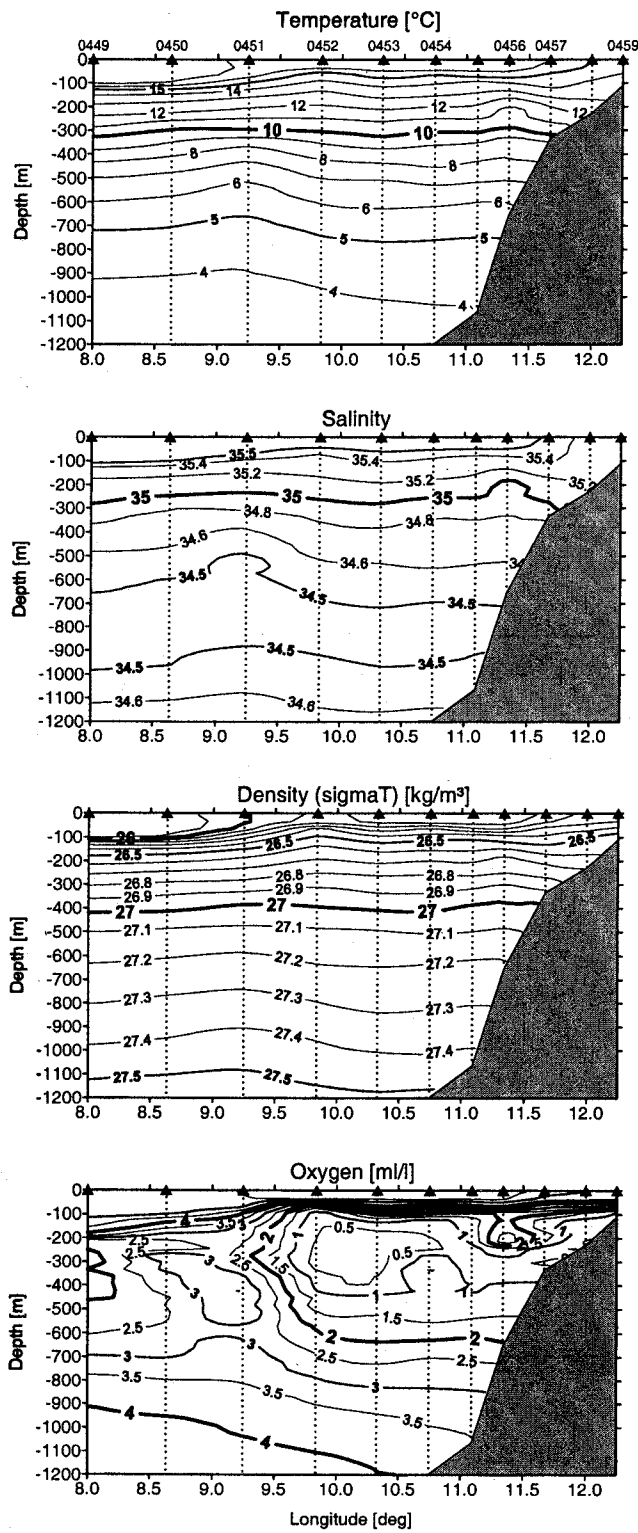


Figure 5.22: Section 06 vertical distribution of T, S,  $\sigma$  and O<sub>2</sub> (0-1200 m).



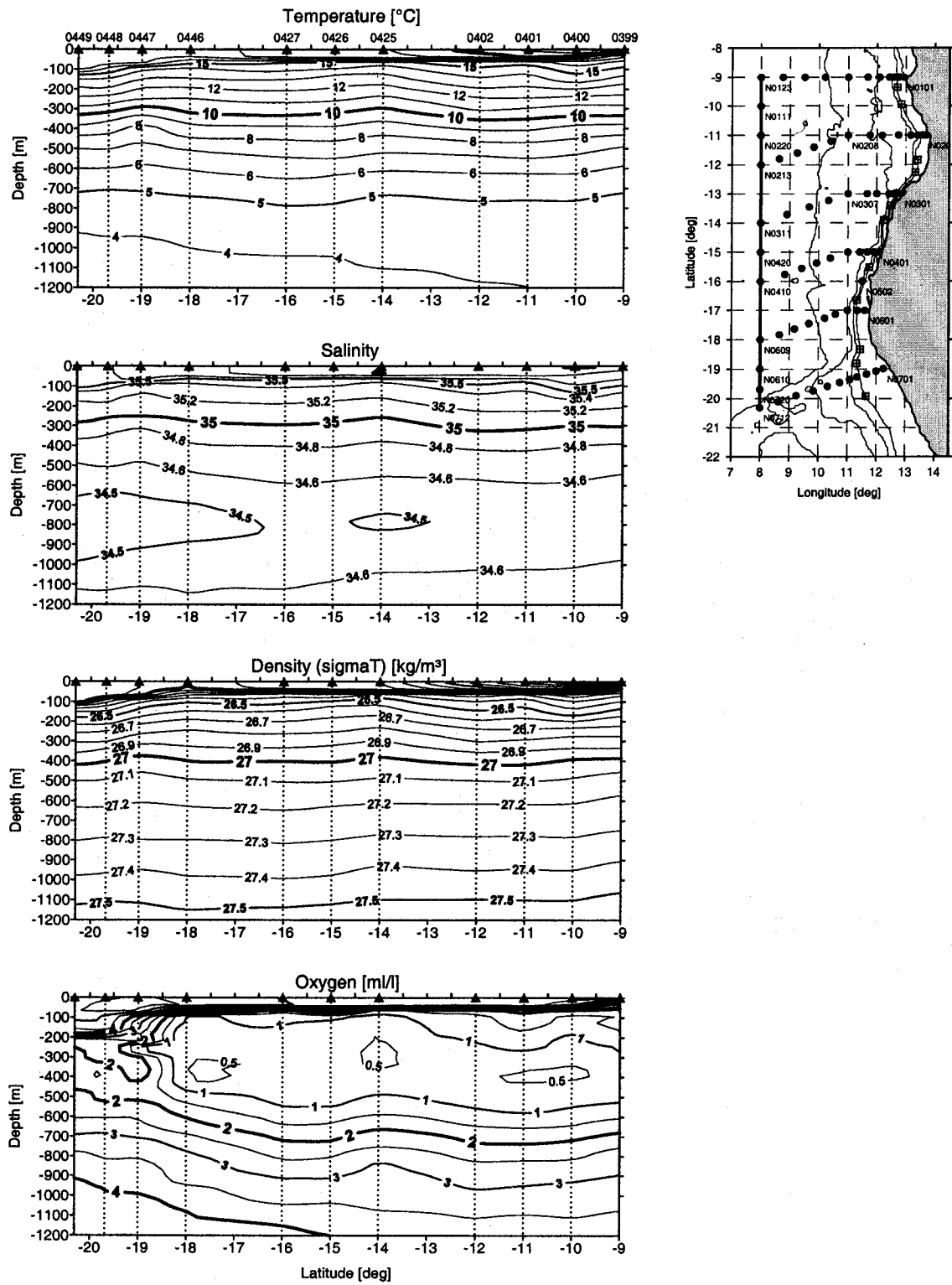


Figure 5.24: Section 10 vertical distribution of T, S,  $\sigma$  and  $\text{O}_2$  (0-1200 m).

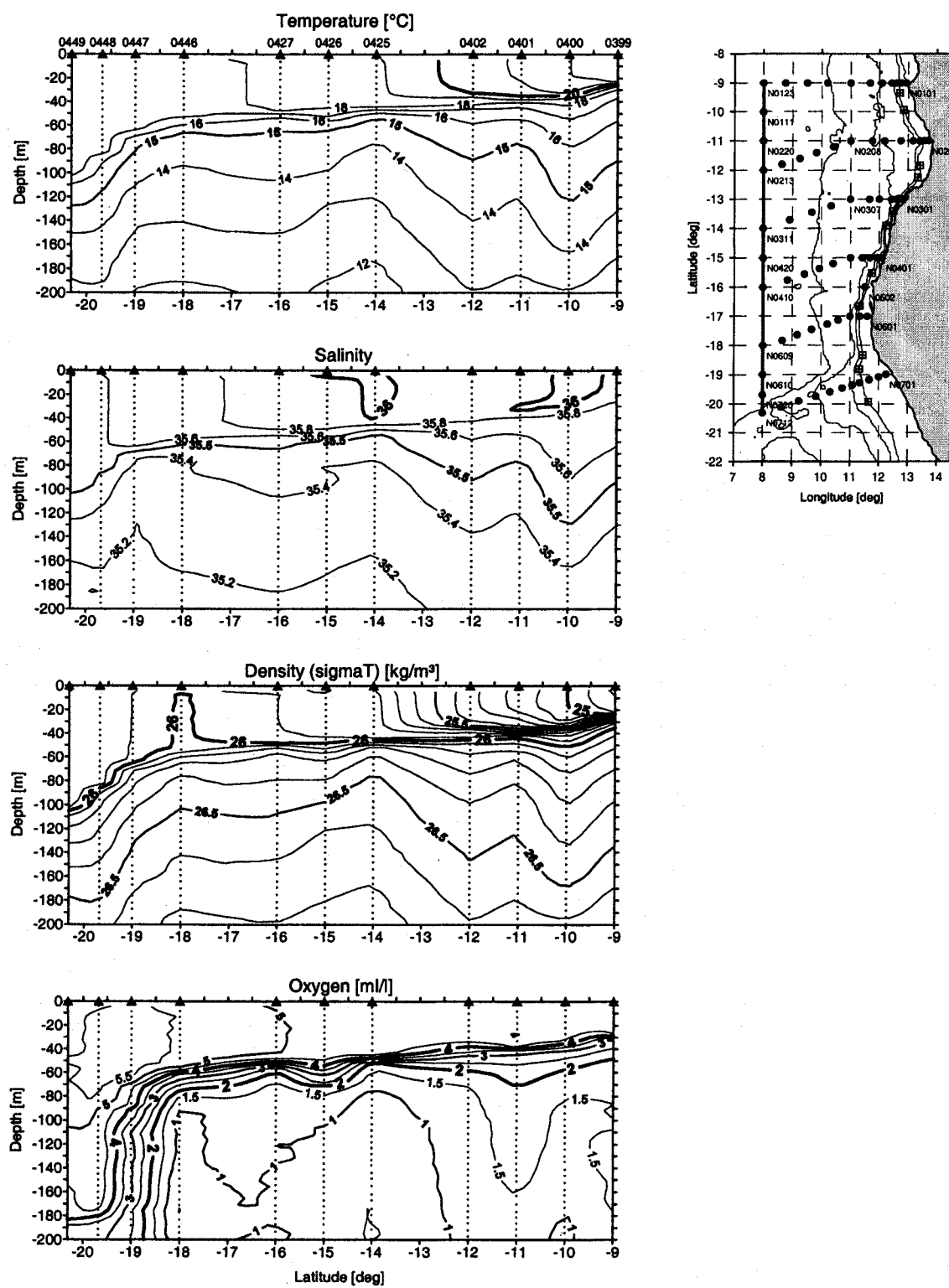


Figure 5.25: Section 10 vertical distribution of T, S,  $\sigma$  and  $O_2$  (0-200 m)

### 5.2.5 Currents

The changes of the tracks of the deployed surface drifter are representative for the current in the surface layer (Figure 5.26). The drifter released in the area of the Angola Gyre (C) did reveal no significant mean motion in September and October 2000. However, inertial oscillations with a period of about 3.1 day and an amplitude varying between 10 to 30  $\text{cm s}^{-1}$  are clearly seen. The drifter released in the Angola current (B) moved from its start southward on the shelf until it turned westward during mid November at the latitude of 22° S. Its track along the shelf edge between 13° - 16° S was effected by anticyclonic small scale eddies. The monthly mean speed in the Angola current varied between 10 and 17  $\text{cm s}^{-1}$ . According to the water temperature measured by this drifter, it turned west well south of the ABFZ in Benguela upwelling water. The mean monthly speed reduced from 12 to 4  $\text{cm s}^{-1}$  along its track toward west. The drifter released on the shelf south of the ABFZ (A) moved westward from the very beginning with a speed changing between 4 - 11  $\text{cm s}^{-1}$ . The drifter tracks in the south exhibit well developed inertial oscillations. Interestingly, the Benguela current drifter moved even westward in October 2000 when the Angola current drifter moved southward at the same latitude some 50 km east of it. This provides the information that the width of the Angola current did not exceed 150 km offshore.

The currents measured by both the vessel mounted and the lowered ADCP provide reliable results at depths below the mixed layer. One has to keep in mind that their measurements are momentary superpositions of geostrophic and non-geostrophic currents, and that both have a speed being of the same order. Generally, the current velocity is decreasing with depth and amounts to a few  $\text{cm s}^{-1}$  in 1200 m depth. In the depth range of the SACW the most coherent pattern of the current is the Angola current stretching southward along the shelf at least to 22° S. The vertical extent of the Angola current is as deep as 300 m. The current direction measured in the depth range of the SACW along the northern sections at 9° S and 11° S is predominantly toward east, except for the coastal boundary layer, where the Angola current flows southward. This eastward directed current could be a representation of the South Equatorial Counter Current. On the sections south of 11° S no clear picture emerges.

Obviously, the weak mean currents are masked as well by ageostrophic currents as by mesoscale geostrophic eddies with a radius of the order of 100 km. Taking this uncertainty into account the observed current field below the thermocline in the central and southern parts of the studied area are not in contradiction to the path of the ridge in the stratification obviously caused by open ocean upwelling. According to these measurements the current should tend to circulate cyclonally around the ridge, i.e. northward and westward to the west and south of the ridge, and southward and eastward to the east and north of the ridge.

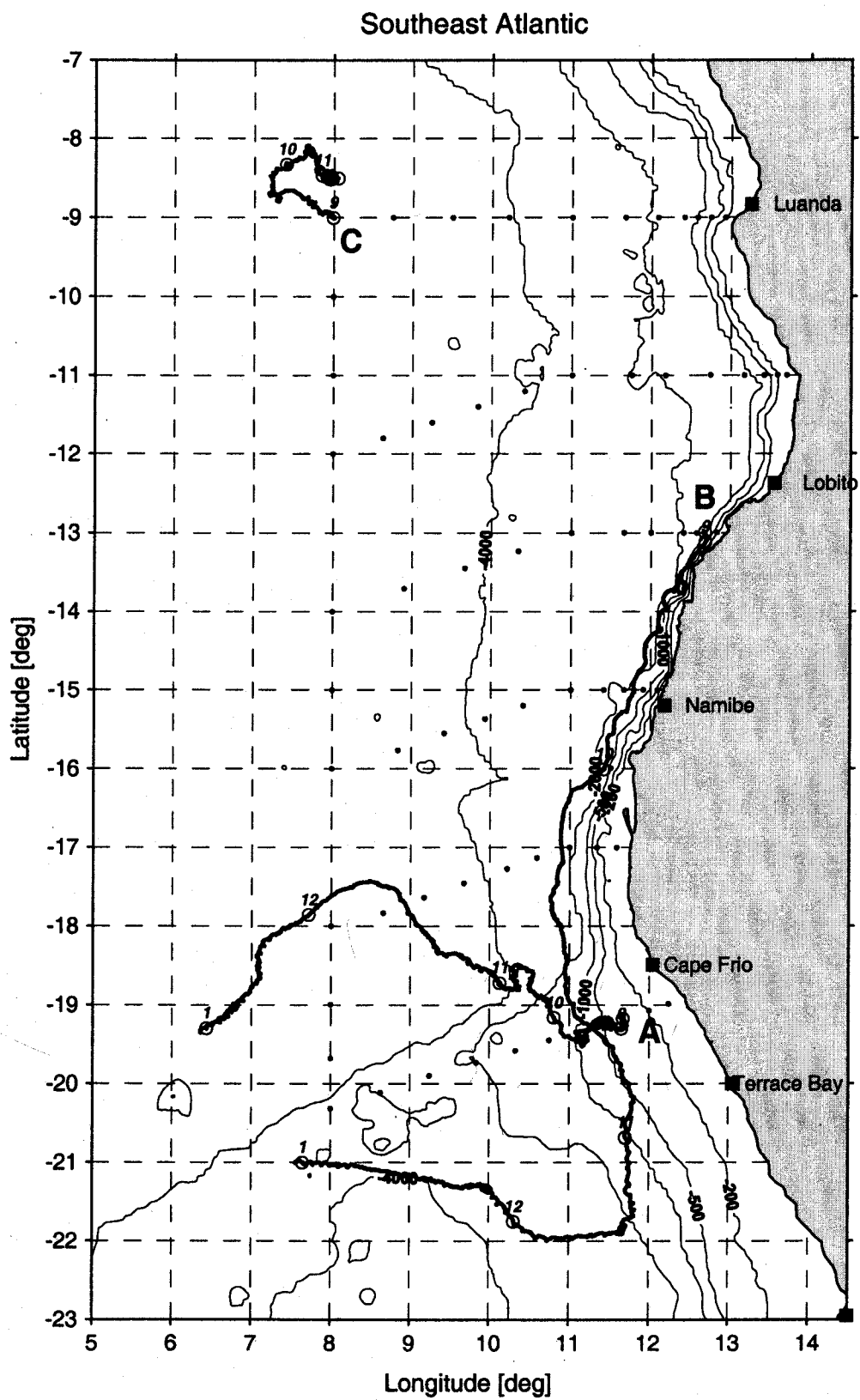


Figure 5.26: Tracks of released ARGOS drifter.

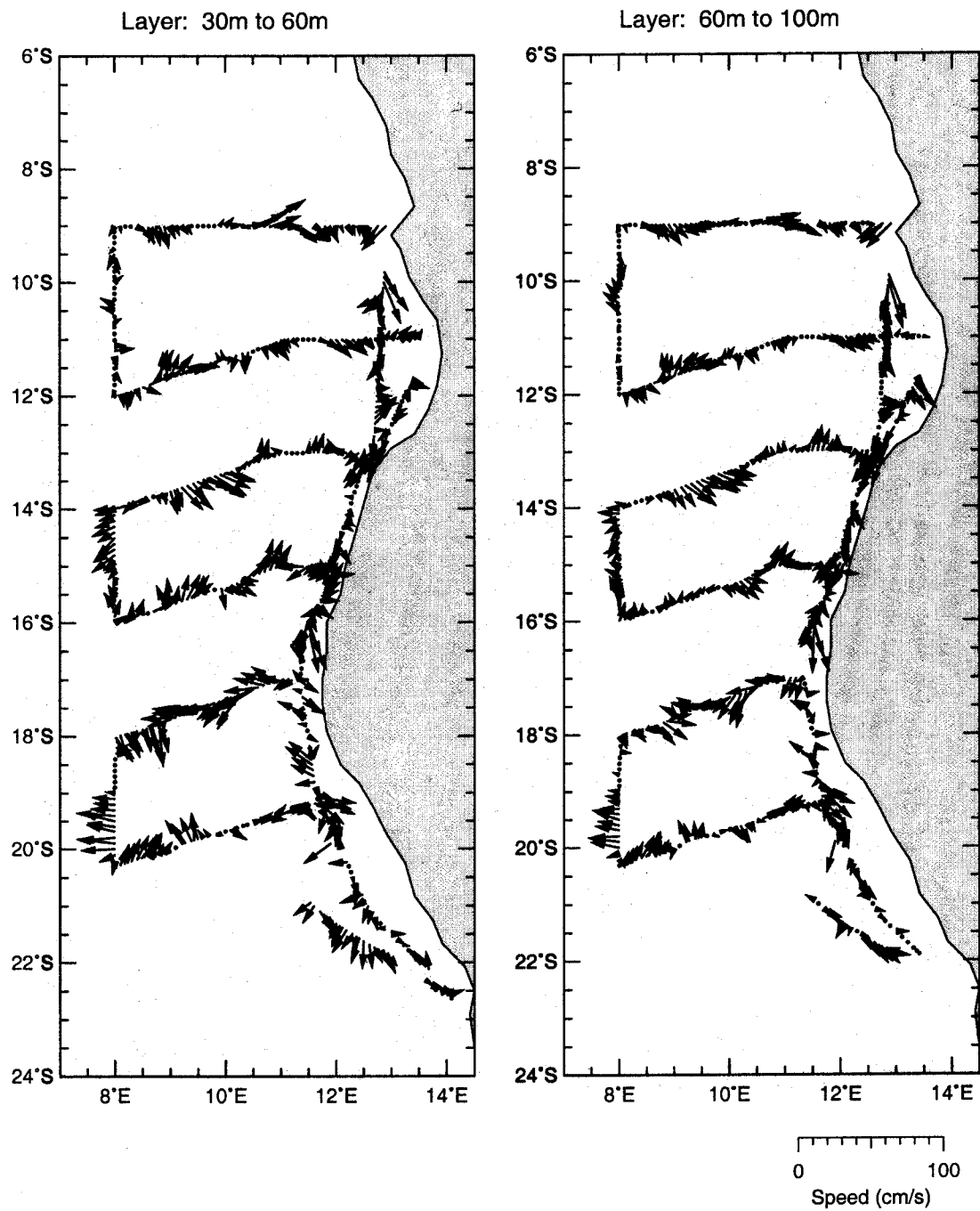


Figure 5.27: Horizontal distribution of currents measured with the vessel mounted ADCP at depth of 30-60 m and 60-100 m.

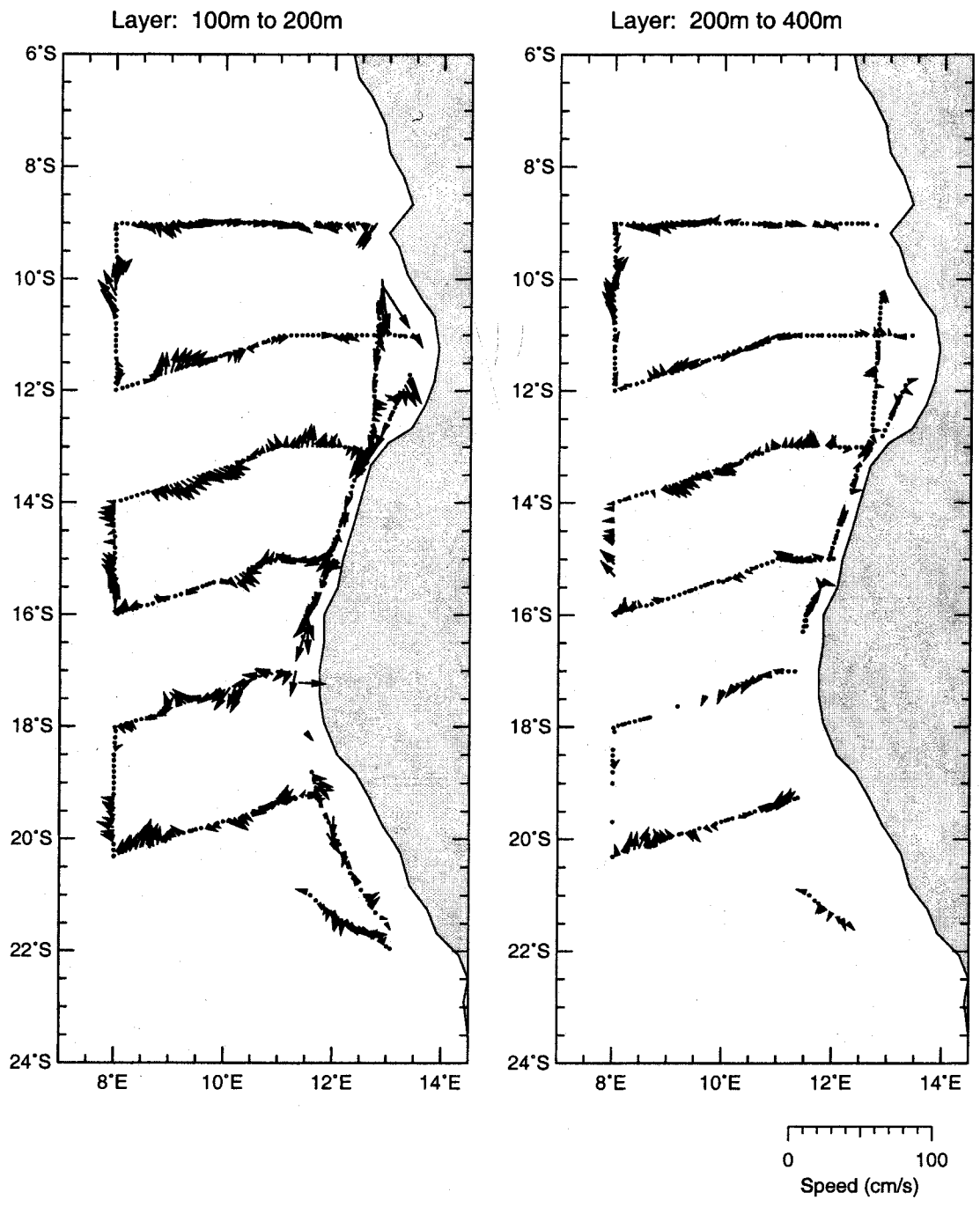


Figure 5.28: Horizontal distribution of currents measured with the vessel mounted ADCP at depth of 100 - 200 m and 200 - 400 m.

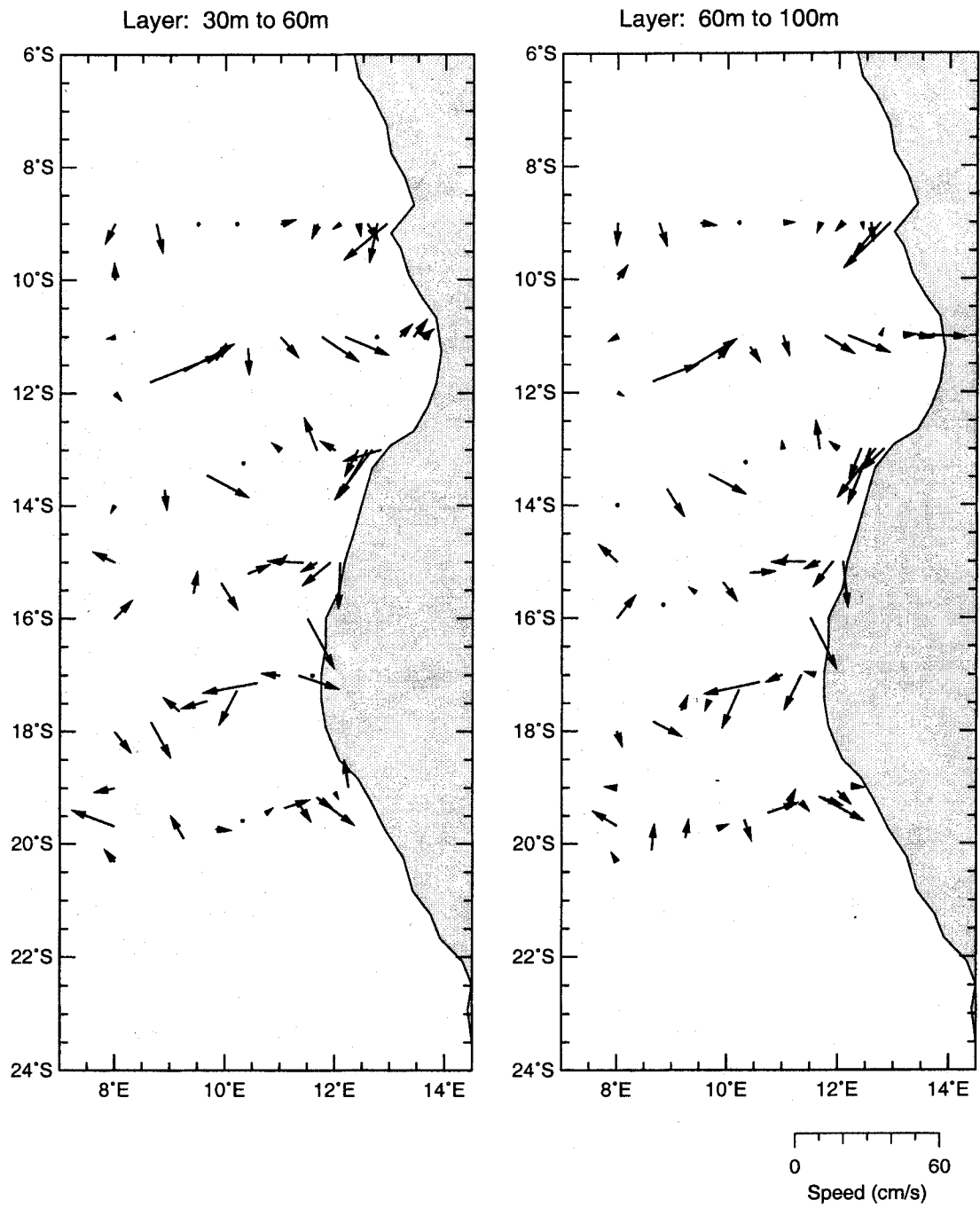


Figure 5.29: Horizontal distribution of currents measured with the lowered ADCP at depth of 30-60 m and 60-100 m.

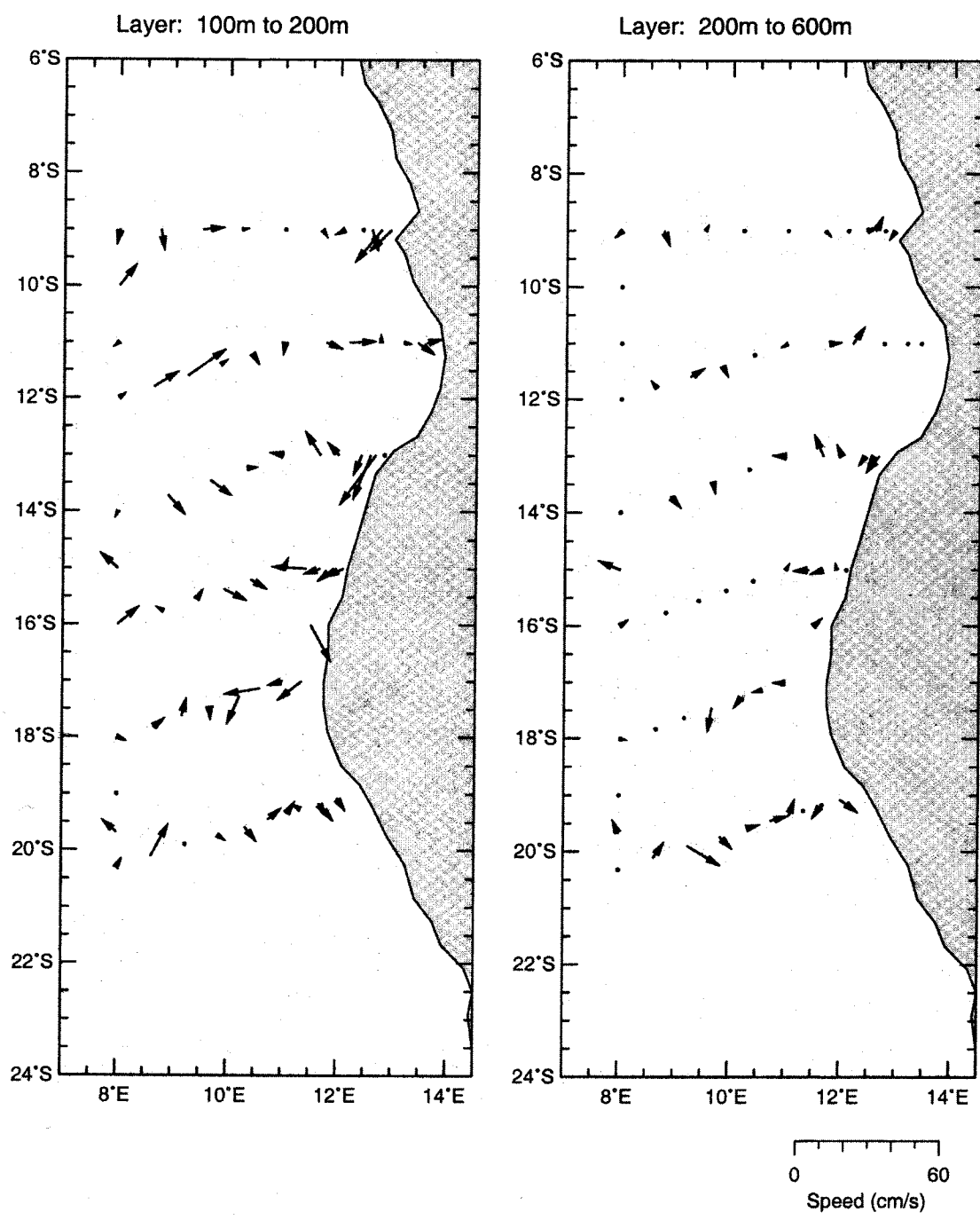


Figure 5.30: Horizontal distribution of currents measured with the lowered ADCP at depth of 100 - 200 m and 200 - 600 m.

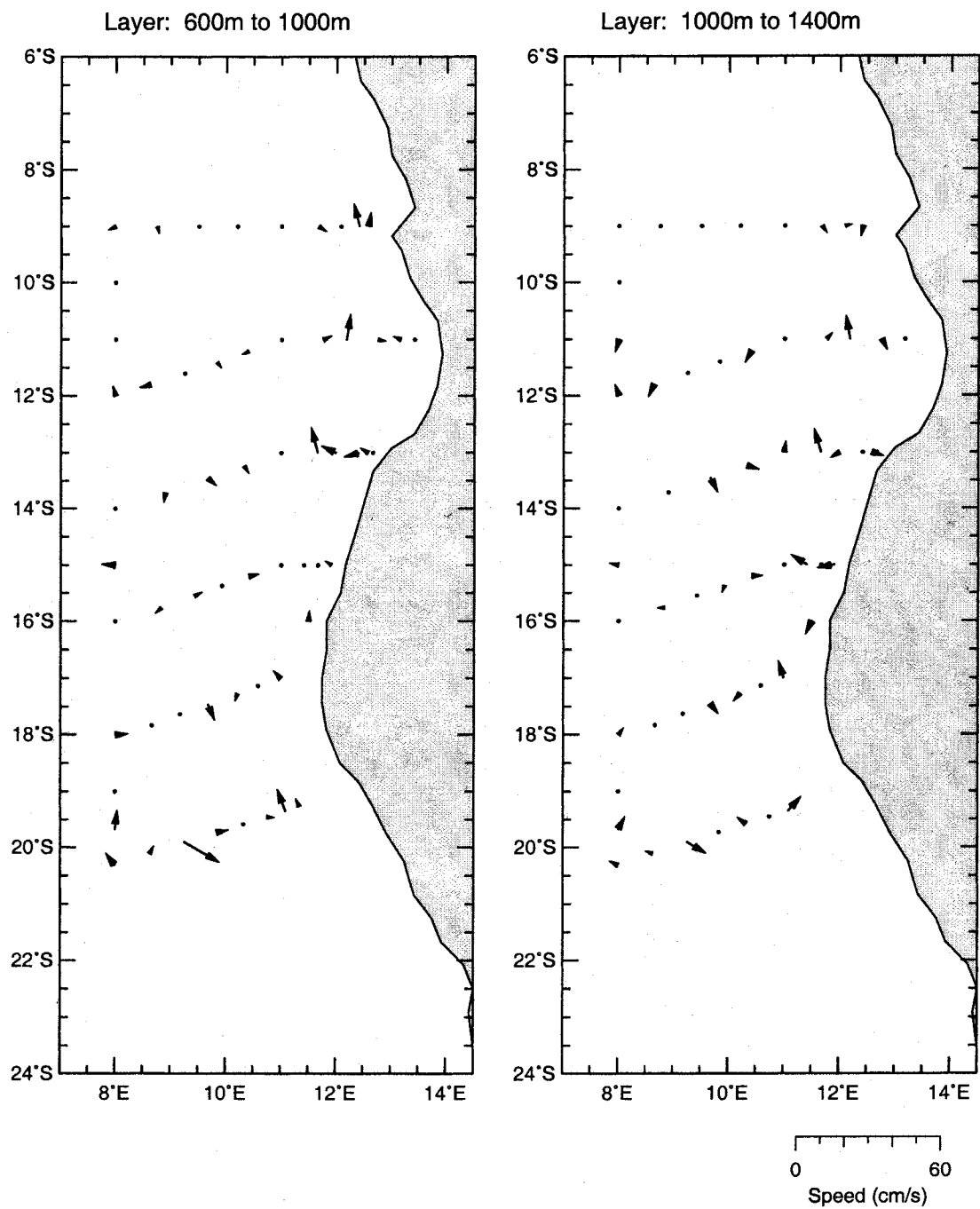


Figure 5.31: Horizontal distribution of currents measured with the lowered ADCP at depth of 600 - 1000 m and 1000 - 1400 m.

## 5.3 Chemical measurements

### 5.3.1 Nutrients

The general nutrient distribution is closely related to the production and degradation of organic material and the transport processes. The most important transport processes in the area under investigation are the wind driven cross shore circulation cell comprising the upwelling of deep water into the surface layer, the Ekman offshore transport in the surface layer and the compensating recirculation in the deep layers, and the longshore circulation consisting of the Angola current north of the ABFZ and the Benguela current and the poleward undercurrent south of it. Thus, the upwelling area south of the Angola-Benguela Frontal Zone is characterized by high phosphate and nitrate concentrations in the surface layer reaching maximum values at the nearshore stations with  $1.5 \mu\text{mol l}^{-1}$  and up to  $19 \mu\text{mol l}^{-1}$  respectively (Figure 5.32). In offshore direction phosphate and nitrate concentrations start to decrease due to consumption by phytoplanktonic organisms, but without limiting primary production. Remarkable are the low silicate concentrations in the surface layer. Near to the coast around  $2 \mu\text{mol l}^{-1}$  were measured whereas in the offshore areas concentrations were often  $< 1 \mu\text{mol l}^{-1}$ , possibly indicating a silicate limitation.

North of the frontal region local upwelling can be observed at all coastal stations of the three northern transects with up to  $0.9 \mu\text{mol l}^{-1}$  phosphate and  $11 \mu\text{mol l}^{-1}$  nitrate. In the open sea areas phosphate decreases to  $0.15\text{-}0.2 \mu\text{mol l}^{-1}$  whereas nitrate is often at the detection limit. The production in these areas is limited most probably by nitrate. This can be seen also by the low N:P-ratios. Again, silicate concentrations are low, only at the nearshore stations around  $5 \mu\text{mol l}^{-1}$  were measured. The silicate maximum in the surface layer was measured in the coastal belt off Luanda at  $9^\circ \text{S}$ . This can be together with the relatively low salinity at this station considered as evidence for freshwater plume from the Zaire river. River water masses are commonly characterized by a higher silicate content.

Below the euphotic zone high nutrient concentrations were detected (Figure 5.33). These are resulting from the current regimes and the enhanced degradation of sedimenting organic material. In the South Atlantic Central Water (SACW) a nutrient pool with concentrations of around  $2 \mu\text{mol l}^{-1}$  phosphate and  $20\text{-}30 \mu\text{mol l}^{-1}$  nitrate were measured (Figure 5.34) north of  $18^\circ \text{S}$  at least between  $8^\circ \text{E}$  and the coast. A weak maximum of the nutrients in  $200\text{m}$  depth extends from the centre of the southernmost section towards  $14^\circ \text{S}$  on the  $8^\circ \text{E}$  section. The nutrient pool is bounded toward the open ocean in the south west of the studied area by a water mass with lower nutrients and higher oxygen concentrations. The highest phosphate and nitrate concentrations of the water column can be found in the Antarctic Intermediate Water (AAIW) between 600 and 1000 m (Figure 5.35). The North Atlantic Deep Water (NADW) is characterized by slightly lower concentrations (Figure 5.36). Silicate concentrations do not follow these patterns. They increase continuously down to 1200 m reaching there highest values with about  $36\text{-}40 \mu\text{mol l}^{-1}$  in the south and  $32\text{-}34 \mu\text{mol l}^{-1}$  in the northern part of the investigated area (Figures 5.36 and 5.39). Below the euphotic zone the relation of inorganic nitrogen and phosphate are more or less in

balance. The N:P-ratio of 14 is near to the Redfield ratio with a slight nitrogen deficit.

Nitrate is by far the dominating inorganic nitrogen compound in all profiles. However, intermediate ammonium and nitrite maxima can be observed. Both are lying in the order of around  $0.5 \mu\text{mol l}^{-1}$  (Figure 5.38) indicating centres of mineralization and nitrification processes. Nitrite can be found also as an intermediate product during denitrification processes when oxygen concentrations are low enough. An interesting feature is the depth of the observed maxima. South of the Benguela-Angola-Front these maxima are very shallow and are lying between 10 and 20 m only. In the northern part of the investigated area, both maxima are deeper. Only in the coastal areas, characterized by local upwelling, the depth is comparable with that south of the front.

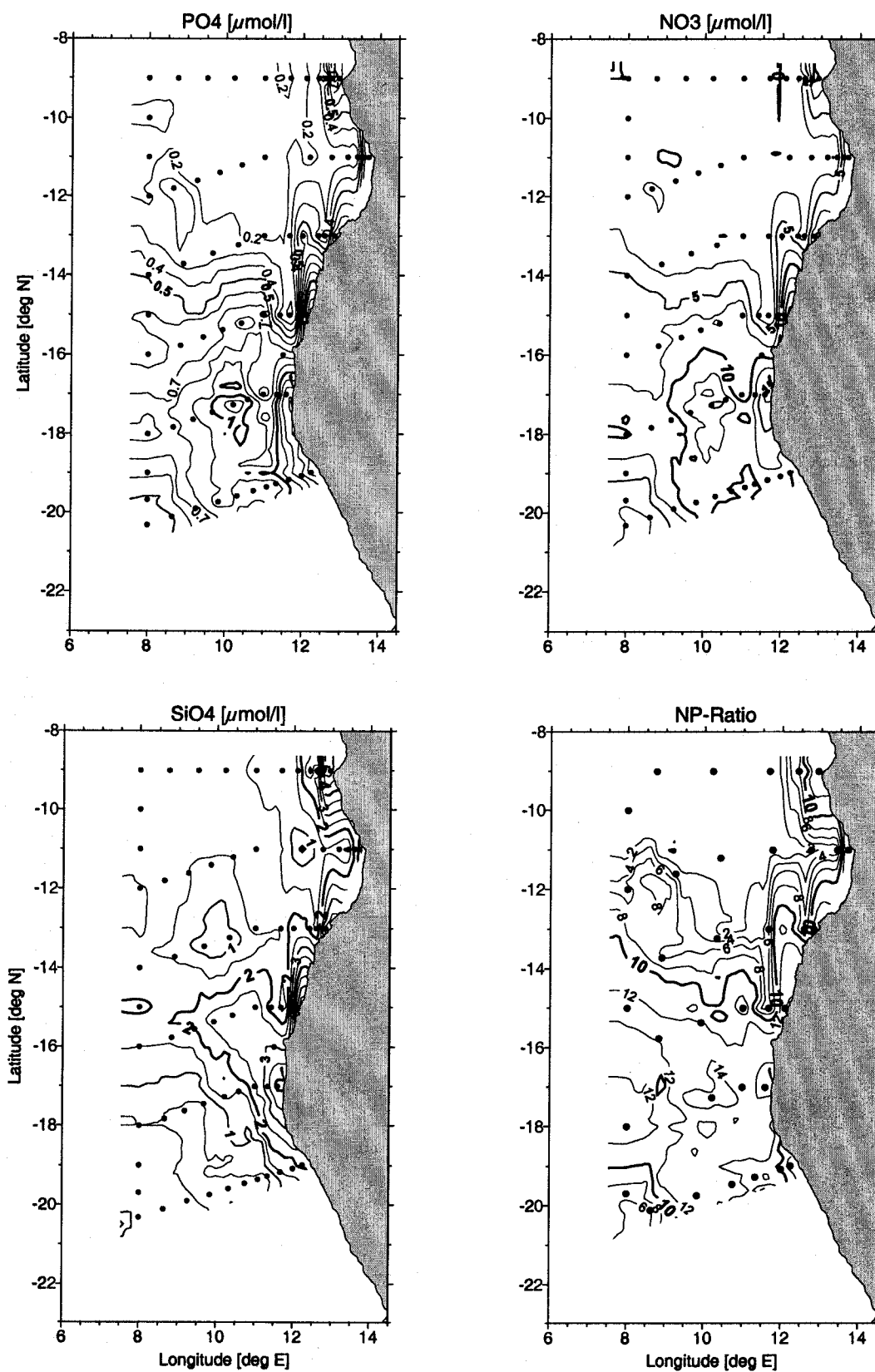


Figure 5.32: Horizontal distribution of  $\text{PO}_4$ ,  $\text{NO}_3$ ,  $\text{SiO}_4$  and N-P ratio at 0 m depth.

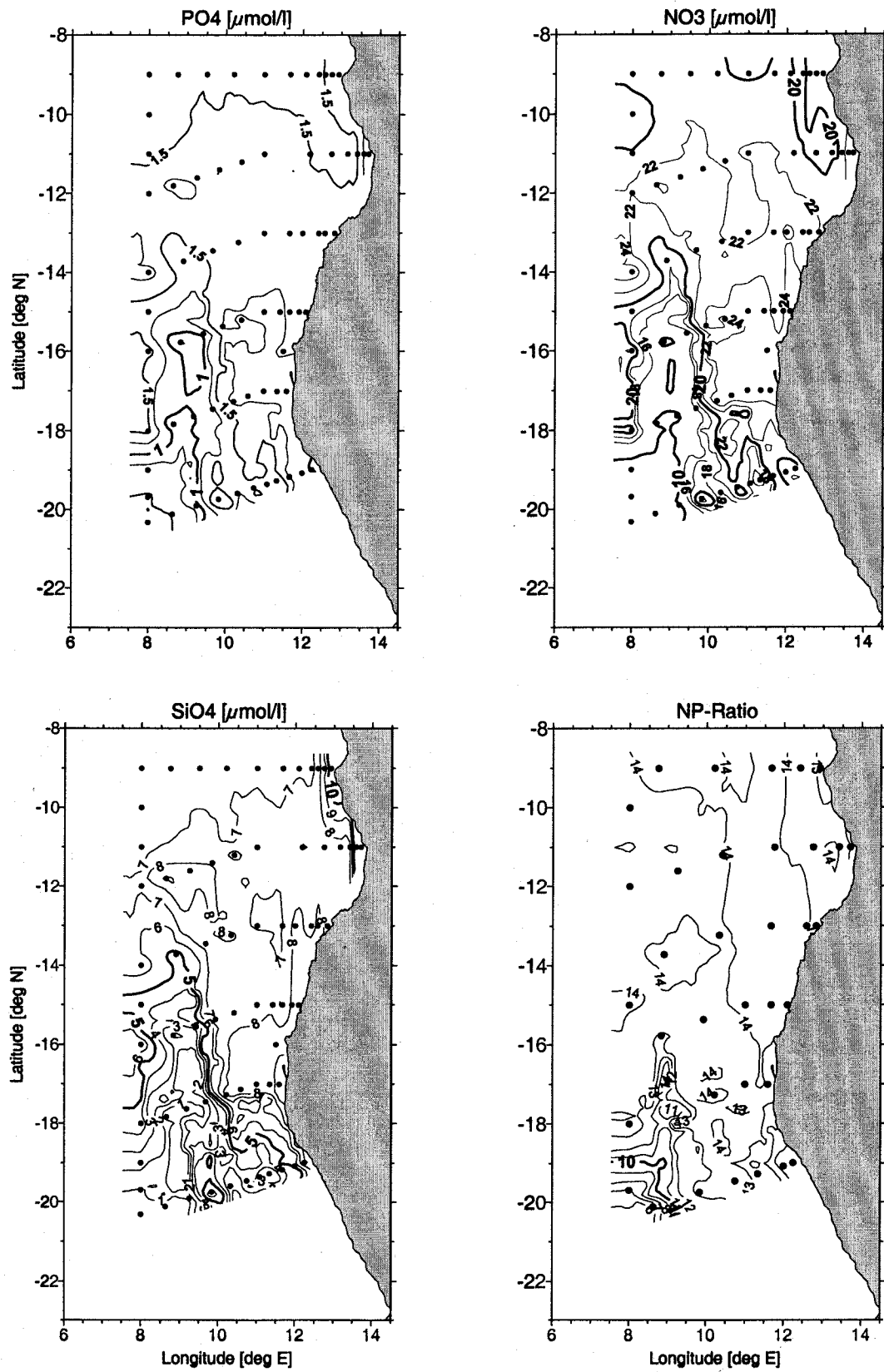


Figure 5.33: Horizontal distribution of  $\text{PO}_4$ ,  $\text{NO}_3$ ,  $\text{SiO}_4$  and N-P ratio at 60 m depth.

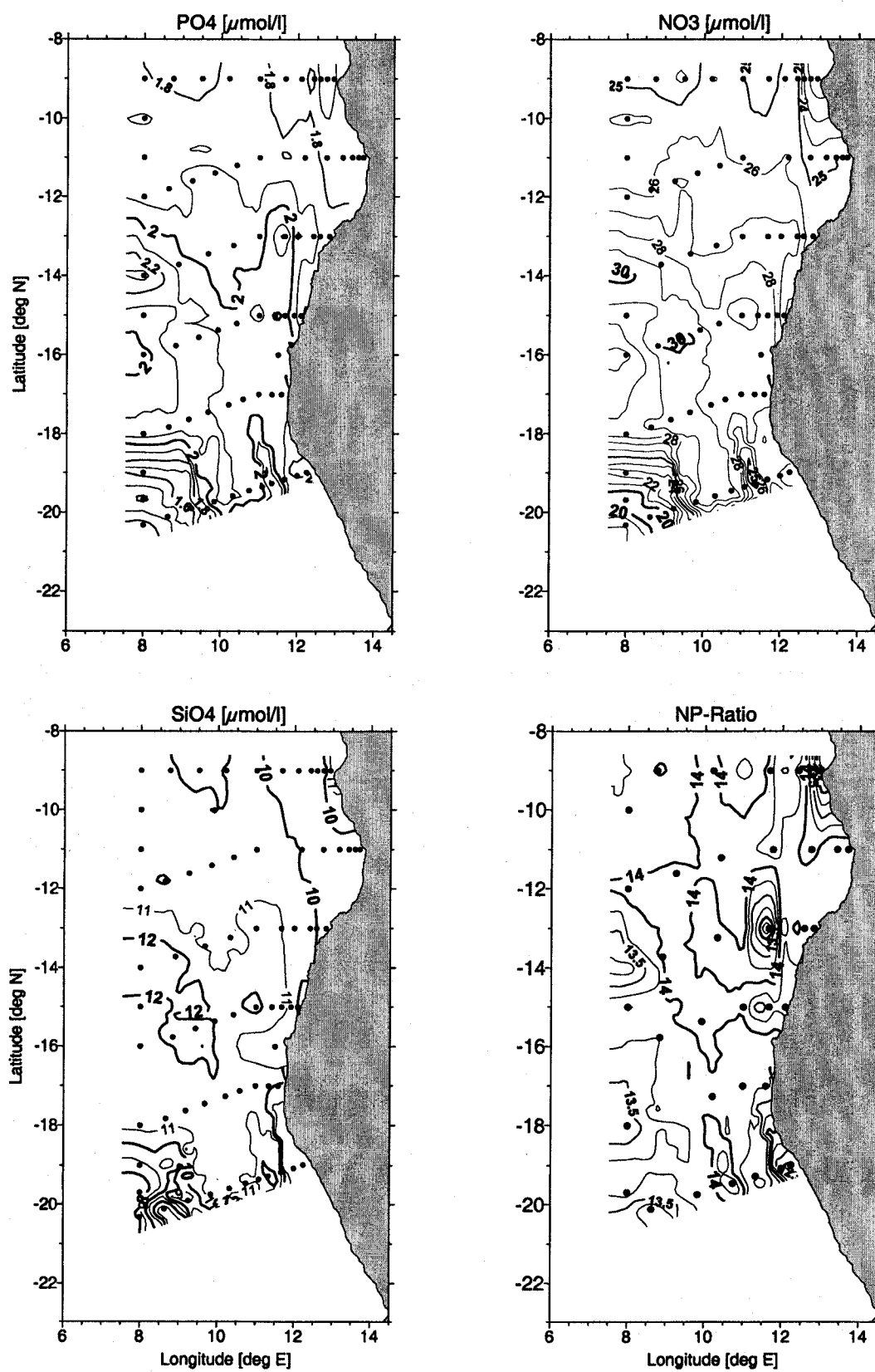


Figure 5.34: Horizontal distribution of PO<sub>4</sub>, NO<sub>3</sub>, SiO<sub>4</sub> and N-P ratio at 200 m depth.

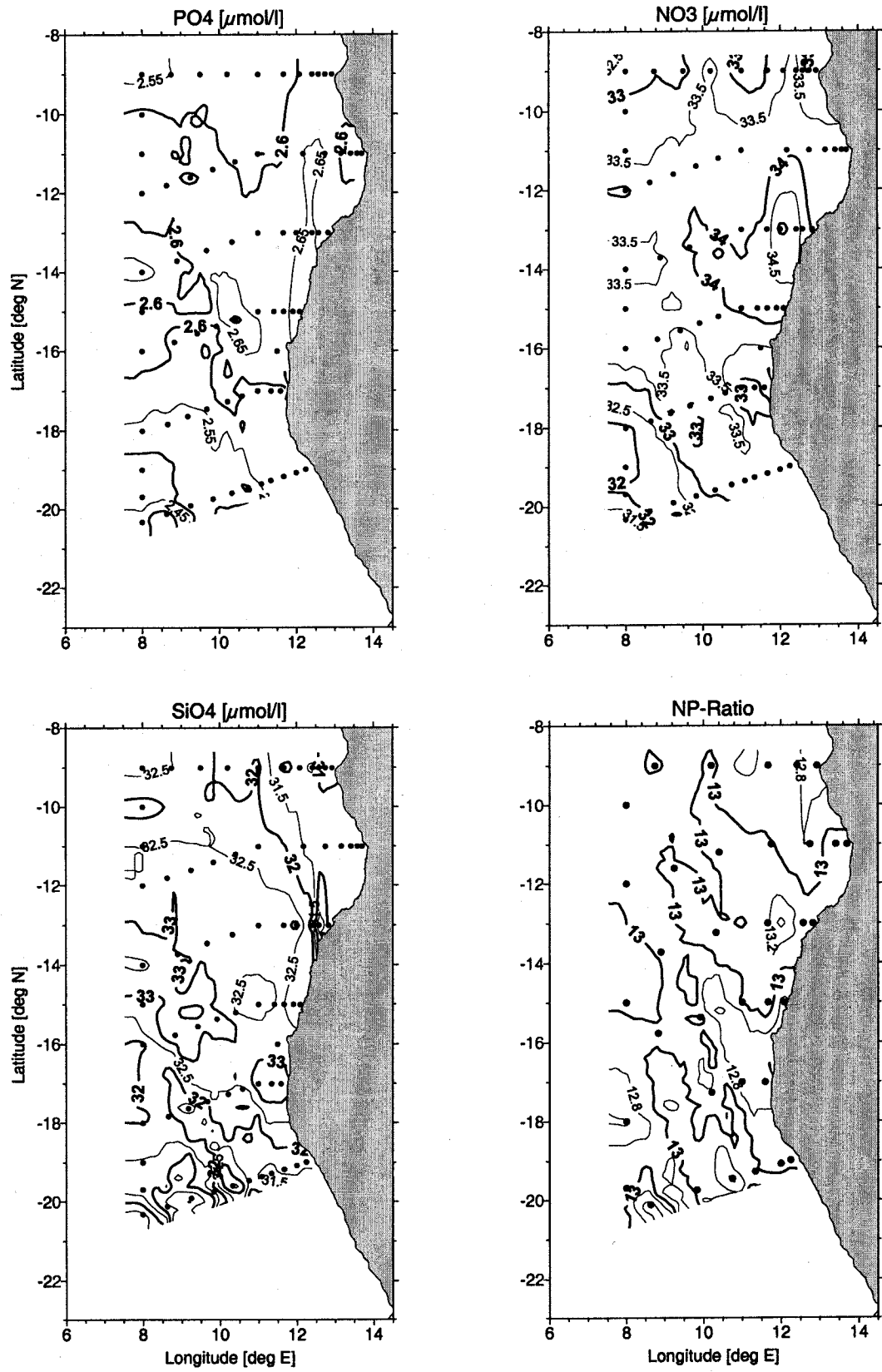


Figure 5.35: Horizontal distribution of PO<sub>4</sub>, NO<sub>3</sub>, SiO<sub>4</sub> and N-P ratio at 800 m depth.

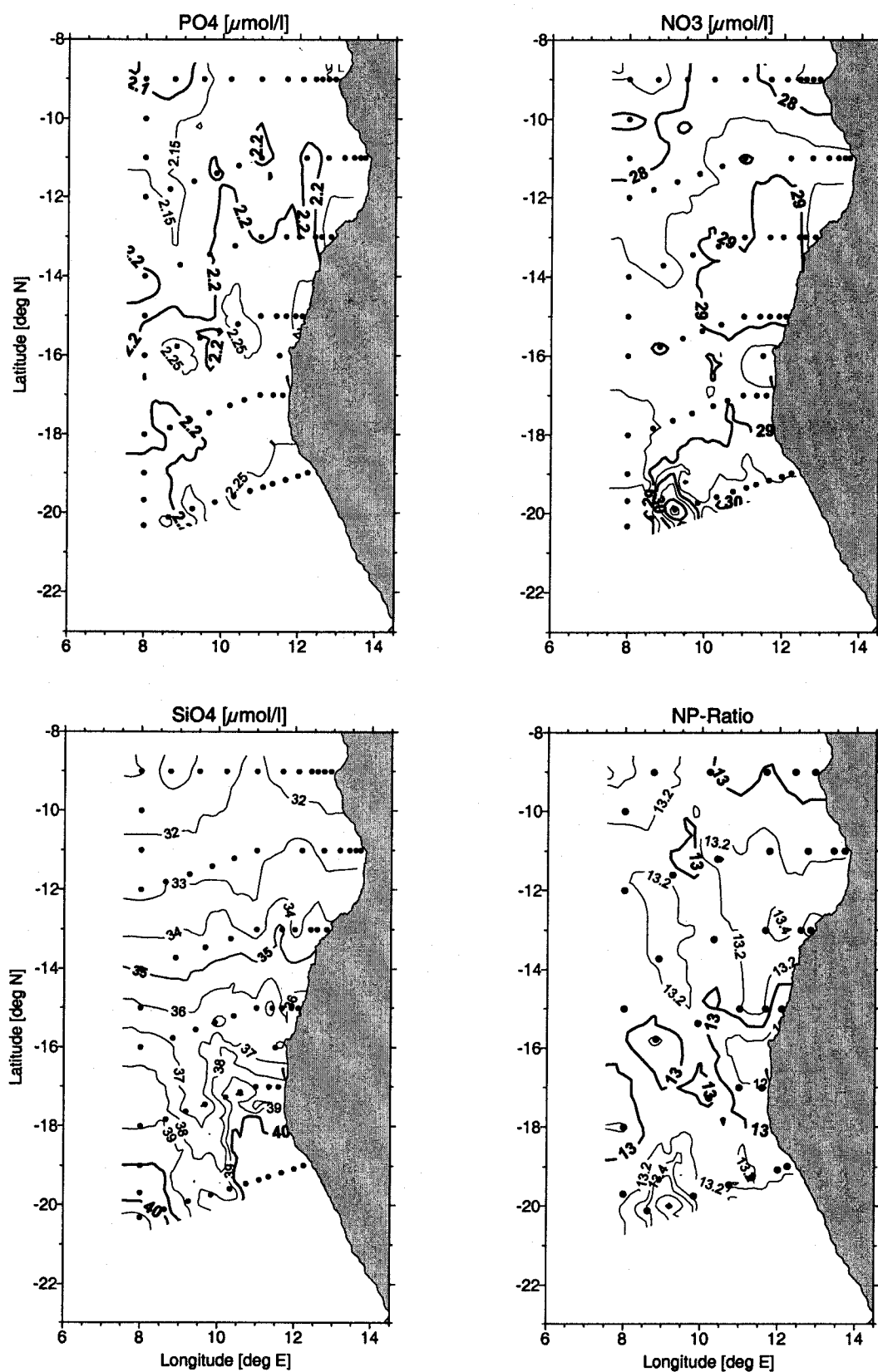


Figure 5.36: Horizontal distribution of PO<sub>4</sub>, NO<sub>3</sub>, SiO<sub>4</sub> and N-P ratio at 1200 m depth.

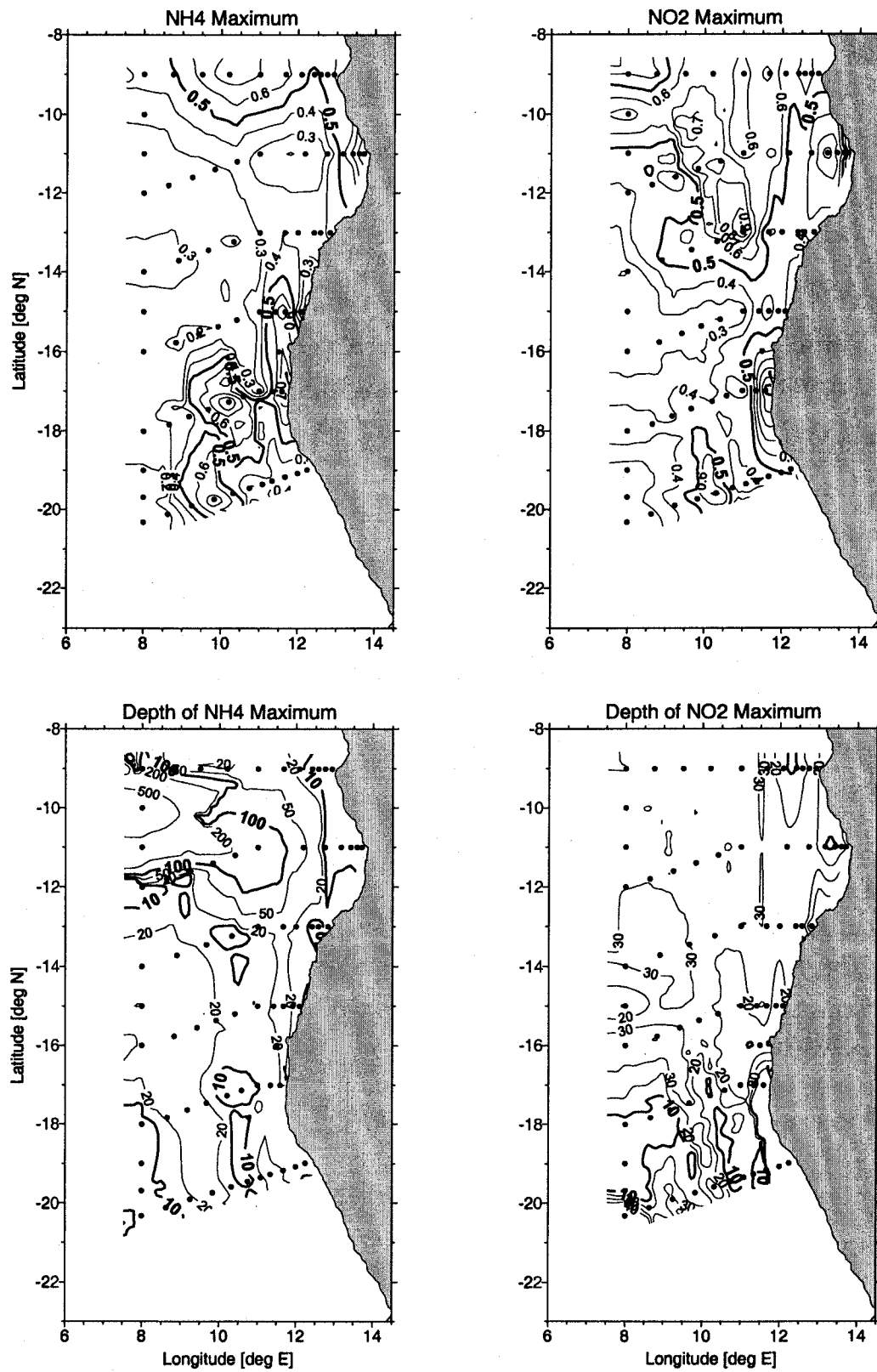


Figure 5.37: Horizontal distribution of  $\text{NO}_2$  and  $\text{NH}_4$  at depth of their maximum near the thermocline.

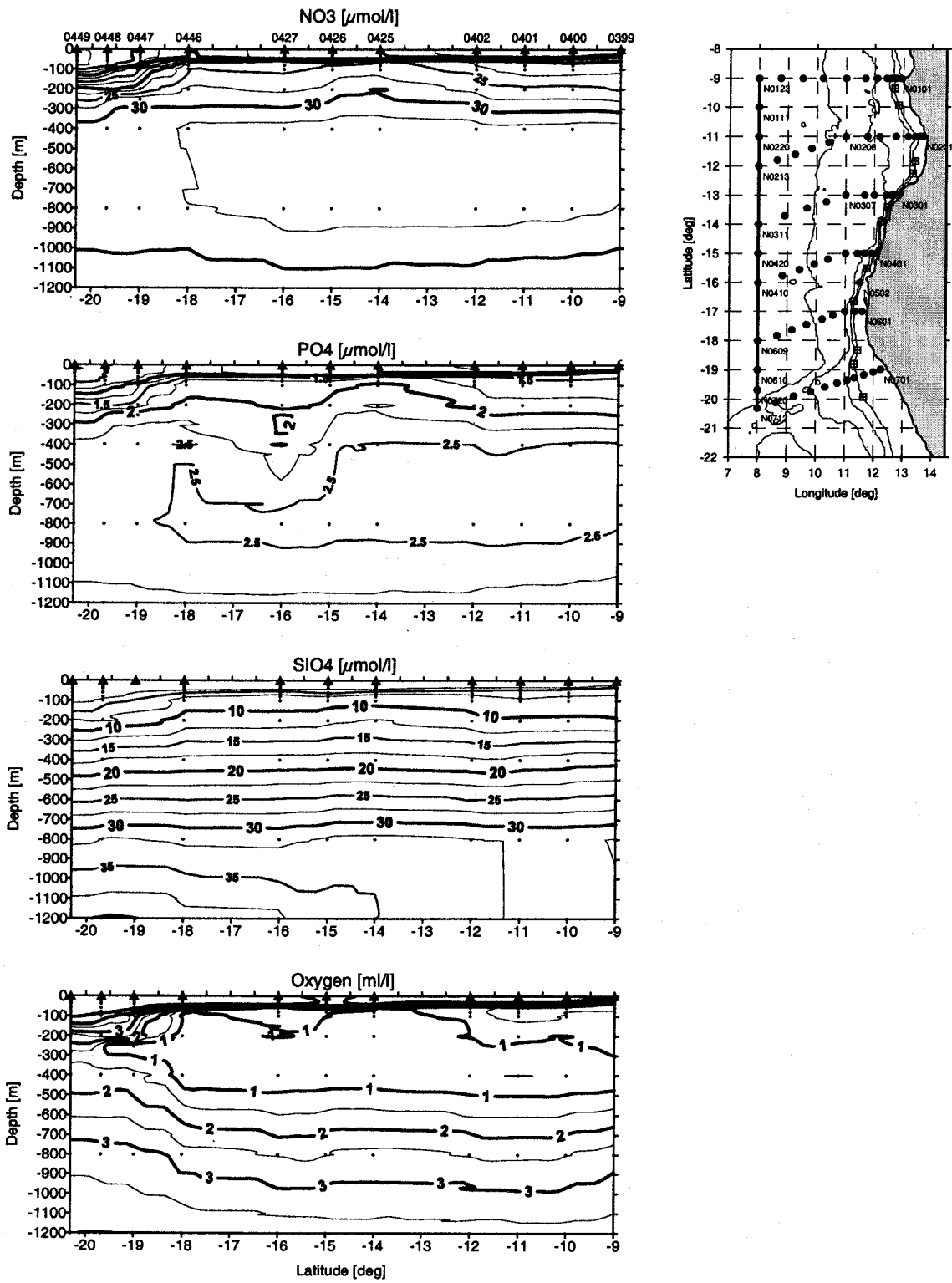


Figure 5.38: Section 10 vertical distribution of PO<sub>4</sub>, NO<sub>3</sub>, SiO<sub>4</sub> and O<sub>2</sub> (0-1200 m).

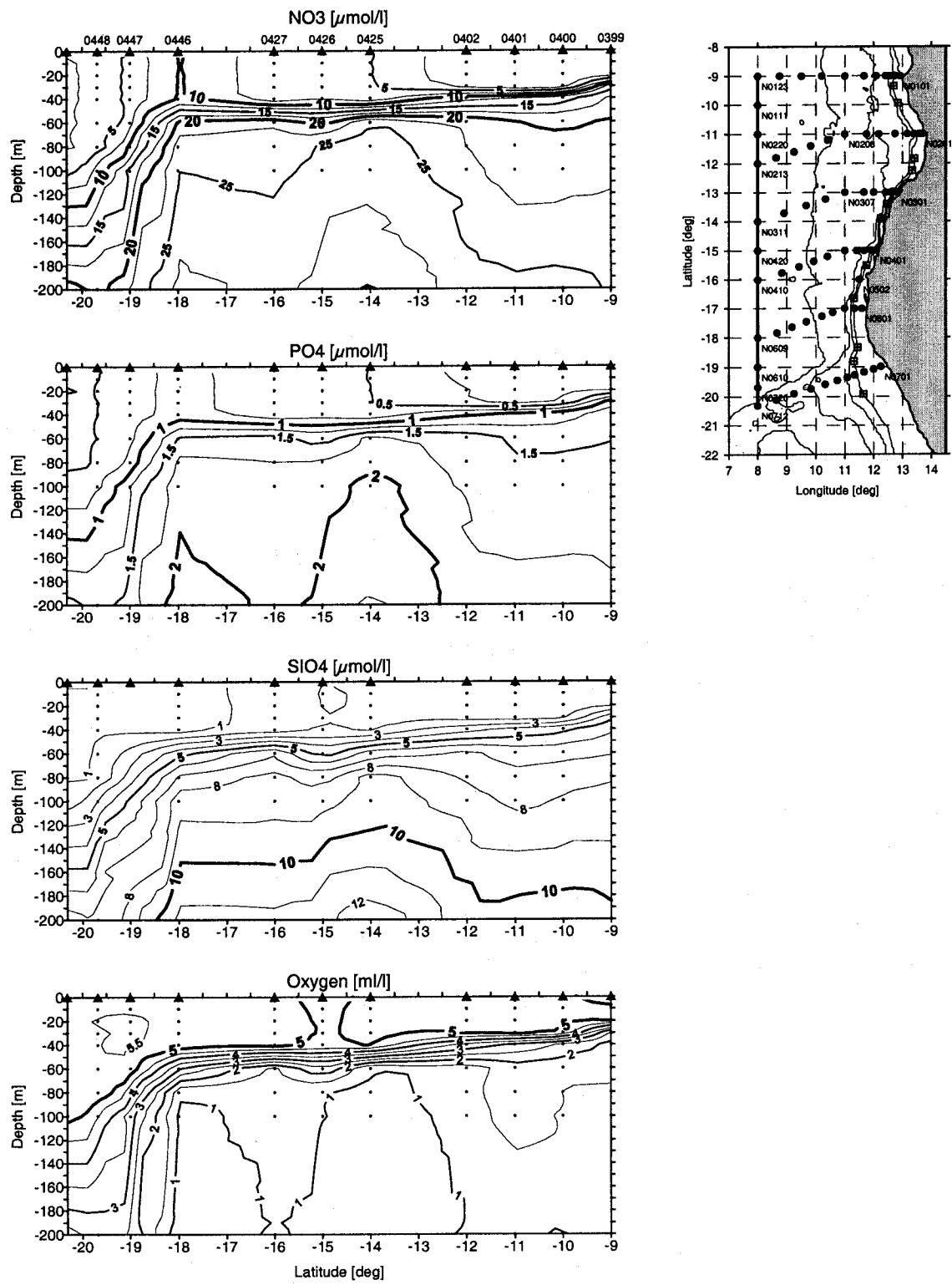


Figure 5.39: Section 10 vertical distribution of PO<sub>4</sub>, NO<sub>3</sub>, SiO<sub>4</sub> and O<sub>2</sub> (0-200 m).

### 5.3.2 Trace metals

#### Cadmium distribution in surface and deep waters

Surface water distribution of cadmium can be affected by several chemical and physical processes, like vertical mixing with deeper water layers (upwelling), atmospheric input and particulate removal (BRULAND, 1980; POHL et al., 1993; RUDGERS VAN DER LOEFF et al., 1997). In coastal regions also influences from anthropogenic sources have to be considered. First results on the cadmium distribution of surface waters in the investigated area (Figure 5.40) showed low Cd levels in the offshore regions ( $0.008 - 0.025 \text{ nmol kg}^{-1}$ ) and by factor 3-5 increasing Cd concentrations close to the Angolan coast with maximum Cd values in the region of Luanda ( $0.133 \text{ nmol kg}^{-1}$ ) and Namibe ( $0.072 \text{ nmol kg}^{-1}$ ). The question arises if the elevated Cd concentrations in the coastal region are a result of terrestrial sources mainly of anthropogenic origin or a result of upwelling water cells from deeper water layers?

Upwelling can be identified by phosphate maxima in the surface layer. Results of the coastal phosphate distribution showed elevated phosphate levels near  $19^\circ \text{ S}$ ,  $17^\circ \text{ S}$ , and in the region of Namibe at  $15^\circ \text{ S}$ . At the other coastal stations at  $13^\circ \text{ S}$ ,  $11^\circ \text{ S}$  and at  $9^\circ \text{ S}$  (Luanda) phosphate concentrations decreased to a level of  $\sim 0,5 \mu\text{mol dm}^{-3}$  so that upwelling can be neglected in this area (see Figure 5.4). That means, that the coastal area around Luanda could be influenced by anthropogenic sources, while for the other areas south of  $13^\circ \text{ S}$  coastal upwelling of the Benguela current has to be considered. As could be demonstrated in (Figure 5.40 and Table 5.1) cadmium is depleted in surface waters to  $0.025 \text{ nmol kg}^{-1}$ , and enriched in the deeper water layer (500 - 1000 m) which was characterized as Antarctic Intermediate Water (AAIW) by a factor of  $\sim 20$ . The increase of Cd in deeper water layers is usually explained by the Cd uptake by phytoplankton in surface waters, the sinking of organic material and the release of Cd after its decomposition. In many times a correlation between phosphate and cadmium has been demonstrated for deep water profiles (BRULAND, 1980). So it seems, that vertical transportation is the major process responsible for the distribution of the Cd (MART and NÜRNBERG, 1986). For our results a correlation between Cd and  $\text{PO}_4$  cannot be observed in the vertical profiles (Figure 5.41).

Table 5.1: Cd concentrations ( $\text{nmol kg}^{-1}$ ) in surface waters and in the deep horizon of the oxygen minimum at several stations in the Southeast Atlantic

Station	Cd (20 m)	Cd (at Oxygen minimum)
NO206	0.025	0.536 (400m)
NO401	0.072	0.139 (150m)
NO403	0.029	0.540 (400m)
NO405	0.020	0.521 (400m)
NO502	0.027	0.530 (400m)
NO602	0.021	0.115 (100m)
NO603	0.031	0.510 (400m)

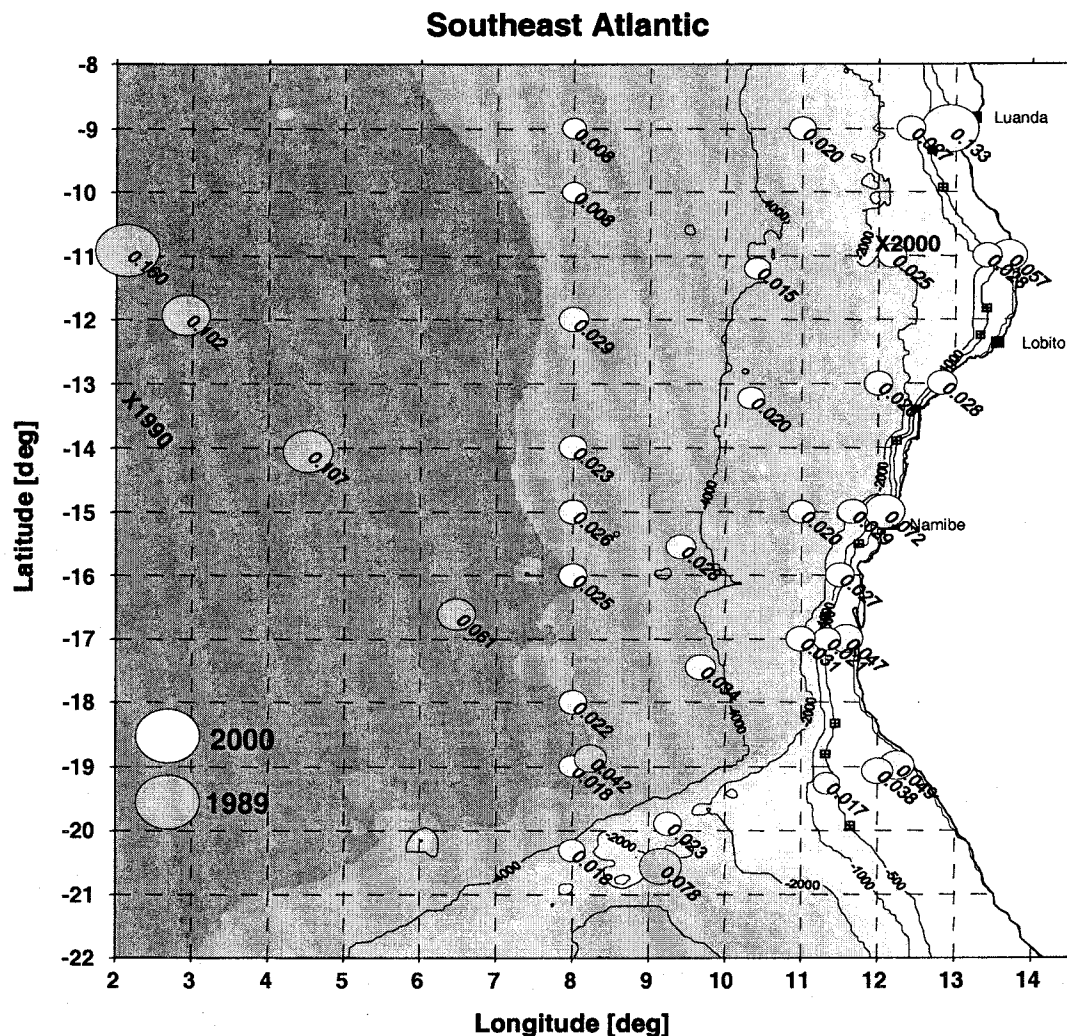


Figure 5.40: Surface water Cd concentrations in  $\text{nmol kg}^{-1}$ , (unfiltered samples)

In contrast to other oceans WESTERLUND and ÖHMAN (1991) observed relatively high concentrations of Cd ( $0.5\text{--}0.8\text{ nmol kg}^{-1}$ ) in the Weddell Sea throughout the whole water-column. Compared to our results this is exactly the same range we found in the water layer of the AAIW. It seems, that horizontal transportation of Cd cannot be neglected because the elevated cadmium concentrations in the AAIW transported by the Benguela current may have their source in the Weddell Sea.

#### Comparison between 1989/1990 and 2000

In 1989 the surface Cd concentrations in the oceanic regions were higher by a factor of 3-4 than in the year 2000, but they are comparable to the concentrations observed in the coastal upwelling regions (Figure 5.40). Upwelling signals are very patchy as demonstrated by the phosphate distribution (see Figure 5.32) and can be transported far offshore by the

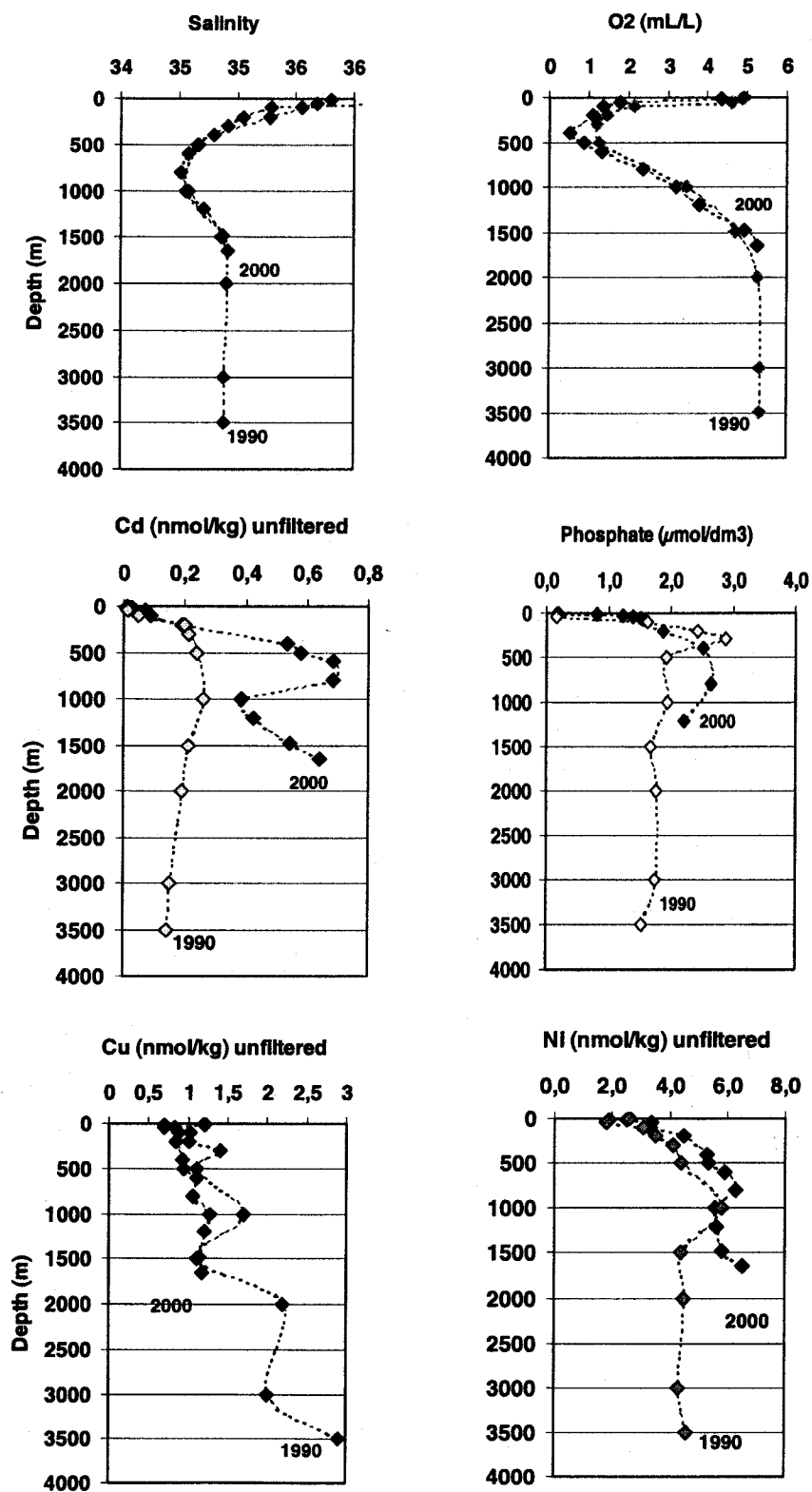


Figure 5.41: Vertical distribution of Cd, Cu and Ni in 1990 and 2000 compared to salinity, oxygen and phosphate in the Southeast Atlantic.

Benguela current (RUDGERS VAN DER LOEFF et al., 1997). This would be an explanation for the elevated Cd concentrations in 1989. In May 1990 the depth profile was sampled in the Angola Basin at  $13^{\circ} 46.0' S$ ,  $2^{\circ} 26.0' E$ , far more offshore than in 2000 ( $11^{\circ} N$ ,  $12^{\circ} 10.0' E$ ). Both profiles, showed the Cd maximum in the water layer of the oxygen minimum, with factor 3 higher Cd concentrations in the year 2000 at the onshore station. Additionally investigations have been carried out for Cu and Ni. In 2000 the results for the vertical distribution of Cu and Ni are similar to that observed in 1990. The gradient for Cu and Ni is small in relation to Cd, so upwelling processes do not have a major influence on the copper and nickel concentrations in surface waters.

## 5.4 Biological measurements

### 5.4.1 Chlorophyll-a and primary production

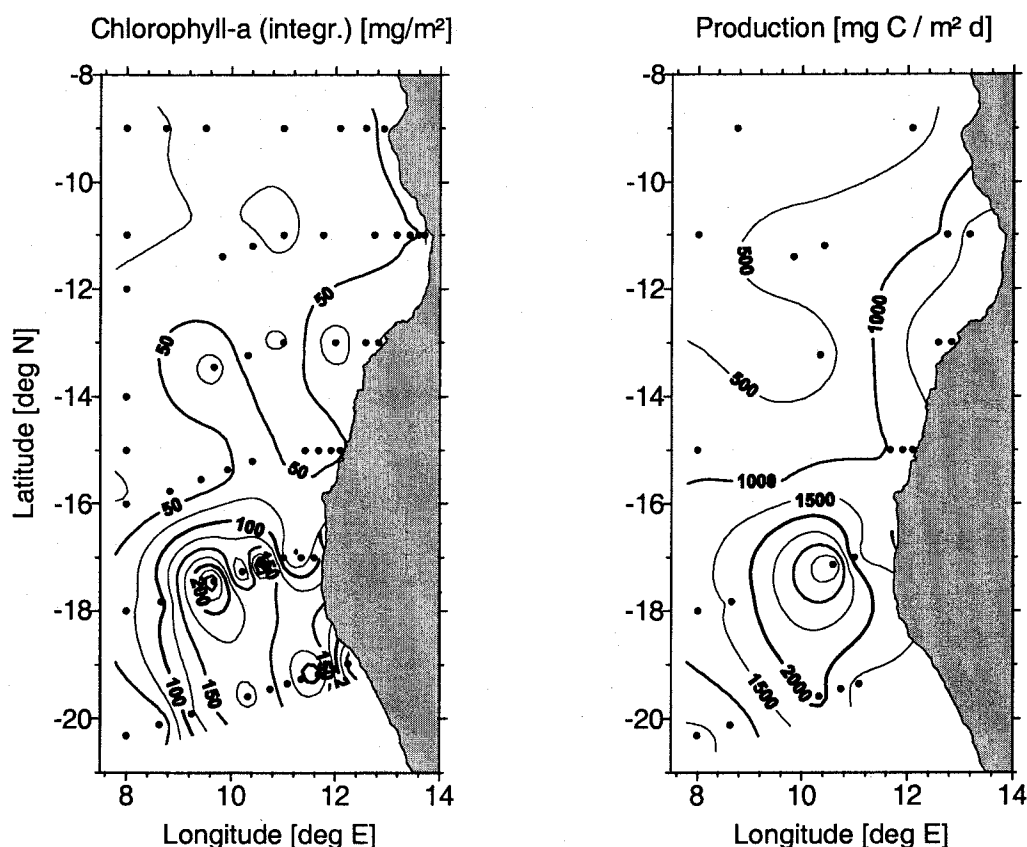


Figure 5.42: Horizontal distribution of chlorophyll-a (integrated over the upper 60 m of the water column, left) and of primary production during cruise M48-3 (integrated over the euphotic zone, right).

The horizontal distribution of chlorophyll-a, integrated over the upper 60 m of the water column, and primary production of phytoplankton in the euphotic zone (see Figure 5.42)

reveal the same pattern: low values north of the Angola-Benguela front but patches of extremely high values in the Benguela upwelling region. It is interesting that one of these chlorophyll-a patches is located near-shore (Stat. 701, maximum of  $6 \text{ mg m}^{-3}$  chl a in 30 m depth) but the other remote from the coast. These remote patches are localised at station 606 (almost even distribution of  $4.4\text{--}4.9 \text{ mg m}^{-3}$  chl-a down to 60 m depth), station 604 (maximum of  $5.8 \text{ mg m}^{-3}$  chl-a at 20 m depth) and station 707 (almost even distribution of  $4.0\text{--}4.2 \text{ mg m}^{-3}$  chl-a down to 30 m depth). At stations 201 and 601, high chlorophyll-a concentrations of  $5.5$  and  $6.0 \text{ mg m}^{-3}$  chl-a were concentrated only at the surface. Unfortunately, no primary production measurements were conducted at the mentioned near-coast stations. Along the 3., 4. and 5. transects, primary production rates increased while approaching the coast (e.g station 301:  $1805 \text{ mg C m}^{-2} \text{ d}^{-1}$ , station 401:  $1362 \text{ mg C m}^{-2} \text{ d}^{-1}$ ). On the 6. transect, the maximum of  $4145 \text{ mg C m}^{-2} \text{ d}^{-1}$  was measured at station 604, whereas no data were available from station 606.

#### 5.4.2 Zooplankton biomass

Basing on the M48/3 material, the conditions north and south of the Angola-Benguela Frontal Zone will be characterized in terms of zooplankton by

- vertical and horizontal biomass distribution,
- biodiversity patterns in relation to water masses,
- spatial patterns of the utilization of primary productivity and
- the balance between the nutritive demand of pelagic fishes of commercial value and the nutrition being produced.

Zooplankton had been studied within five size categories between  $55 \mu\text{m}$  and  $> 1 \text{ mm}$  (see section 3.9.2). Currently, the analysis is concentrated on biomass patterns in terms of ash free dry mass, originated at 17 stations (Table A.3, Figure 2.4) mostly in three different depth strata from the sea surface down to 200 m and three times down to 500 m (see section 3.9.2).

The average zooplankton AFDM decreases with growing depths in all size categories as usual (Table 5.2). Significant changes appear mainly between 25 and 75 m. This concerns the total of all size classes, and therein the organisms smaller than  $100 \mu\text{m}$  on one hand and individuals between 200 and  $1000 \mu\text{m}$  on the other hand. The gradient is steepest below 75 m for the fraction  $100\text{--}200 \mu\text{m}$  and the largest group ( $> 1000 \mu\text{m}$ ).

Comparing the average AFDM dominance of the different size classes at all 17 stations, the proportion of organisms  $> 1000 \mu\text{m}$  raised with increasing depth from 19 to 31 %, while the 200 to  $500 \mu\text{m}$  size class behaved contrary to the largest (Fig. 5.43). It could be caused by differences in the percentage of trophic types. The coming results of taxonomic analysis may be used to verify this hypothesis.

Table 5.2: Statistics of the zooplankton AFDM concentrations in different size classes and depth levels off Angola / Namibia (C.V. [%] means coefficient of variation, which is standard deviation [st. dev.] divided by mean and multiplied by 100)

		Ash free dry mass ( $\text{mg m}^{-3}$ )					
Size fraction ( $\mu\text{m}$ )		> 1000	1000 - 500	500 - 200	200 - 100	100 - 55	Total
0 - 25 m N = 17	mean	4.25	4.69	6.45	3.91	2.91	22.22
	st. dev.	4.07	6.79	3.87	2.98	3.28	16.22
	minimum	0.56	0.25	0.31	1.02	0.80	2.94
	maximum	17.30	29.50	14.15	10.97	14.36	73.95
	C.V. (%)	96	145	60	76	113	73
25 - 75 m N = 17	mean	2.89	1.84	2.40	2.78	1.08	10.98
	st. dev.	2.28	1.70	1.80	3.48	0.79	8.18
	minimum	0.26	0.18	0.39	0.39	0.43	1.74
	maximum	6.78	4.98	5.72	14.63	3.04	34.14
	C.V. (%)	79	92	75	126	73	74
75 - 200 m N = 17	mean	0.71	0.42	0.42	0.50	0.26	2.31
	st. dev.	0.86	0.77	0.51	0.38	0.14	2.40
	minimum	0.15	0.05	0.09	0.08	0.05	0.42
	maximum	3.40	3.22	2.15	1.66	0.57	10.05
	C.V. (%)	121	181	122	76	56	104
200 - 500 m N = 3	mean	0.89	0.37	0.19	0.18	0.10	1.73
	st. dev.	0.90	0.51	0.22	0.10	0.03	1.72
	minimum	0.09	0.04	0.05	0.07	0.07	0.32
	maximum	1.87	0.95	0.45	0.27	0.12	3.65
	C.V. (%)	101	138	117	57	27	99

Within the particular depth levels, the regional variability is more pronounced in the bigger size categories, indicated by coefficients of variation (C.V.) of  $> 100\%$ . The average biomass concentrations are similar to those of areas outside of regions influenced by near coastal upwelling. For example, the dry mass off the Namibian upwelling site ranges between 40 to 80  $\text{mg m}^{-3}$  for zooplankton larger than 200  $\mu\text{m}$  in the upper 30 m (POSTEL, 1990, POSTEL et al., 1995). A conversion of the sum of the average AFDM for the same size categories of the 0 - 25 m layer (Table 5.2) lead to concentrations which are smaller by the factor of 2 to 4.

The horizontally distribution of AFDM concentration and of the ash content is shown for the sum of all size categories and three depth levels of the entire region in Figures 5.44 and 5.45.

According to the AFDM concentrations, the area is separated into three sub-regions in agreement with the observations made on the early R/V "Meteor" cruise between 1925 and 1927. The northernmost area fits with the southernmost extension of a plankton rich zone, which was called "Congo Province" by HENTSCHEL (1936). Like 75 years ago, the

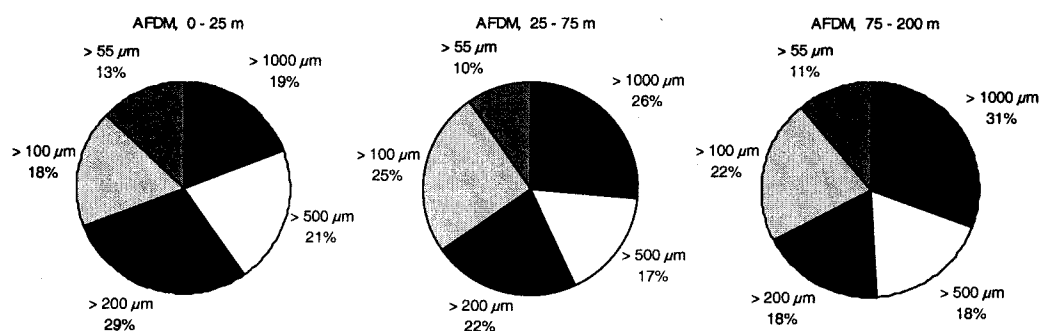


Figure 5.43: The average AFDM dominance of the different size classes in three depth levels above 200 m (N = 17 stations)

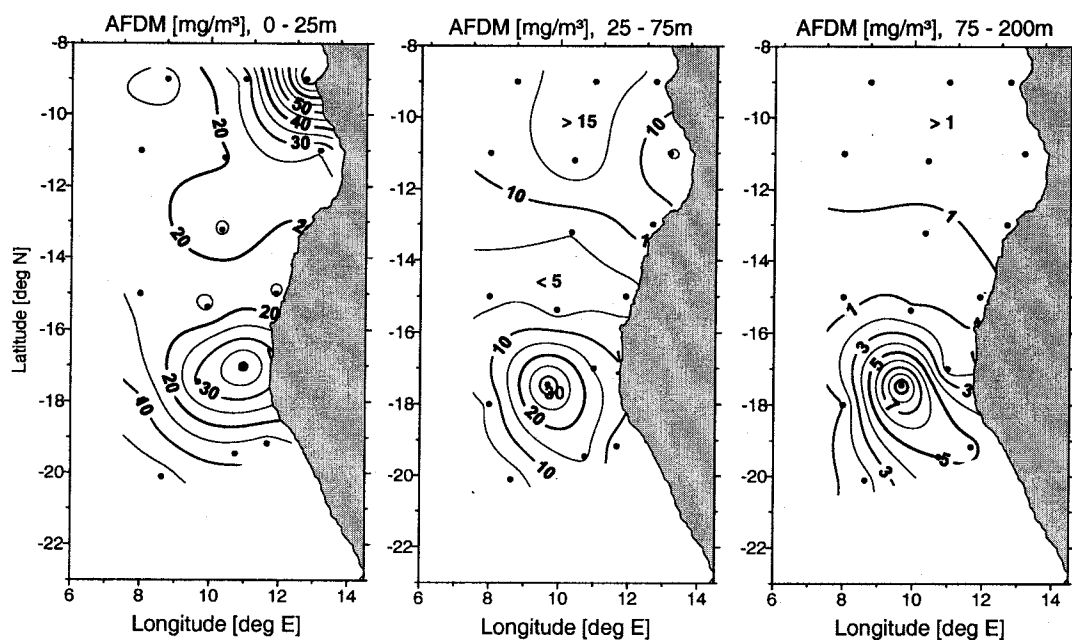


Figure 5.44: Horizontally distribution of total AFDM concentration for the sum of all size categories at three depth levels.

"Congo area" is followed by a "Minimal Area" and finally exchanged by the "Southwest African Tongue" in poleward direction. While the northern plankton rich area is restricted to the latitude of about 10 to 11° S, the southern zone covers a third of the investigation area, beginning at 15 to 16° S. The latter is probably fed by the near coastal upwelling off Namibia. These patterns are fully developed in the upper 25 m, partly in the successive depth level till 75 m, however not in deeper layers, where the northern plankton rich zone is missing.

The ash content of zooplankton depend on species composition. Copepods contain 2-6 %

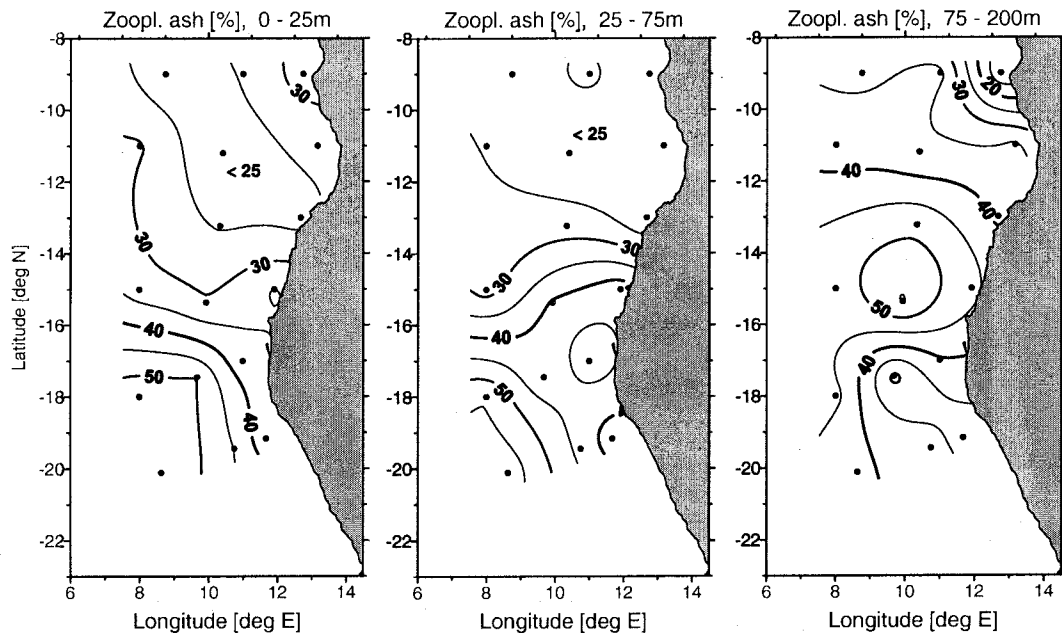


Figure 5.45: Horizontally distribution of the total ash content for the sum of all size categories at three depth levels.

of dry mass, Euphausiids about 8 % (Pacific) and 20 % (Continental shelf off New York), Pteropods 28-47 %, Cnidarians and Ctenophores 50-75 %, Tunicates (69-77 %), according to CURL (1962) and OMORI (1969). Consequently, the distribution of ash percentage (Fig. 5.45) is caused by different species assemblages. The high amounts in the upper 75 m of the south westerly part in the area of investigation may indicate the dominance of gelatinous plankton. It coincides with stations of AFDM which is lower than in the adjacent "Southwest African Tongue". Similar conditions occur between 12 and 17° S, the "Minimal Area" north of the Angola-Benguela Frontal Zone in the 75-200 m depth level.

The vertical patterns shown by horizontal plots of AFDM concentration in three depth levels are confirmed by the LADCP results on section 10 (8° E, 9-20° 19' S; Figure 5.46) although the latter must be interpreted with caution. Strictly spoken, the correlation between the backscattering signals and the AFDM of all size categories (Table 4.6) is valid only in the depth layers between 25 and 200 m. In addition, the absolute amounts are in question because the influence of the backscattering properties of the sea water are not removed until now. Nevertheless, there are plausible differences north and south the Angola-Benguela Frontal Zone. Remarkable is the high biomass in the upper 75 to 100 m north of 16° S. South of this latitudes, a spreading of isolines indicate a deeper extension of higher zooplankton concentrations, the 10 mg m<sup>-3</sup> reach more than 200 m and the 2 mg m<sup>-3</sup> isolines more than 900 m. This pattern coincides with other parameter, e.g. the increased vertical extension of oxygen rich water (Figure 5.24). The higher biomass in the intermediate layer at 11° S and 15° S is also noticeable. Additionally, the daily vertical migration might have influenced the patterns to a certain extent. The lower amounts in the deeper waters at

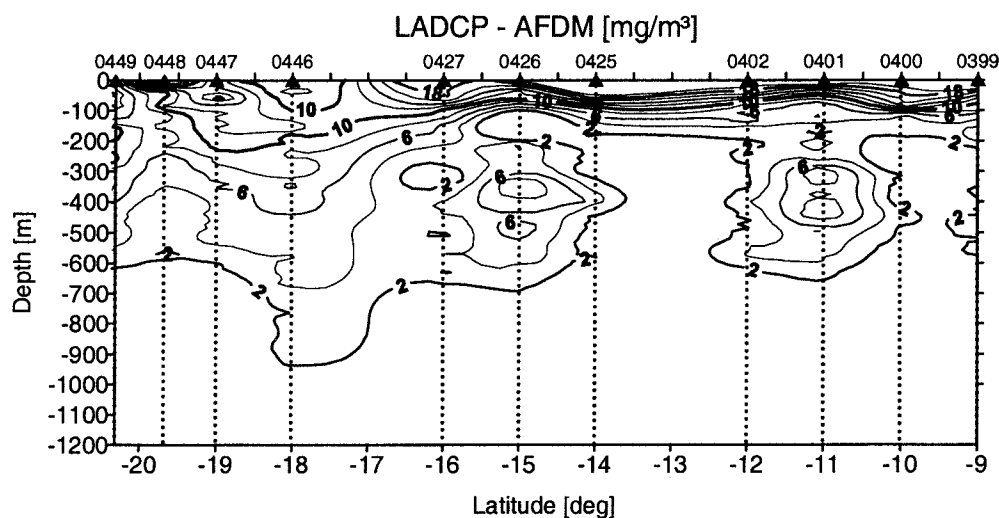


Figure 5.46: Vertical distribution of ash free dry mass concentration at section 10

stations 400 (2:20 UTC), 425 (2:31), 427 (22:07) and 448 (0:36) could be an example of it. All, the other stations had been processed during day time (see Table A.1).

## Acknowledgement

This cruise with R/V "Meteor" was granted by the Deutsche Forschungsgemeinschaft (DFG) Grant no. Ba 725/4-1 and LA 1137/3-1. We thank the captain, his officers and the crew of the R/V "Meteor" for the perfect assistance during the cruise. The BENEFIT office generously supported the Angolan participants.

We thank the participants of the cruise for their excellent field work and for the contributions to this report. The help and technical support of Siegfried Krüger and his team (IOW) who prepared the CTD system is greatly acknowledged here. We also thank all the individuals and authorities who gave valuable support in the preparation of the Cruise.

The kindly providing of ERS 2 satellite data by CERSAT at IFREMER is acknowledged. We thank Toralf Heene for the preparing most of the figures. V. Mohrholz was supported by the Deutsche Forschungsgemeinschaft Grant no. LA 1137/1-1.

## Bibliography

- ANONYMOUS, 1968: Zooplankton sampling. Monographs on oceanographic methodology 2. UNESCO Press, 174 S.
- BARANGE, M. and PILLAR, S.C., 1992: Cross-shelf circulation, zonation and maintenance mechanisms of *Nyctiphanes capensis* and *Euphausia hanseni* (Euphausiacea) in the northern Benguela upwelling system. *Cont. Shelf Res.*, 12, 1027-1042.
- BRULAND, K.W., 1980: Oceanographic distributions of cadmium, zinc, nickel and copper in the North Pacific. *Earth Planet. Sci. Lett.*, 47, 176-198.
- CONKRIGHT, M.E., S. LEVITUS, T. O'BRIEN, T.P. BOYER, C. STEPHENS, D. JOHNSON, L. STATHOPOLOS, O. BARANOVA, J. ANTONOV, R. GELFELD, J. BURNEY, J. ROCHESTER and C. FORGY, 1998: World Ocean Database 1998 Documentation and Quality Control. National Oceanographic Data Center, Silver Spring, MD. [http://www.nodc.noaa.gov/OC5/WOA98F/open\\_1st.html](http://www.nodc.noaa.gov/OC5/WOA98F/open_1st.html)
- COSSA, D., MARTIN, J.M., TAKAYANAGI, K. and J. SANJUAN, 1997: The distribution and cycling of mercury species in the western Mediterranean. *Deep Sea Res. II*, 44, 721-740.
- CURL, H, 1961: Standing crops of carbon, nitrogen and phosphorus, and transfer between trophic levels, in continental shelf waters south of New York. *Rapp. Proc.-Verb. Réunion. Cons. int. Explor. Mer*, 153, 183-189.
- DANIELSSON, L.G., MAGNUSSON, B. and S. WESTERLUND, 1978: An improved metal extraction procedure for the determination of trace metals in sea-water by atomic absorption spectrometry with electrothermal atomization. *Anal. Chim. Acta*, 98, 47-57.
- EDLER, L, (ed), 1979: Recommendations on methods for marine biological studies in the Baltic Sea. *Phytoplankton and chlorophyll*. Baltic Marine Biologists Publication, 5, 1-38.
- FIEKAS, V., ELKEN, J., MÜELLER, J., AITSAM, A. and W. ZENK, 1992: A View of the Canary Basin Thermocline Circulation in Winter. *J. Geophys. Res.*, 97(C8), 12.495-12.510.
- FILIBE, V. L.L. The Angola Dome observed in April 1997, 1998: Proceedings of international symposium and "On the variability of the marine ecosystems off the southern Africa", Swakopmund.
- FIRING, E., RANADA, J. and P. CALDWELL, 1995: Processing ADCP data with CODAS Software, Version 3.1. Technical Report, Joint Institute for Marine and Atmospheric Research, University of Hawaii, USA, 218 S.

- GARGAS, E., AERTEBJERG NIELSEN, G. and S. MORTENSEN, 1978: Phytoplankton production, chlorophyll-a and nutrients in the open Danish waters 1975-1977. The National Agency of Envir. Prot., Denmark, 1-61.
- GARZOLI, S.L. and GORDON, A. L., 1996: Origins and variability of the Benguela Current. *J. Geophys. Res.*, 101, C1, 897-906.
- GORDON, A. L., J.R.E. LUTHJEHARMS and M.L. GRÜNDLING, 1987: Stratification and circulation at the Agulhas Retroflexion. *Deep-Sea Res.*, 34, 565-599.
- GORDON, A. L., R.F. WEISS, W.M. SMETHIE, JR. and M.J. WARNER, 1991: Thermocline and intermediate water communication between the South Atlantic and the Indian Oceans. *J. Geophys. Res.*, 97, C5, 7223-7240.
- GORDON, A. L. and K. L. BOSLEY, 1991: Cyclonic gyre in the tropical South Atlantic. *Deep-Sea Res.*, 38(suppl. 1A), 323-343.
- GRASSHOFF, K., EHRHARDT, M. and K. KREMLING, 1983: *Methods of Seawater Analysis*. Chapter 4: Determination of nutrients. Verlag Chemie, Weinheim.
- HART, T.J. and CURRIE, R.I., 1960: The Benguela Current. *Discovery Reports*, 31, 123-298.
- HATCH, W.R. and W.L. OTT, 1968: Determination of submicrogram quantities of mercury by atomic absorption spectrophotometry. *Anal. Chem.*, 40, 2085-2087.
- HELCOM, 1991: Third biological intercalibration workshop, 27-31 August 1990, Visby, Sweden. *Baltic Mar. Environ. Proc.*, 38, 1-153.
- HELLERMAN, S., 1980: Charts of the variability of the wind stress over the tropical Atlantic. *Deep Sea Res. Part A*, , Suppl. II to Vol. 26, 63-76.
- HENTSCHEL, E., 1936: *Allgemeine Biologie des Südatlantischen Ozeans*. In A. Defant (Hrsg.) *Deutsche Atlantische Expedition auf dem Forschungsschiff Meteor" 1925-1927*. 11 (2), Walter de Gruyter und Co., Berlin und Leipzig, 1-343
- IKEDA, T., TORRES, J.J., HERNANDEZ-LEON, S. and S.P. GEIGER, 2000: Metabolism. Chapter 10, in: *The Zooplankton Methodology Manual*, International Council for the Exploration of the Sea. Academic Press, London. Pp. 455 - 532.
- JOHN, H.-CH. and C. ZELCK, 1997: Features, boundaries and connecting mechanisms of the Mauretanian Province exemplified by oceanic fish larvae. *Helgoländer Meeresunters.*, 51(2), 213-240.
- KELL, V. and R. BÖRNER, 1980: Untersuchungen zur Primärproduktion des Phytoplanktons in den Darß-Zingster Boddengewässern (südliche Ostsee). *Wiss. Ztschr. Wilhelm-Pieck-Univ. Rostock* 29, Math.-nat. R., 4/5, 55-60.

- LASS, H. U., SCHMIDT, M., MOHRHOLZ, V. and G. NAUSCH, 2000: Hydrographic and current measurements in the Angola-Benguela front area. *J. Phys. Oceanogr.*, 30, 2589-2609.
- LUND, J.W.C., KIPLING, C., and E.D. LECREN, 1958: The inverted microscope method of estimating algal numbers and the statistical basis of estimations by counting. *Hydrobiologia*, 11, 143-170.
- MART, L., NÜRNBERG, H.W. 1986: The distribution of cadmium in the sea. In: MISLIN, H., RAVERA, O. (eds.), *Cadmium in the environment*, 28-40
- MAZEIKA, P. A., 1967: Thermal domes in the Eastern Atlantic Ocean. *Limnol. Oceanogr.*, 12, 537-539.
- MEEUWIS, J. M. and J. R. E. LUTJEHARMS, 1990: Surface Thermal Characteristics of the Angola - Benguela Front. *S. Afr. J. mar. Sci.*, 9, 261-279.
- MOHRHOLZ, V., SCHMIDT, M. and J.R.E. LUTJEHARMS, 2001: The hydrography and dynamics of the Angola-Benguela Frontal Zone and environment in April 1999. *South Afr. J. Sci.*, 97, 199 - 208.
- MOLINARI, R. L., 1982: Observations of eastward currents in the tropical South Atlantic Ocean: 1978-1980. *J. Geophys. Res.*, 87, 9707-9714.
- MOLINARI, R. L., VOITUREZ, B. and P. DUNCAN, 1981: Observations in the subthermocline undercurrent of the South Atlantic Ocean: 1978 - 1980. *Oceanolog. Acta*, 4, 451-456.
- MOROSHKIN, K. V., BUBNOV, V. A. and R. P. BULATOV, 1970: Water circulation in the eastern South Atlantic Ocean. *Oceanology*, 10(1), 27-34.
- OMORI, M., 1969: Weight and chemical composition of some important oceanic zooplankton in the North Pacific Ocean. *Mar.Biol.*, 3, 4-10.
- PATTERSON, C. and D. SETTLE, 1976: The reduction of orders of magnitude errors in lead analysis of biological materials and natural waters by evaluating and controlling the extent and sources of industrial lead contamination introduced during sample collecting, handling, and analysis. United States/ National Bureau of Standards/ Special publication, No. 422, P. LaFleur, *Accuracy in trace analysis: Sampling, Sample handling, Analysis*, 321-351.
- POHL, C., KATTNER, G. and SCHULZ-BALDES, M. 1993: Cadmium, copper, lead and zinc on transects through Arctic and Eastern Atlantic surface and deep waters. *J. Mar. Syst.*, 4, 17-29.
- POHL, C., 1997: Trace Metals (Cu, Pb, Zn, Cd, Al, Li, Fe, Mn, Ni, Co) in Marine Suspended Particulate Matter: An International ICES Intercomparison Exercise. *Accred. Qual. Assur.*, 2, 2-10.

- POOL, R., M. TOMCZAK, 1999: Optimum multiparameter analysis of the water mass structure in the Atlantic Ocean thermocline. *Deep-Sea Res.*, 46, 1895-1921.
- POSTEL, L., ARNDT, E.A. and U. BRENNING, 1995: Rostock zooplankton studies off West Africa. *Helgoländer Meeresunters.* 49, 829-847.
- POSTEL, L., FOCK, H. and W. HAGEN, 2000: Biomass and abundance. In Harris, R., Wiebe, P. Lenz, J. Skjoldal, H.R., Huntley, M. (eds.), *ICES Zooplankton Methodological Manual*. Academic Press, San Diego, San Francisco, New York, Boston, London, Sydney, Tokyo, 83- 192.
- POSTEL, L., 1990: The mesozooplankton response to coastal upwelling off West Africa with particular regard to biomass. *Mar. Sci. Rep.* 1, 1-127.
- REID, J. L., JR., 1964: Evidence of a South Equatorial Counter Current in the Atlantic Ocean in July 1963. *Nature London*, 203, 182S.
- ROHDE, K. H. and D. NEHRING, 1979: Die Bestimmung von Nährstoffen und Schadstoffen im Meer- und Brackwasser. *Geod. Geophys. Veröff.* R.IV, H.29.
- RUTGERS VAN DER LOEFF, M., HELMERS, E. and KATTNER, G., 1997: Continuous transects of cadmium, copper, and aluminium in surface waters of the Atlantic Ocean, 50° N to 50° S: Correspondence and contrast with nutrient - like behaviour. *Geochim. et Cosmochim. Acta*, 61/1, 47-61.
- SHANNON, L.V. and NELSON, G, 1996: The Benguela: Large scale features and processes and system variability. *The South Atlantic: Present and past circulation*, Wefer, G., Berger, W. H., Siedler, G. Webb, D. J. (Eds.), 163-210.
- STRAMMA, L. and ENGLAND, M., 1999: On the water masses and mean circulation of the South Atlantic Ocean. *J. Geophys. Res.*, 104, C9, 20863-20883.
- TOMCZAK, M., 1998: Water mass analysis as a Tool for Climate Research, a workshop held in IAMAS/IAPSO General Assambly in Melbourne, 1997. *International WOCE Newsletter*, 30, 43S.
- UNESCO, 1968: Zooplankton sampling. *Monographs on oceanographic methodology* 2. The Unesco Press, Paris, 174 pp.
- VISBECK, M., 2000: Deep Velocity Profiling using Lowered Acoustic Doppler Current Profiler: Bottom Track and Inverse Solutions. *J. Atmos. Oceanic Technology*, submitted.
- VOITURIEZ, B., 1981: Les sous-courants équatoriaux nord et sud et la formation des dômes thermiques tropicaux. *Oceanologica Acta*, 4, 497-506.
- VOITURIEZ, B. and A. HERBLAND, 1982: Comparaison des systèmes productifs de l'Atlantique Tropical Est: dômes thermiques, upwellings côtiers et upwelling équatorial. *Rapp. Proc.-Verb. Réun. Cons. Int. Explor. Mer*, 180, 114-130.

- WACONGNE, S. and B. PITON, 1992: The near-surface circulation in the northeastern corner of the South Atlantic ocean. *Deep Sea Res.*, 39(7/8), 1273-1298.
- WESTERLUND, S. and ÖHMAN, P., 1991: Cadmium, copper, cobalt, nickel, lead and zinc in the water column of the Weddell Sea, Antarctica. *Geochim. Cosmochim. Acta*, 55, 2127-2146.
- WINKLER, L.W., 1888: . *Ber. dtsh. chem. Ges.*, 21, 2843-2855.
- WLOST, K. P., 1999: IOW-ReiseAssistent-Softwarepaket.
- WOCE, 1990: WOCE Hydrographic Operations and Methods. Dissolved Oxygen., unpublished.
- YAMAGATA, I. and S. IIZUKA, 1995: Simulation of the Subtropical Domes in the Atlantic: A Seasonal Cycle. *J. Phys. Oceanogr.*, 25(9), 2129-2124.

## List of Figures

1.1	Principle circulation in the Southeast Atlantic . . . . .	7
2.1	Map of hydrographical sections . . . . .	14
2.2	Map of hydrographical stations . . . . .	15
2.3	Map of phytoplankton stations . . . . .	16
2.4	Map of Multinet stations . . . . .	17
3.1	Multinet sampling performance . . . . .	43
4.1	Calibration of the thermosalinograph - temperature . . . . .	46
4.2	Calibration of the therosalinograph - salinity . . . . .	47
4.3	Relationship between dry mass and ash free dry mass of zooplankton . . . . .	52
5.1	Time series of wind and air pressure . . . . .	55
5.2	Time series of air temperature and moist, global- and long wave radiation . . . . .	56
5.3	Time series of ship position and echo sounding depth . . . . .	57
5.4	Sea surface temperature, salinity, phosphate and ERS-2 wind. . . . .	58
5.5	T-S diagram of all CTD measurements. . . . .	61
5.6	Horizontal distribution of T, S, O <sub>2</sub> and Chl.a-fluorescence at 0 m depth. . . . .	62
5.7	Horizontal distribution of T, S, O <sub>2</sub> and Chl.a-fluorescence at 50 m depth. . . . .	63
5.8	Horizontal distribution of T, S, O <sub>2</sub> and Chl.a-fluorescence at 200 m depth. . . . .	64
5.9	Horizontal distribution of T, S, O <sub>2</sub> and Chl.a-fluorescence at 400 m depth. . . . .	65
5.10	Horizontal distribution of T, S, O <sub>2</sub> and Chl.a-fluorescence at 800 m depth. . . . .	66
5.11	Horizontal distribution of T, S, O <sub>2</sub> and Chl.a-fluorescence at 1200 m depth. . . . .	67
5.12	Section 01 vertical distribution of T, S, $\sigma$ and O <sub>2</sub> (0-1200 m). . . . .	68
5.13	Section 01 vertical distribution of T, S, $\sigma$ and O <sub>2</sub> (0-200 m) . . . . .	69
5.14	Section 02 vertical distribution of T, S, $\sigma$ and O <sub>2</sub> (0-1200 m). . . . .	70
5.15	Section 02 vertical distribution of T, S, $\sigma$ and O <sub>2</sub> (0-200 m) . . . . .	71
5.16	Section 03 vertical distribution of T, S, $\sigma$ and O <sub>2</sub> (0-1200 m). . . . .	72
5.17	Section 03 vertical distribution of T, S, $\sigma$ and O <sub>2</sub> (0-200 m) . . . . .	73
5.18	Section 04 vertical distribution of T, S, $\sigma$ and O <sub>2</sub> (0-1200 m). . . . .	74
5.19	Section 04 vertical distribution of T, S, $\sigma$ and O <sub>2</sub> (0-200 m) . . . . .	75
5.20	Section 05 vertical distribution of T, S, $\sigma$ and O <sub>2</sub> (0-1200 m). . . . .	76
5.21	Section 05 vertical distribution of T, S, $\sigma$ and O <sub>2</sub> (0-200 m) . . . . .	77
5.22	Section 06 vertical distribution of T, S, $\sigma$ and O <sub>2</sub> (0-1200 m). . . . .	78
5.23	Section 06 vertical distribution of T, S, $\sigma$ and O <sub>2</sub> (0-200 m) . . . . .	79
5.24	Section 10 vertical distribution of T, S, $\sigma$ and O <sub>2</sub> (0-1200 m). . . . .	80
5.25	Section 10 vertical distribution of T, S, $\sigma$ and O <sub>2</sub> (0-200 m) . . . . .	81
5.26	Tracks of released ARGOS drifter. . . . .	83
5.27	Vector plot of currents at 30-60 m and 60-100 m depth (VMADCP) . . . . .	84
5.28	Vector plot of currents at 100-200 m and 200-400 m depth (VMADCP) . . . . .	85
5.29	Vector plot of currents at 30-60 m and 60-100 m depth (LADCP) . . . . .	86
5.30	Vector plot of currents at 100-200 m and 200-600 m depth (LADCP) . . . . .	87
5.31	Vector plot of currents at 600-1000 m and 1000-1400 m depth (LADCP) . . . . .	88
5.32	Horizontal distribution of PO <sub>4</sub> , NO <sub>3</sub> , SiO <sub>4</sub> and N-P ratio at 0 m depth. . . . .	91
5.33	Horizontal distribution of PO <sub>4</sub> , NO <sub>3</sub> , SiO <sub>4</sub> and N-P ratio at 60 m depth. . . . .	92

5.34	Horizontal distribution of PO <sub>4</sub> , NO <sub>3</sub> , SiO <sub>4</sub> and N-P ratio at 200 m depth. . . . .	93
5.35	Horizontal distribution of PO <sub>4</sub> , NO <sub>3</sub> , SiO <sub>4</sub> and N-P ratio at 800 m depth. . . . .	94
5.36	Horizontal distribution of PO <sub>4</sub> , NO <sub>3</sub> , SiO <sub>4</sub> and N-P ratio at 1200 m depth. . . . .	95
5.37	Horizontal distribution of NO <sub>2</sub> and NH <sub>4</sub> at depth of their maximum. . . . .	96
5.38	Section 10 vertical distribution of PO <sub>4</sub> , NO <sub>3</sub> , SiO <sub>4</sub> and O <sub>2</sub> (0-1200 m). . . . .	97
5.39	Section 10 vertical distribution of PO <sub>4</sub> , NO <sub>3</sub> , SiO <sub>4</sub> and O <sub>2</sub> (0-200 m). . . . .	98
5.40	Surface water Cd concentrations in nmol kg <sup>-1</sup> , (unfiltered samples) . . . . .	100
5.41	Vertical distribution of Cd, Cu and Ni . . . . .	101
5.42	Horizontal distribution of chlorophyll-a and of primary production. . . . .	102
5.43	The average zooplankton AFDM dominance of the different size classes . . . . .	105
5.44	Horizontally distribution of total AFDM concentration for the sum of all size categories at three depth levels. . . . .	105
5.45	Horizontally distribution of the total ash content for the sum of all size categories . .	106
5.46	Vertical distribution of ash free dry mass concentration at section 10 . . . . .	107

## List of Tables

3.1	Mean values and standard deviation of heading . . . . .	21
3.2	Table of basic meteorological sensors . . . . .	22
3.3	Configuration of the vessel mounted ADCP . . . . .	25
3.4	Configuration of the CTD SBE 911+ . . . . .	28
3.5	Configuration of the CTD SBE 911+ Software . . . . .	28
3.6	Slope correction factor of oxygen sensor OX9904 for different station ranges . . . . .	31
3.7	Calibration data of the salinometer . . . . .	32
3.8	Calibration data of reversing thermometer . . . . .	32
3.9	Configuration of the lowered ADCP . . . . .	34
3.10	Specifications of ARGOS surface drifter released by R/V Meteor . . . . .	35
4.1	File format of validated DVS meta data . . . . .	48
4.2	Error thresholds for bad VMADCP data . . . . .	49
4.3	VMADCP calibration coefficients . . . . .	49
4.4	CTD sensor calibration coefficients . . . . .	50
4.5	LADCP post processing parameter . . . . .	50
4.6	Correlation between the ash free dry mass and the LADCP backscattering . . . . .	52
5.1	Cd concentrations (nmol kg <sup>-1</sup> ) in surface waters and at oxygen minimum. . . . .	99
5.2	Statistics of the zooplankton ash free dry mass concentrations. . . . .	104
	List of CTD-Stations . . . . .	115
	List of Phytoplankton-Stations . . . . .	118
	List of Multinet tows . . . . .	120

## Appendix A Station lists

The CTD-casts can be identified from a consecutive cast number from 387 to 459 and a station label (shown in figure 2.2). Additionally the station list shows station date, time and position. Because LADCP-casts were performed at each CTD-cast they are not listed separately. The particular LADCP cast number is the CTD cast number with prefix 'm'.

Table A.1: List of CTD stations

Cast	Serie	Station name	Time [UTC]	Date	Latitude [deg]	Longitude [deg]	Magnetic deviation [deg]
387	1	N0703	10:10	27.08.00	19° 09.98' S	11° 40.47' E	-13.5°
387	2	N0703	11:29	27.08.00	19° 10.59' S	11° 40.93' E	
387	3	N0703	11:34	27.08.00	19° 10.61' S	11° 40.90' E	
387	4	N0703	11:41	27.08.00	19° 10.66' S	11° 40.83' E	
389	1	N0101	19:54	30.08.00	09° 00.18' S	12° 55.60' E	-7.0°
390	1	N0102	21:34	30.08.00	09° 00.05' S	12° 45.07' E	-7.0°
391	1	N0103	1:22	31.08.00	09° 00.07' S	12° 34.76' E	-7.2°
391	2	N0103	2:30	31.08.00	09° 00.04' S	12° 34.86' E	
392	1	N0104	4:04	31.08.00	09° 00.00' S	12° 24.89' E	-7.8°
393	1	N0105	6:53	31.08.00	09° 00.03' S	12° 05.05' E	-7.8°
393	2	N0105	7:54	31.08.00	09° 00.04' S	12° 05.09' E	
394	1	N0106	10:44	31.08.00	09° 00.01' S	11° 40.29' E	-7.1°
395	1	N0107	15:37	31.08.00	09° 00.00' S	11° 00.20' E	-7.1°
396	1	N0120	22:35	31.08.00	08° 59.99' S	10° 12.37' E	-7.6°
396	2	N0120	23:48	31.08.00	08° 59.98' S	10° 12.35' E	
397	1	N0121	4:07	01.09.00	09° 00.00' S	09° 30.25' E	-7.7°
398	1	N0122	9:15	01.09.00	09° 00.02' S	08° 45.01' E	-8.1°
399	1	N0123	18:11	01.09.00	09° 00.01' S	07° 59.95' E	-8.5°
400	1	N0111	1:07	02.09.00	10° 00.00' S	07° 59.93' E	-9.1°
400	2	N0111	2:20	02.09.00	09° 59.99' S	08° 00.04' E	
400	3	N0111	2:23	02.09.00	10° 00.00' S	08° 00.04' E	
401	1	N0220	8:38	02.09.00	10° 59.94' S	08° 00.01' E	-9.7°
402	1	N0213	17:09	02.09.00	11° 59.97' S	08° 00.03' E	-10.3°
403	1	N0212	21:27	02.09.00	11° 47.85' S	08° 37.93' E	-9.9°
403	2	N0212	21:43	02.09.00	11° 47.97' S	08° 38.23' E	
403	3	N0212	22:56	02.09.00	11° 47.95' S	08° 38.48' E	
403	4	N0212	23:00	02.09.00	11° 47.94' S	08° 38.50' E	
404	1	N0211	2:51	03.09.00	11° 36.00' S	09° 15.12' E	-9.5°
405	1	N0210	6:58	03.09.00	11° 23.94' S	09° 49.60' E	-9.1°
405	2	N0210	7:12	03.09.00	11° 24.00' S	09° 50.02' E	
405	3	N0210	7:59	03.09.00	11° 24.00' S	09° 50.15' E	
406	1	N0209	11:28	03.09.00	11° 12.03' S	10° 24.68' E	-9.0°
407	1	N0208	17:33	03.09.00	10° 59.98' S	11° 00.28' E	-8.5°
407	2	N0208	18:21	03.09.00	11° 00.00' S	11° 00.33' E	
408	1	N0207	22:35	03.09.00	10° 59.98' S	11° 45.32' E	-8.0°
408	2	N0207	23:40	03.09.00	11° 00.01' S	11° 45.34' E	
408	3	N0207	23:54	03.09.00	11° 00.01' S	11° 45.36' E	

Table A.1: List of CTD stations (continued)

Cast	Serie	Station name	Time [UTC]	Date	Latitude [deg]	Longitude [deg]	Magnetic deviation [deg]
409	1	N0206	2:24	04.09.00	11° 00.10' S	12° 10.68' E	-8.0°
409	2	N0206	3:47	04.09.00	11° 00.13' S	12° 10.88' E	
410	1	N0205	7:54	04.09.00	10° 59.77' S	12° 44.64' E	-8.0°
410	2	N0205	8:09	04.09.00	11° 00.02' S	12° 44.94' E	
410	3	N0205	8:58	04.09.00	11° 00.12' S	12° 45.07' E	
411	1	N0204	11:45	04.09.00	10° 59.95' S	13° 09.99' E	-7.0°
412	1	N0203	16:38	04.09.00	10° 59.96' S	13° 25.05' E	-7.5°
413	1	N0202	18:03	04.09.00	10° 59.75' S	13° 34.92' E	-7.4°
413	2	N0202	18:17	04.09.00	10° 59.95' S	13° 35.11' E	
413	3	N0202	18:28	04.09.00	10° 59.98' S	13° 35.21' E	
414	1	N0201	19:10	04.09.00	10° 59.84' S	13° 41.92' E	-7.4°
414	2	N0201	19:22	04.09.00	10° 59.97' S	13° 42.33' E	
414	3	N0201	19:33	04.09.00	10° 59.97' S	13° 42.34' E	
415	1	N0301	8:05	05.09.00	12° 59.68' S	12° 49.93' E	-9.4°
415	2	N0301	8:16	05.09.00	13° 00.01' S	12° 49.72' E	
415	3	N0301	8:30	05.09.00	13° 00.03' S	12° 49.63' E	
416	1	N0302	9:23	05.09.00	12° 59.93' S	12° 40.45' E	-8.8°
416	2	N0302	9:35	05.09.00	13° 00.03' S	12° 40.12' E	
416	3	N0302	10:21	05.09.00	13° 00.18' S	12° 39.97' E	
417	1	N0303	12:56	05.09.00	13° 00.05' S	12° 34.72' E	-9.0°
418	1	N0304	14:51	05.09.00	13° 00.04' S	12° 24.85' E	-9.0°
419	1	N0305	17:56	05.09.00	12° 59.92' S	12° 00.02' E	-9.2°
419	2	N0305	18:05	05.09.00	13° 00.01' S	11° 59.91' E	
419	3	N0305	18:55	05.09.00	13° 00.05' S	11° 59.85' E	
420	1	N0306	20:50	05.09.00	12° 59.83' S	11° 39.88' E	-9.3°
420	2	N0306	21:03	05.09.00	12° 59.98' S	11° 39.79' E	
421	1	N0307	1:40	06.09.00	12° 59.98' S	11° 00.13' E	-9.5°
421	2	N0307	3:05	06.09.00	12° 59.97' S	11° 00.14' E	
421	3	N0307	3:20	06.09.00	13° 00.24' S	10° 59.43' E	
422	1	N0308	7:11	06.09.00	13° 13.79' S	10° 20.15' E	-10.0°
422	2	N0308	7:23	06.09.00	13° 14.00' S	10° 19.79' E	
422	3	N0308	8:13	06.09.00	13° 14.08' S	10° 19.92' E	
423	1	N0309	14:54	06.09.00	13° 27.03' S	09° 40.10' E	-10.4°
424	1	N0310	20:13	06.09.00	13° 42.73' S	08° 54.25' E	-11.0°
424	2	N0310	20:25	06.09.00	13° 42.96' S	08° 54.05' E	
424	3	N0310	21:13	06.09.00	13° 43.12' S	08° 54.26' E	
425	1	N0311	2:31	07.09.00	13° 59.97' S	07° 59.95' E	-11.5°
426	1	N0420	9:57	07.09.00	15° 00.00' S	07° 59.93' E	-12.3°
427	1	N0410	22:07	07.09.00	16° 00.03' S	07° 59.96' E	-12.9°
427	2	N0410	23:20	07.09.00	15° 59.97' S	08° 00.10' E	
428	1	N0409	4:24	08.09.00	15° 45.97' S	08° 50.12' E	-12.3°
429	1	N0408	8:33	08.09.00	15° 33.03' S	09° 25.06' E	-11.9°
429	2	N0408	8:45	08.09.00	15° 33.01' S	09° 25.56' E	
429	3	N0408	9:34	08.09.00	15° 33.02' S	09° 25.79' E	
430	1	N0407	12:34	08.09.00	15° 22.04' S	09° 55.68' E	-11.9°

Table A.1: List of CTD stations (continued)

Cast	Serie	Station name	Time [UTC]	Date	Latitude [deg]	Longitude [deg]	Magnetic deviation [deg]
431	1	N0406	18:34	08.09.00	15° 11.99' S	10° 24.29' E	-11.3°
431	2	N0406	18:46	08.09.00	15° 11.99' S	10° 24.73' E	
431	3	N0406	19:34	08.09.00	15° 12.03' S	10° 24.91' E	
432	1	N0405	22:58	08.09.00	14° 59.99' S	11° 00.15' E	-11.0°
433	1	N0404	2:20	09.09.00	15° 00.01' S	11° 24.98' E	-11.0°
434	1	N0403	4:49	09.09.00	15° 00.02' S	11° 40.16' E	-10.7°
435	1	N0402	7:03	09.09.00	14° 59.85' S	11° 54.70' E	-10.4°
435	2	N0402	7:18	09.09.00	15° 00.03' S	11° 54.94' E	
435	3	N0402	8:08	09.09.00	14° 59.85' S	11° 54.50' E	
436	1	N0401	11:31	09.09.00	15° 00.07' S	12° 05.36' E	-10.5°
437	1	N0502	18:16	09.09.00	15° 59.65' S	11° 30.43' E	-11.3°
437	2	N0502	18:28	09.09.00	16° 00.10' S	11° 30.20' E	
437	3	N0502	19:17	09.09.00	16° 00.33' S	11° 30.27' E	
438	1	N0601	1:14	10.09.00	17° 00.02' S	11° 35.39' E	-10.7°
438	2	N0601	1:45	10.09.00	17° 00.03' S	11° 35.45' E	
439	1	N0602	3:31	10.09.00	17° 00.01' S	11° 20.50' E	-11.0°
440	1	N0603	5:51	10.09.00	16° 59.98' S	10° 59.79' E	-11.2°
441	1	N0604	10:56	10.09.00	17° 07.80' S	10° 35.19' E	-12.5°
442	1	N0605	14:05	10.09.00	17° 16.04' S	10° 12.82' E	-12.7°
443	1	N0606	18:06	10.09.00	17° 26.96' S	09° 40.48' E	-13.1°
444	1	N0607	23:59	10.09.00	17° 37.94' S	09° 10.48' E	-13.5°
445	1	N0608	4:07	11.09.00	17° 50.00' S	08° 39.71' E	-13.8°
446	1	N0609	8:55	11.09.00	17° 59.94' S	08° 00.18' E	-14.6°
446	2	N0609	9:06	11.09.00	18° 00.13' S	08° 00.11' E	
447	1	N0610	18:41	11.09.00	18° 59.48' S	07° 59.94' E	-15.0°
447	2	N0610	18:54	11.09.00	18° 59.95' S	07° 59.99' E	
447	3	N0610	19:43	11.09.00	18° 59.93' S	08° 00.23' E	
448	1	N0720	0:36	12.09.00	19° 40.95' S	07° 59.97' E	-15.5°
448	2	N0720	1:49	12.09.00	19° 40.95' S	07° 59.94' E	
449	1	N0712	6:04	12.09.00	20° 18.76' S	07° 59.95' E	-15.8°
449	2	N0712	6:15	12.09.00	20° 18.97' S	08° 00.00' E	
449	3	N0712	7:04	12.09.00	20° 19.04' S	08° 00.11' E	
450	1	N0721	11:00	12.09.00	20° 06.71' S	08° 37.90' E	-15.5°
451	1	N0709	19:22	12.09.00	19° 53.98' S	09° 14.96' E	-15.0°
452	1	N0708	0:02	13.09.00	19° 44.01' S	09° 50.13' E	-14.5°
452	2	N0708	1:11	13.09.00	19° 43.99' S	09° 50.13' E	
453	1	N0707	4:23	13.09.00	19° 34.97' S	10° 19.52' E	-14.3°
454	1	N0706	7:45	13.09.00	19° 27.00' S	10° 44.79' E	-14.0°
455	1	N0705	12:35	13.09.00	19° 20.98' S	11° 05.31' E	-13.7°
456	1	N0704	14:54	13.09.00	19° 16.00' S	11° 20.39' E	-13.5°
457	1	N0703	17:25	13.09.00	19° 09.99' S	11° 40.22' E	-13.3°
458	1	N0702	21:43	13.09.00	19° 04.28' S	12° 00.03' E	-13.0°
459	1	N0701	23:41	13.09.00	18° 58.97' S	12° 14.93' E	-12.8°

Table A.2: List of Phytoplankton stations

Cast	Station name	Time [UTC]	Date	Latitude [deg]	Longitude [deg]
387	N0703	9:53	27.08.00	19° 10.07' S	11° 40.06' E
389	N0101	19:35	30.08.00	09° 00.51' S	12° 55.71' E
391	N0103	1:14	31.08.00	09° 00.03' S	12° 34.77' E
393	N0105	6:45	31.08.00	09° 00.02' S	12° 05.05' E
395	N0107	15:31	31.08.00	09° 00.00' S	11° 00.18' E
397	N0121	4:01	01.09.00	09° 00.00' S	09° 30.24' E
398	N0122	9:05	01.09.00	08° 59.90' S	08° 45.02' E
399	N0123	18:05	01.09.00	08° 59.97' S	07° 59.96' E
401	N0220	8:29	02.09.00	10° 59.94' S	08° 00.00' E
402	N0213	17:05	02.09.00	11° 59.98' S	08° 00.03' E
405	N0210	6:58	03.09.00	11° 23.95' S	09° 49.57' E
406	N0209	11:23	03.09.00	11° 12.01' S	10° 24.71' E
407	N0208	17:31	03.09.00	10° 59.98' S	11° 00.27' E
408	N0207	22:31	03.09.00	10° 59.97' S	11° 45.32' E
410	N0205	7:54	04.09.00	10° 59.77' S	12° 44.63' E
411	N0204	11:40	04.09.00	10° 59.96' S	13° 10.01' E
412	N0203	16:28	04.09.00	10° 59.88' S	13° 24.99' E
413	N0202	18:03	04.09.00	10° 59.75' S	13° 34.91' E
414	N0201	19:09	04.09.00	10° 59.84' S	13° 41.85' E
415	N0301	8:04	05.09.00	12° 59.65' S	12° 49.94' E
417	N0303	12:51	05.09.00	13° 00.03' S	12° 34.74' E
419	N0305	17:56	05.09.00	12° 59.91' S	12° 00.03' E
421	N0307	1:34	06.09.00	12° 59.96' S	11° 00.14' E
422	N0308	7:11	06.09.00	13° 13.78' S	10° 20.17' E
423	N0309	14:51	06.09.00	13° 27.02' S	09° 40.05' E
425	N0311	2:27	07.09.00	13° 59.98' S	07° 59.95' E
426	N0420	9:52	07.09.00	15° 00.00' S	07° 59.95' E
427	N0410	22:01	07.09.00	16° 00.03' S	07° 59.94' E
428	N0409	4:20	08.09.00	15° 45.98' S	08° 50.11' E
429	N0408	8:33	08.09.00	15° 33.04' S	09° 25.05' E
430	N0407	12:29	08.09.00	15° 22.01' S	09° 55.66' E
431	N0406	18:34	08.09.00	15° 11.99' S	10° 24.26' E
433	N0404	2:20	09.09.00	15° 00.01' S	11° 24.98' E
434	N0403	4:44	09.09.00	15° 00.00' S	11° 40.19' E
435	N0402	7:02	09.09.00	14° 59.85' S	11° 54.65' E
436	N0401	11:23	09.09.00	15° 00.01' S	12° 05.39' E
438	N0601	1:09	10.09.00	17° 00.02' S	11° 35.38' E
439	N0602	3:28	10.09.00	17° 00.02' S	11° 20.46' E
440	N0603	5:47	10.09.00	16° 59.97' S	10° 59.78' E
441	N0604	10:51	10.09.00	17° 07.81' S	10° 35.21' E
442	N0605	14:01	10.09.00	17° 16.02' S	10° 12.82' E
443	N0606	18:00	10.09.00	17° 26.98' S	09° 40.48' E
445	N0608	4:03	11.09.00	17° 50.00' S	08° 39.69' E
446	N0609	8:55	11.09.00	17° 59.94' S	08° 00.19' E
449	N0712	6:04	12.09.00	20° 18.75' S	07° 59.95' E

Table A.2: List of Phytoplankton stations (continued)

Cast	Station name	Time [UTC]	Date	Latitude [deg]	Longitude [deg]
450	N0721	10:55	12.09.00	20° 06.71' S	08° 37.88' E
451	N0709	19:15	12.09.00	19° 53.97' S	09° 14.93' E
453	N0707	4:18	13.09.00	19° 34.96' S	10° 19.51' E
454	N0706	7:40	13.09.00	19° 26.98' S	10° 44.77' E
456	N0704	14:50	13.09.00	19° 15.99' S	11° 20.39' E
457	N0703	17:25	13.09.00	19° 09.99' S	11° 40.22' E
458	N0702	21:38	13.09.00	19° 04.27' S	12° 00.00' E
459	N0701	23:36	13.09.00	18° 58.99' S	12° 14.97' E

Table A.3: List of Multinet tows

Station number	Cast MN	Serie MN	Station name	Time [UTC]	Date	Latitude [deg]	Longitude [deg]
389	0	0	N0101	19:54	30.08.00	12° 51.47' S	12° 47.38' E
390	1	0	N0102	22:11	30.08.00	10° 59.35' S	12° 44.98' E
390	1	1	N0102	22:11	30.08.00	10° 59.34' S	12° 44.98' E
390	1	2	N0102	23:42	30.08.00	10° 56.99' S	12° 44.54' E
395	2	0	N0107	16:40	31.08.00	10° 59.88' S	11° 00.15' E
395	2	1	N0107	16:40	31.08.00	10° 59.88' S	11° 00.15' E
395	2	2	N0107	17:54	31.08.00	10° 58.63' S	10° 58.84' E
398	3	0	N0122	10:29	01.09.00	10° 59.43' S	08° 44.60' E
398	3	1	N0122	10:29	01.09.00	10° 59.43' S	08° 44.60' E
398	3	2	N0122	13:33	01.09.00	10° 58.74' S	08° 39.91' E
401	4	0	N0220	9:52	02.09.00	12° 59.56' S	08° 00.24' E
401	4	1	N0220	9:52	02.09.00	12° 59.55' S	08° 00.24' E
401	4	2	N0220	10:50	02.09.00	12° 58.22' S	08° 00.30' E
406	5	0	N0209	12:21	03.09.00	12° 47.76' S	10° 24.70' E
406	5	1	N0209	12:21	03.09.00	12° 47.76' S	10° 24.70' E
406	5	2	N0209	13:44	03.09.00	12° 45.93' S	10° 24.89' E
411	6	0	N0204	12:40	04.09.00	12° 59.99' S	13° 09.99' E
411	6	1	N0204	12:40	04.09.00	12° 59.99' S	13° 09.99' E
411	6	2	N0204	13:51	04.09.00	12° 58.90' S	13° 10.14' E
416	7	0	N0302	10:27	05.09.00	14° 59.77' S	12° 39.94' E
416	7	1	N0302	10:27	05.09.00	14° 59.77' S	12° 39.94' E
416	7	2	N0302	11:45	05.09.00	14° 58.13' S	12° 38.67' E
422	8	0	N0308	9:59	06.09.00	14° 44.15' S	10° 19.23' E
422	8	1	N0308	9:59	06.09.00	14° 44.15' S	10° 19.23' E
422	8	2	N0308	10:28	06.09.00	14° 43.72' S	10° 19.07' E
426	9	0	N0420	10:51	07.09.00	16° 59.88' S	08° 00.03' E
426	9	1	N0420	10:51	07.09.00	16° 59.88' S	08° 00.03' E
426	9	2	N0420	14:34	07.09.00	16° 56.43' S	08° 00.54' E
430	10	0	N0407	13:27	08.09.00	16° 37.65' S	09° 55.76' E
430	10	1	N0407	13:27	08.09.00	16° 37.65' S	09° 55.76' E
430	10	2	N0407	15:25	08.09.00	16° 34.57' S	09° 55.69' E
435	11	0	N0402	8:14	09.09.00	15° 00.12' S	11° 54.56' E
435	11	1	N0402	8:14	09.09.00	15° 00.12' S	11° 54.58' E
435	11	2	N0402	9:54	09.09.00	15° 00.72' S	11° 56.09' E
440	12	0	N0603	6:46	10.09.00	18° 59.74' S	10° 59.74' E
440	12	1	N0603	6:46	10.09.00	18° 59.74' S	10° 59.74' E
440	12	2	N0603	8:24	10.09.00	18° 58.00' S	10° 58.61' E
443	13	0	N0606	18:59	10.09.00	18° 32.97' S	09° 40.73' E
443	13	1	N0606	18:59	10.09.00	18° 32.97' S	09° 40.73' E
443	13	2	N0606	20:33	10.09.00	18° 31.70' S	09° 41.85' E
446	14	0	N0609	9:57	11.09.00	19° 59.54' S	08° 00.32' E
446	14	1	N0609	9:58	11.09.00	19° 59.52' S	08° 00.33' E
446	14	2	N0609	12:00	11.09.00	19° 57.03' S	08° 01.81' E
450	15	0	N0721	11:53	12.09.00	21° 53.24' S	08° 37.97' E
450	15	1	N0721	11:53	12.09.00	21° 53.24' S	08° 37.98' E

Table A.3: List of Multinet tows (continued)

Station number	Cast MN	Serie MN	Station name	Time [UTC]	Date	Latitude [deg]	Longitude [deg]
450	15	2	N0721	14:28	12.09.00	21° 50.93' S	08° 38.69' E
454	16	0	N0706	8:38	13.09.00	20° 32.90' S	10° 45.18' E
454	16	1	N0706	8:38	13.09.00	20° 32.90' S	10° 45.19' E
454	16	2	N0706	10:20	13.09.00	20° 31.49' S	10° 47.65' E
457	17	0	N0703	17:54	13.09.00	20° 49.85' S	11° 40.46' E
457	17	1	N0703	17:54	13.09.00	20° 49.85' S	11° 40.46' E
457	17	2	N0703	19:30	13.09.00	20° 48.71' S	11° 43.05' E

# Meereswissenschaftliche Berichte

## MARINE SCIENCE REPORTS

---

- 1 (1990) Postel, Lutz:  
Die Reaktion des Mesozooplanktons, speziell der Biomasse, auf küstennahen Auftrieb vor Westafrika (The mesozooplankton response to coastal upwelling off West Africa with particular regard to biomass)
- 2 (1990) Nehring, Dietwart:  
Die hydrographisch-chemischen Bedingungen in der westlichen und zentralen Ostsee von 1979 bis 1988 – ein Vergleich (Hydrographic and chemical conditions in the western and central Baltic Sea from 1979 to 1988 – a comparison)  
Nehring, Dietwart; Matthäus, Wolfgang:  
Aktuelle Trends hydrographischer und chemischer Parameter in der Ostsee, 1958 – 1989 (Topical trends of hydrographic and chemical parameters in the Baltic Sea, 1958 – 1989)
- 3 (1990) Zahn, Wolfgang:  
Zur numerischen Vorticityanalyse mesoskaliger Strom- und Massenfelder im Ozean (On numerical vorticity analysis of mesoscale current and mass fields in the ocean)
- 4 (1992) Lemke, Wolfram; Lange, Dieter; Endler, Rudolf (Eds.):  
Proceedings of the Second Marine Geological Conference – The Baltic, held in Rostock from October 21 to October 26, 1991
- 5 (1993) Endler, Rudolf; Lackschewitz, Klas (Eds.):  
Cruise Report RV "Sonne" Cruise SO82, 1992
- 6 (1993) Kulik, Dmitri A.; Harff, Jan:  
Physicochemical modeling of the Baltic Sea water-sediment column:  
I. Reference ion association models of normative seawater and of Baltic brackish waters at salinities 1–40 ‰, 1 bar total pressure and 0 to 30 °C temperature  
(system Na–Mg–Ca–K–Sr–Li–Rb–Cl–S–C–Br–F–B–N–Si–P–H–O)
- 7 (1994) Nehring, Dietwart; Matthäus, Wolfgang; Lass, Hans-Ulrich; Nausch, Günther:  
Hydrographisch-chemische Zustandseinschätzung der Ostsee 1993
- 8 (1995) Hagen, Eberhard; John, Hans-Christian:  
Hydrographische Schnitte im Ostrandstromsystem vor Portugal und Marokko 1991 - 1992
- 9 (1995) Nehring, Dietwart; Matthäus, Wolfgang; Lass, Hans Ulrich; Nausch, Günther; Nagel, Klaus:  
Hydrographisch-chemische Zustandseinschätzung der Ostsee 1994  
Seifert, Torsten; Kayser, Bernd:  
A high resolution spherical grid topography of the Baltic Sea
- 10 (1995) Schmidt, Martin:  
Analytical theory and numerical experiments to the forcing of flow at isolated topographic features
- 11 (1995) Kaiser, Wolfgang; Nehring, Dietwart; Breuel, Günter; Wasmund, Norbert; Siegel, Herbert; Witt, Gesine; Kerstan, Eberhard; Sadkowiak, Birgit:  
Zeitreihen hydrographischer, chemischer und biologischer Variablen an der Küstenstation Warnemünde (westliche Ostsee)  
Schneider, Bernd; Pohl, Christa:  
Spurenmittelkonzentrationen vor der Küste Mecklenburg-Vorpommerns

- 12 (1996) Schinke, Holger:  
Zu den Ursachen von Salzwassereinbrüchen in die Ostsee
- 13 (1996) Meyer-Harms, Bettina:  
Ernährungsstrategie calanoider Copepoden in zwei unterschiedlich trophierten Seegebieten der Ostsee (Pommernbucht, Gotlandsee)
- 14 (1996) Reckermann, Marcus:  
Ultraplankton and protozoan communities and their interactions in different marine pelagic ecosystems (Arabian Sea and Baltic Sea)
- 15 (1996) Kerstan, Eberhard:  
Untersuchung der Verteilungsmuster von Kohlenhydraten in der Ostsee unter Berücksichtigung produktionsbiologischer Meßgrößen
- 16 (1996) Nehring, Dietwart; Matthäus, Wolfgang; Lass, Hans Ulrich; Nausch, Günther; Nagel, Klaus:  
Hydrographisch-chemische Zustandseinschätzung der Ostsee 1995
- 17 (1996) Brosin, Hans-Jürgen:  
Zur Geschichte der Meeresforschung in der DDR
- 18 (1996) Kube, Jan:  
The ecology of macrozoobenthos and sea ducks in the Pomeranian Bay
- 19 (1996) Hagen, Eberhard (Editor):  
GOBEX - Summary Report
- 20 (1996) Harms, Andreas:  
Die bodennahe Trübezone der Mecklenburger Bucht unter besonderer Betrachtung der Stoffdynamik bei Schwermetallen
- 21 (1997) Zülicke, Christoph; Hagen, Eberhard:  
GOBEX Report - Hydrographic Data at IOW
- 22 (1997) Lindow, Helma:  
Experimentelle Simulationen windangeregter dynamischer Muster in hochauflösenden numerischen Modellen
- 23 (1997) Thomas, Helmuth:  
Anorganischer Kohlenstoff im Oberflächenwasser der Ostsee
- 24 (1997) Matthäus, Wolfgang; Nehring, Dietwart; Lass, Hans Ulrich; Nausch, Günther; Nagel, Klaus; Siegel, Herbert:  
Hydrographisch-chemische Zustandseinschätzung der Ostsee 1996
- 25 (1997) v. Bodungen, Bodo; Hentzsch, Barbara (Herausgeber):  
Neue Forschungslandschaften und Perspektiven der Meeresforschung - Reden und Vorträge zum Festakt und Symposium am 3. März 1997.
- 26 (1997) Lakaschus, Sönke:  
Konzentrationen und Depositionen atmosphärischer Spurenmetalle an der Küstenstation Arkona
- 27 (1997) Löffler, Annetrin:  
Die Bedeutung von Partikeln für die Spurenmetallverteilung in der Ostsee, insbesondere unter dem Einfluß sich ändernder Redoxbedingungen in den zentralen Tiefenbecken
- 28 (1998) Leipe, Thomas; Eidam, Jürgen; Lampe, Reinhard; Meyer, Hinrich; Neumann, Thomas; Osadczuk, Andrzej; Janke, Wolfgang; Puff, Thomas; Blanz, Thomas; Gingele, Franz Xaver; Dannenberger, Dirk; Witt, Gesine:  
Das Oderhaff. Beiträge zur Rekonstruktion der holozänen geologischen Entwicklung und anthropogenen Beeinflussung des Oder-Ästuars.
- 29 (1998) Matthäus, Wolfgang; Nausch, Günther; Lass, Hans Ulrich; Nagel, Klaus; Siegel, Herbert:  
Hydrographisch-chemische Zustandseinschätzung der Ostsee 1997
- 30 (1998) Fennel, Katja:  
Ein gekoppeltes, dreidimensionales Modell der Nährstoff- und Plankton-

- dynamik für die westliche Ostsee
- 31 (1998) Lemke, Wolfram:  
Sedimentation und paläogeographische Entwicklung im westlichen Ostseeraum (Mecklenburger Bucht bis Arkonabecken) vom Ende der Weichselvereisung bis zur Litorinatransgression
- 32 (1998) Wasmund, Norbert; Alheit, Jürgen; Pollehne, Falk; Siegel, Herbert; Zettler, Michael L.:  
Ergebnisse des Biologischen Monitorings der Ostsee im Jahre 1997 im Vergleich mit bisherigen Untersuchungen
- 33 (1998) Mohrholz, Volker:  
Transport- und Vermischungsprozesse in der Pommerschen Bucht
- 34 (1998) Emeis, Kay-Christian; Struck, Ulrich (Editors):  
Gotland Basin Experiment (GOBEX) - Status Report on Investigations concerning Benthic Processes, Sediment Formation and Accumulation
- 35 (1999) Matthäus, Wolfgang; Nausch, Günther; Lass, Hans Ulrich; Nagel, Klaus; Siegel, Herbert:  
Hydrographisch-chemische Zustandseinschätzung der Ostsee 1998
- 36 (1999) Schernewski, Gerald:  
Der Stoffhaushalt von Seen: Bedeutung zeitlicher Variabilität und räumlicher Heterogenität von Prozessen sowie des Betrachtungsmaßstabs - eine Analyse am Beispiel eines eutrophen, geschichteten Sees im Einzugsgebiet der Ostsee (Belauer See, Schleswig-Holstein)
- 37 (1999) Wasmund, Norbert; Alheit, Jürgen; Pollehne, Falk; Siegel, Herbert; Zettler, Michael L.:  
Der biologische Zustand der Ostsee im Jahre 1998 auf der Basis von Phytoplankton-, Zooplankton- und Zoobenthosuntersuchungen
- 38 (2000) Wasmund, Norbert; Nausch, Günther; Postel, Lutz; Witek, Zbigniew; Zalewski, Mariusz; Gromisz, Sławomira; Łysiak-Pastuszek, Elżbieta; Olenina, Irina; Kavolyte, Rima; Jasinskaite, Aldona; Müller-Karulis, Bärbel; Ikauniece, Anda; Andrushaitis, Andris; Ojaveer, Henn; Kallaste, Kalle; Jaanus, Andres:  
Trophic status of coastal and open areas of the south-eastern Baltic Sea based on nutrient and phytoplankton data from 1993 - 1997
- 39 (2000) Matthäus, Wolfgang; Nausch, Günther; Lass, Hans Ulrich; Nagel, Klaus; Siegel, Herbert:  
Hydrographisch-chemische Zustandseinschätzung der Ostsee 1999
- 40 (2000) Schmidt, Martin; Mohrholz, Volker; Schmidt, Thomas; John, H.-Christian; Weinreben, Stefan; Diesterheft, Henry; Iita, Aina; Filipe, Vianda; Sangolay, Bomba-Bazik; Kreiner, Anja; Hashoongo, Victor; da Silva Neto, Domingos:  
Data report of R/V "Poseidon" cruise 250 ANDEX'1999
- 41 (2000) v. Bodungen, Bodo; Dannowski, Ralf; Erbguth, Wilfried; Humborg, Christoph; Mahlburg, Stefan; Müller, Chris; Quast, Joachim; Rudolph, K.-U.; Schernewski, Gerald; Steidl, Jörg; Wallbaum, Volker:  
Oder Basin - Baltic Sea Interactions (OBBSI): Endbericht
- 42 (2000) Zettler, Michael L.; Bönsch, Regine; Gosselck, Fritz:  
Verbreitung des Makrozoobenthos in der Mecklenburger Bucht (südliche Ostsee) - rezent und im historischen Vergleich
- 43 (2000) Wasmund, Norbert; Alheit, Jürgen; Pollehne, Falk; Siegel, Herbert:  
Der biologische Zustand der Ostsee im Jahre 1999 auf der Basis von Phytoplankton- und Zooplanktonuntersuchungen
- 44 (2001) Eichner, Christiane:  
Mikrobielle Modifikation der Isotopensignatur des Stickstoffs in marinem partikulärem Material
- 45 (2001) Matthäus, Wolfgang; Nausch, Günther (Editors):  
The hydrographic-hydrochemical state of the western and central Baltic

- Sea in 1999/2000 and during the 1990s
- 46 (2001) Wasmund, Norbert; Pollehne, Falk; Postel, Lutz; Siegel, Herbert; Zettler, Michael L.:
- Biologische Zustandseinschätzung der Ostsee im Jahre 2000
- 47 (2001) Lass, Hans Ulrich; Mohrholz, Volker; Nausch, Günther; Pohl, Christa; Postel, Lutz; Rüß, Dietmar; Schmidt, Martin; da Silva, Antonio; Wasmund, Norbert:
- Data report of R/V "Meteor" cruise 48/3 ANBEN'2000